



# LUND UNIVERSITY

## Laser Diagnostics for Soot in Small-Scale and Practical Systems

Simonsson, Johan

2018

*Document Version:*

Publisher's PDF, also known as Version of record

[Link to publication](#)

*Citation for published version (APA):*

Simonsson, J. (2018). *Laser Diagnostics for Soot in Small-Scale and Practical Systems*. [Doctoral Thesis (compilation), Combustion Physics]. Division of Combustion Physics, Department of Physics, Lund University.

*Total number of authors:*

1

### General rights

Unless other specific re-use rights are stated the following general rights apply:

Copyright and moral rights for the publications made accessible in the public portal are retained by the authors and/or other copyright owners and it is a condition of accessing publications that users recognise and abide by the legal requirements associated with these rights.

- Users may download and print one copy of any publication from the public portal for the purpose of private study or research.
- You may not further distribute the material or use it for any profit-making activity or commercial gain
- You may freely distribute the URL identifying the publication in the public portal

Read more about Creative commons licenses: <https://creativecommons.org/licenses/>

### Take down policy

If you believe that this document breaches copyright please contact us providing details, and we will remove access to the work immediately and investigate your claim.

LUND UNIVERSITY

PO Box 117  
221 00 Lund  
+46 46-222 00 00

The background of the cover is a collage of six grayscale microscopic images of soot particles. The particles exhibit various fractal-like structures, including branched chains, clusters, and large, interconnected networks. The images are arranged in a 2x3 grid, with the central text box overlapping the top-left and middle-left panels.

# Laser Diagnostics for Soot in Small-Scale and Practical Systems

JOHAN SIMONSSON

DEPARTMENT OF PHYSICS | FACULTY OF ENGINEERING | LUND UNIVERSITY





# Laser Diagnostics for Soot in Small-Scale and Practical Systems

Johan Simonsson



**LUND**  
UNIVERSITY

DOCTORAL DISSERTATION

by due permission of the Faculty of Engineering, Lund University, Sweden.  
To be defended in lecture hall F (K404), Fysicum, Professorsgatan 1,  
June 1, 2018 at 09:15

*Faculty opponent*

Dr Christopher R. Shaddix, Combustion Research Facility,  
Sandia National Laboratories, Livermore, California, USA

Organization LUND UNIVERSITY Division of Combustion Physics Department of Physics Box 118, SE-22100 Lund, Sweden		Document name Doctoral Dissertation	
		Date of issue May 7, 2018	
		CODEN LUTFD2/TFCP-212-SE	
Author: Johan Simonsson		Sponsoring organization	
Title and subtitle: Laser Diagnostics for Soot in Small-Scale and Practical Systems			
Abstract <p>In this work, laser-diagnostic techniques have been used to investigate soot in both small-scale laboratory burners as well as in large-scale and more applied systems. The aims of the investigations have been both to do fundamental investigations of soot optical properties and to perform more applied measurements in order to see how different running conditions in large-scale systems affect the soot formation. The main laser-diagnostic techniques used are extinction, laser-induced incandescence and elastic light scattering.</p> <p>Extinction measurements, using twelve lasers with wavelengths from 405 nm to 1064 nm, were conducted in two premixed ethylene/air flames in order to investigate the wavelength dependence of the absorption properties in soot. For the more mature soot particles, found at higher heights above burner (HAB), the results show the expected inverse relation to wavelength from Rayleigh theory for absorbing spheres. However, for nascent soot particles, a much stronger wavelength dependence was found. The results also indicated that wavelengths longer than 700 nm should be used when performing extinction measurements of soot in order to avoid additional absorption by soot precursors, such as polycyclic aromatic hydrocarbons. The ethylene/air flames have also been investigated using laser-induced incandescence, where the changes in soot properties caused by the ageing process was studied. This investigation showed that nascent soot is more transparent, and absorbed less light compared to more mature soot.</p> <p>Extinction measurements were also applied in an entrained-flow gasifier to investigate how different operating conditions affected the soot formation. The investigation was performed using two fuels (wood and peat), two burners, and was done at two different distances from the burner. The main difference in measured soot concentrations was found when changing between the fuels, with much lower soot concentrations when, under the same air-fuel equivalence ratios, using peat compared to wood. The primary reason for the lower concentrations found for peat powder is most likely the lower volatile content in peat, and may additionally be due to higher ash concentrations.</p> <p>The effects of seven metal salts, selected based on metals found in the biofuel feed-stock, on soot formation were investigated using laser-induced incandescence, elastic light scattering and extinction. The salts were seeded into a small-scale ethylene/air flame at three different concentrations. Soot volume fractions and particle sizes were evaluated, and the flames seeded with potassium chloride, calcium chloride, and sodium chloride, showed significant decreases in soot volume fractions. For potassium and sodium chloride additives, decreased scattering signals were also observed, at lower HAB, before visible soot appeared, indicating that also the soot precursors are affected by the salt additions, either by size or concentration. Soot primary particle size evaluation was performed both using laser-diagnostics (LII and ELS) and by evaluation of soot samples in a transmission electron microscope. For the flame seeded with potassium chloride, both the evaluation of images from the microscope and the evaluation from LII and ELS showed decreased soot primary particle sizes.</p>			
Key words: Soot, extinction, laser-induced incandescence, combustion, gasification, elastic light scattering			
Classification system and/or index terms (if any)			
Supplementary bibliographical information		Language: English	
ISSN and key title: 1102-8718		ISBN 978-91-7753-665-9 (print) ISBN 978-91-7753-666-6 (pdf)	
Recipient's notes	Number of pages: 208		Price
	Security classification		

I, the undersigned, being the copyright owner of the abstract of the above-mentioned dissertation, hereby grant to all reference sources permission to publish and disseminate the abstract of the above-mentioned dissertation.

Signature \_\_\_\_\_



Date 2018-04-18



# Laser Diagnostics for Soot in Small-Scale and Practical Systems

Johan Simonsson



**LUND**  
UNIVERSITY

Cover image by Johan Simonsson


pp. 7-104      Copyright Johan Simonsson  
Paper I          © 2015 Springer-Verlag Berlin Heidelberg  
Paper II         © 2015 Springer-Verlag Berlin Heidelberg  
Paper III        © 2015 SAE International  
Paper IV        © 2016 American Chemical Society  
Paper V         © 2016 The Combustion Institute, published by Elsevier  
Paper VI        © 2017 The Combustion Institute, published by Elsevier  
Paper VII       © 2018 by the authors

Lund University  
Faculty of Engineering  
Department of Physics

Lund Reports on Combustion Physics, LRCP-212  
ISBN 978-91-7753-665-9 (print)  
ISBN 978-91-7753-666-6 (pdf)  
ISSN 1102-8718  
ISRN LUTFD2/TFCP-212-SE

Printed in Sweden by Media-Tryck, Lund University  
Lund 2018



MADE IN SWEDEN 

Media-Tryck is an environmental-  
ly certified and ISO 14001 certified  
provider of printed material.  
Read more about our environmental  
work at [www.mediatryck.lu.se](http://www.mediatryck.lu.se)



# Table of Contents

Abstract .....	7
Populärvetenskaplig sammanfattning .....	9
List of Papers .....	11
Related work .....	12
Chapter 1 Introduction .....	13
Chapter 2 Combustion and Gasification .....	17
2.1 Combustion .....	17
2.1.1 Premixed and Non-Premixed Flames .....	18
2.1.2 Oxy-fuel Combustion .....	19
2.2 Gasification .....	20
2.2.1 Gasification Techniques.....	22
Chapter 3 Soot and Experimental Soot Sources.....	25
3.1 Soot.....	25
3.1.1 Soot Formation.....	25
3.2 Experimental Soot Sources .....	28
3.2.1 Laboratory Burners .....	28
3.2.2 The miniCAST Soot-Generator.....	32
3.2.3 Large-Scale and Practical Systems .....	34
Chapter 4 Soot Diagnostics and Theoretical Considerations.....	39
4.1 Extinction .....	39
4.1.1 The Complex Refractive Index of Soot .....	41
4.1.2 Uncertainties – Extinction .....	43
4.2 Laser-Induced Incandescence (LII) .....	45
4.2.1 Laser Profiles and Fluence Curves .....	46
4.2.2 Time-Resolved LII Measurements .....	48
4.2.3 Time-Gated LII Measurements.....	49
4.2.4 Calibration of LII signals to Soot Volume Fractions.....	50
4.2.5 Uncertainties - LII .....	51

4.3 Elastic Light Scattering (ELS) .....	52
4.3.1 Soot Particle Size Measurements .....	53
4.3.2 Uncertainties - ELS.....	54
4.4 Transmission Electron Microscopy (TEM).....	55
4.4.1 Uncertainties - TEM.....	57
Chapter 5 Optical Arrangements and Experimental Equipment .....	59
5.1 Extinction Measurements .....	59
5.1.1 Diode Laser System .....	60
5.1.2 Photodiodes and Data Collection .....	61
5.2 LII and ELS Measurements .....	62
Chapter 6 Results .....	65
6.1 Investigation of Soot Optical Properties.....	65
6.2 Applied Extinction Measurements .....	71
6.3 Influence of Metal Salts on Soot Formation.....	75
6.4 Applied Measurements Using LII and Extinction .....	81
Chapter 7 Summary, Conclusions, and Outlook .....	85
7.1 Summary and Conclusions .....	85
7.2 Outlook .....	87
Chapter 8 Bibliography .....	89
Acknowledgements .....	99
Summary of Papers .....	101



# Abstract

In this work, laser-diagnostic techniques have been used to investigate soot in both small-scale laboratory burners as well as in large-scale and more applied systems. The aims of the investigations have been both to do fundamental investigations of soot optical properties and to perform more applied measurements in order to see how different running conditions in large-scale systems affect the soot formation. The main laser-diagnostic techniques used are extinction, laser-induced incandescence and elastic light scattering.

Extinction measurements, using twelve lasers with wavelengths from 405 nm to 1064 nm, were conducted in two premixed ethylene/air flames in order to investigate the wavelength dependence of the absorption properties in soot. For the more mature soot particles, found at higher heights above burner (HAB), the results show the expected inverse relation to wavelength from Rayleigh theory for absorbing spheres. However, for nascent soot particles, a much stronger wavelength dependence was found. The results also indicated that wavelengths longer than 700 nm should be used when performing extinction measurements of soot in order to avoid additional absorption by soot precursors, such as polycyclic aromatic hydrocarbons. The ethylene/air flames have also been investigated using laser-induced incandescence, where the changes in soot properties caused by the ageing process was studied. This investigation showed that nascent soot is more transparent, and absorbed less light compared to more mature soot.

Extinction measurements were also applied in an entrained-flow gasifier to investigate how different operating conditions affected the soot formation. The investigation was performed using two fuels (wood and peat), two burners, and was done at two different distances from the burner. The main difference in measured soot concentrations was found when changing between the fuels, with much lower soot concentrations when, under the same air-fuel equivalence ratios, using peat compared to wood. The primary reason for the lower concentrations found for peat powder is most likely the lower volatile content in peat, and may additionally be due to higher ash concentrations.

The effects of seven metal salts, selected based on metals found in the biofuel feedstock, on soot formation were investigated using laser-induced incandescence, elastic light scattering and extinction. The salts were seeded into a small-scale ethylene/air flame at three different concentrations. Soot volume fractions and particle sizes were evaluated, and the flames seeded with potassium chloride, calcium chloride, and sodium chloride, showed significant decreases in soot volume fractions. For potassium

and sodium chloride additives, decreased scattering signals were also observed, at lower HAB, before visible soot appeared, indicating that also the soot precursors are affected by the salt additions, either by size or concentration. Soot primary particle size evaluation was performed both using laser-diagnostics (LII and ELS) and by evaluation of soot samples in a transmission electron microscope. For the flame seeded with potassium chloride, both the evaluation of images from the microscope and the evaluation from LII and ELS showed decreased soot primary particle sizes.



# Populärvetenskaplig sammanfattning

*Den här avhandlingen syftar till att utveckla och använda olika lasermättekniker både i mindre laboratorieflammar, i syfte för att öka kunskaperna om sotpartiklarnas optiska egenskaper, men också att använda dessa tekniker i större anläggningar för att få ökade kunskaper om hur olika körfall påverkar bildningen av sot.*

Energianvändningen ökar kontinuerligt i världen och den energi som används genereras till största del genom förbränning av olika bränslen, där fossila bränslen så som kol, olja och naturgas är de mest vanliga. Intresset ökar för att ersätta dessa fossila bränslen med förnybara alternativ för att minska den globala uppvärmningen. En möjlighet är att använda biobränslen, till exempel rester från skogsindustrin, för att genom förgasning skapa mer flexibla bränslen som till exempel biogas. Den biogas som produceras kan då ha samma innehåll som motsvarande naturgas, men istället ha ett ursprung som gör att utsläppen av koldioxid i atmosfären inte ökar.

Förgasning kan liknas vid förbränning men sker i en atmosfär som innehåller för lite syre i förhållande till hur mycket bränsle som tillsätts. På så vis skapas de energirika molekyler som utgör förstadiet till den färdiga biogasen. Det kan även skapas andra önskade kolbaserade restprodukter som till exempel sot. Sot är mycket små kolbaserade partiklar, som kan klumpa ihop sig till större strukturer. En källa till sotpartiklar som många kan relatera till är stearinljus, där de upphettade sotpartiklarna är orsaken till det tydligt gul-orangea sken som syns. Sotpartiklar har visat sig både vara hälsofarligt, då det kan orsaka till exempel astmabesvär och lungcancer, och skadligt för miljön. Sot som kommer ut i atmosfären har visat sig ha liknande effekt som koldioxid, och anses vara en av de tre största orsakerna till den globala uppvärmningen tillsammans med koldioxid och metan.

För att undersöka sot kan lasermetoder med fördel användas. Dessa kan användas för att ta reda på mängden sot, hur stora sotpartiklarna är, men även temperaturen hos sotpartiklarna i till exempel en flamma eller en större förgasningsanläggning. De vanligaste teknikerna för mätning av sot med laser är extinktion, laserinducerad inkandescens (glödning) och elastisk ljusspridning.

Extinktion är en teknik där ljus passerar genom till exempel en flamma med sotpartiklar. Genom att jämföra intensiteten av ljuset före och efter flammen kan man ta reda på hur mycket av ljuset som har absorberats av sotpartiklarna. Detta kan sedan användas för att beräkna hur mycket sot det finns längs ljusets väg. För laserinducerad inkandescens används intensiva laserpulser för att hetta upp sotpartiklarna. Dessa hettas då upp till flera tusen grader över normal flamtemperatur och när temperaturen ökar

så ökar även den strålning som partiklarna sänder ut. Denna strålning, utöver den normala strålning som en flamma avger, mäts och kan även den relateras till hur mycket sot som finns vid mätpunkten. Genom att kombinera laserinducerad inkandescens med elastisk ljusspridning kan även storlek på sotpartiklarna beräknas under vissa förutsättningar. Elastisk ljusspridning är en teknik där det spridda ljuset från inkommande laserpulser mäts. Ljuset sprids från sotpartiklarna mot detektorn som oftast är placerad vinkelrätt mot den inkommande laserpulsen.

För att kunna göra noggranna mätningar av sot så är det viktigt att veta hur sotpartiklarna påverkas av olika saker, till exempel på vilken färg (våglängd) som laserstrålen har. Sotet kan också ha olika egenskaper som påverkar mätningarna beroende på om det är alldeles nyskapat eller har fått växa till sig och mogna. Mätningar där sotets egenskaper har undersökts har utförts i stabila flammor på mindre laboratoriebrännare. Dessa mätningar har visat att nyskapat sot är mer genomskinligt, och absorberar ljus sämre än sotpartiklar som åldrats. Det yngre sotet har också visat sig ha ett starkt våglängdsberoende på det inkommande ljuset vid absorption.

Vid praktiska mätningar i större anläggningar, så är extinktionsmätningar väldigt praktiska, då utrustningen är relativt liten till sin storlek och enkel att hantera. Mätning av mängden sot kan då utföras kontinuerligt, och ofta kan man direkt se hur en förändring av driften påverkar mängden sot i anläggningen. Den här typen av mätning har utförts i en förgasningsanläggning i Piteå, där körfall med olika bränslen undersökts. Resultaten visade på stora skillnader i mängden sot som bildades beroende på om pulver av vanligt trä eller torv användes, även under liknande bränsleluftblandningar. Denna skillnad kan bero på att innehållet mellan trä och torv skiljer sig åt. Torv innehåller bland annat en mindre andel lättflyktiga ämnen och har även en högre andel askkomponenter, som till exempel metaller. Vissa metaller har visat sig kunna påverka mängden sot kraftigt.

För att kunna undersöka hur metaller påverkar sotbildningen i flammor genomfördes ett experiment där sju olika salter med metaller, som återfinns i råmaterialet för biobränslen, har undersökts. Dessa salter matades in tillsammans med blandningen av bränsle och luft och undersöktes sedan med laserinducerad inkandescens, elastisk ljusspridning och extinktion. Resultaten visar tydligt att salter som innehåller kalium, kalcium och natrium har en tydlig påverkan på sotbildningen och minskar mängden sot i flammorna.

# List of Papers

- I. **J. Simonsson**, N.-E. Olofsson, S. Török, P.-E. Bengtsson, and H. Bladh, *Wavelength dependence of extinction in sooting flat premixed flames in the visible and near-infrared regimes*, Applied Physics B, **119**: pp. 657-667 (2015)
- II. N.-E. Olofsson, **J. Simonsson**, S. Török, H. Bladh, and P.-E. Bengtsson, *Evolution of properties for aging soot in premixed flat flames studied by laser-induced incandescence and elastic light scattering*, Applied Physics B, **119**: pp. 669-683 (2015)
- III. Y. Gallo, **J. Simonsson**, T. Lind, P.-E. Bengtsson, H. Bladh, and Ö. Andersson, *A study of in-cylinder soot oxidation by laser extinction measurements during an EGR-sweep in an optical diesel engine*, SAE Technical Paper 2015-01-0800 (2018), <https://doi.org/10.4271/2015-01-0800>
- IV. **J. Simonsson**, H. Bladh, M. Gullberg, E. Pettersson, A. Sepman, Y. Ögren, H. Wiinikka, and P.-E. Bengtsson, *Soot concentrations in an atmospheric entrained flow gasifier with variations in fuel and burner configuration studied using diode-laser extinction measurements*, Energy & Fuels **30**: pp. 2174-2186 (2016)
- V. **J. Simonsson**, N.-E. Olofsson, H. Bladh, M. Sanati, and P.-E. Bengtsson, *Influence of potassium and iron chloride on the early stages of soot formation studied using imaging LII/ELS and TEM techniques*, Proceedings of the Combustion Institute **36**: pp. 853-860 (2017)
- VI. **J. Simonsson**, N.-E. Olofsson, A. Hosseinnia, and P.-E. Bengtsson, *Influence of potassium chloride and other metal salts on soot formation studied using imaging LII and ELS, and TEM techniques*, Combustion and Flame **190**: pp. 188-200 (2018)

- VII. **J. Simonsson**, A. Gunnarsson, M. Naduvil Mannazhi, D. Bäckström, K. Andersson, and P.-E. Bengtsson, *In-situ soot characterization of propane flames and influence of additives in a 100 kW oxy-fuel furnace using two-dimensional laser-induced incandescence*, Submitted to the Proceedings of the Combustion Institute (2018), (accepted for presentation at the 37th International Symposium on Combustion 2018, under review for publication)

## Related work

- R-I. H. Bladh, N.-E. Olofsson, T. Mouton, **J. Simonsson**, X. Mercier, A. Faccinetto, P.-E. Bengtsson, and P. Desgroux, *Probing the smallest soot particles in low-sooting premixed flames using laser-induced incandescence*, Proceedings of the Combustion Institute **35**: pp.1843-1850 (2015)
- R-II. E. Nordström, N.-E. Olofsson, **J. Simonsson**, J. Johnsson, H. Bladh, and P.-E. Bengtsson, *Local gas heating in sooting flames by heat transfer from laser-heated particles investigated using rotational CARS and LII*, Proceedings of the Combustion Institute **35**: pp. 3707-3713 (2015)
- R-III. Y. Gallo, V. B. Malmborg, **J. Simonsson**, E. Svensson, M. Shen, P.-E. Bengtsson, J. Pagels, M. Tunér, A. Garcia, and Ö. Andersson, *Investigation of late-cycle soot oxidation using laser extinction and in-cylinder gas sampling at varying inlet oxygen concentrations in diesel engines*, Fuel **193**: pp. 308-314 (2017)
- R-IV. S. Török, V. Berg Malmborg, **J. Simonsson**, A. Eriksson, J. Martinsson, M. Naduvil Mannazhi, J. Pagels, and P.-E. Bengtsson, *Characterization of light absorption and physicochemical properties for soot of different maturity from a mini-CAST soot generator*, Aerosol Science and Technology (2018), <https://doi.org/10.1080/02786826.2018.1457767>

# Chapter 1 Introduction

The overall energy consumption in the world is increasing every year [1], and during 2015 a total of 81.4 % of the world's energy fuel supply originated from coal, oil, and natural gas [1]. In Sweden, the numbers are significantly lower, with only 28.2 % of the energy originating from fossil fuels during the same year [2]. The total energy consumption in Sweden is also decreasing, and an increased amount of carbon-neutral fuels are used [2].

Carbon dioxide is considered to be the most important anthropogenic greenhouse gas contributing to global warming [3], and emission of greenhouse gases must decrease to prevent possible effects such as increased temperatures, increased sea levels, and extreme weather [4]. Gasification of biofuels is one way of reducing the net emissions of carbon dioxide while, for example, creating carbon neutral fuel for the transport sector. Oxy-fuel combustion is another way of minimizing the amount of CO<sub>2</sub>-emissions if used in combination with carbon storage. However, both gasification and the oxy-fuel technique, described in **Chapter 2**, are likely to form soot regardless of whether fossil fuel or biomass is used.

Soot is a result of incomplete combustion and has been shown to be negative for both health [5] and climate [6]. Health issues caused by soot include, for example, lung cancer, chronic lung diseases, and asthma [5]. For the climate, soot has in recent studies been found to be one of the main contributors to global warming along with carbon dioxide and methane [4, 6]. The effect of soot particles is not always negative, for example, the high radiative intensity of soot compared to the combustion gases makes soot necessary for achieving effective heat transfer in furnaces. However, it is important to limit the amount of soot in the exhaust from such devices. A more detailed description of soot and soot formation can be found in **Chapter 3**.

In Sweden, the emissions of soot particles have decreased by around 40 % between the year 2000 and 2016 to approximately 3 million kilograms per year [7]. Emissions from the heating of houses and buildings have increased by 30 % during the same period, making this the main contributor to soot emissions in Sweden. The previous largest contributor to soot emissions in Sweden (domestic transports mainly from heavy-duty traffic) decreased by over 60 % during the same period [7].

Experimental studies of soot in combustion can be separated into two categories: fundamental studies and practical studies. In fundamental studies the focus is on investigating only a limited number of properties and parameters in small-scale systems, while in practical studies the overall performance of various fuels and operating conditions are investigated. Both fundamental and practical investigations are

important to get a better understanding of soot, for example, regarding soot optical properties and soot formation. Investigation of soot in either small or large-scale environments can result in questions leading to both a more practical or a more fundamental approach in the ongoing soot research.

Experimental studies of soot can either be performed intrusively using probes for soot extraction and evaluation in an external instrument [8], or using non-intrusive laser diagnostics for measurements *in situ* with advantages of, for example, increased spatial and temporal resolution. The most commonly used laser diagnostic techniques for soot are extinction, laser-induced incandescence (LII) [9, 10], and elastic light scattering measurements (ELS) [11]. These techniques, along with related theory are described in **Chapter 4**.

Extinction measurement of soot can advantageously be used in practical and large-scale systems as the equipment needed is small, and often relatively cheap. However, extinction is a line-of-sight technique, which relies on measuring the transmitted light intensity through an absorbing medium. It is therefore important to use light which is only absorbed by the species of interest, in this case, soot particles. Furthermore, it is important to know the optical properties and their uncertainties for the investigated soot and how these properties change, for example, during the soot ageing process. In **Paper I**, results from an investigation of wavelength dependence of soot using extinction to find suitable wavelengths for soot measurements are presented. Results on how soot maturity affected the optical properties are also shown in this paper. Soot maturity was also investigated in the work leading up to **Paper II**, where laser-induced incandescence and elastic light scattering measurements were used to investigate how absorption properties change for soot at different stages of maturity. Soot temperatures were also investigated in this work, where results from the wavelength dependence investigation in **Paper I**, were used.

The extinction technique and the gained knowledge from the small-scale experiments were applied in an engine (**Paper III**) and an atmospheric gasifier (**Paper IV**) under various running conditions. The measurement from the gasifier showed significant differences in soot concentrations depending on which fuel was used (stem wood or peat), under approximately the same operating conditions. The main reason for the difference in soot concentrations was believed to be the higher volatile content in the wood powder resulting in higher concentrations of soot. However, the lower concentration of soot when using peat powder could also be related to higher concentrations of ash components. The ash components include metal compounds, which are found in both peat and bark mixtures [12], and some metals have showed to reduce the soot formation [13-15].

A controlled study of how metal compounds affect the soot formation was performed by seeding metal salt solutions into a premixed flame on a small-scale burner. The metal salts were selected based on metal compounds found in high abundance in the bio-fuel feed-stock [12]. A combination of laser-induced incandescence, elastic light scattering, and extinction were used to evaluate, for example, soot concentrations and particle

sizes. Part of the results, with additives of potassium chloride, showing significant reduction in concentration of both soot precursors and soot were presented in **Paper V**. A more extensive presentation of the results from all investigated metal salts were made in **Paper VI**.

In an attempt to combine extinction and imaging laser-induced incandescence in a large-scale environment, a 100 kW<sub>th</sub> oxy-fuel test furnace was investigated using propane as fuel. The combination of LII and extinction allowed for spatially resolved LII measurements calibrated to soot volume fractions over a large area inside the furnace. The furnace was operated at various running conditions in oxy-fuel mode, with air, and with oxygen-enriched air. The measured spatially resolved soot volume fraction data can, for example, be used for validation of radiative heat transfer models, of importance for improving efficiency and operation of furnaces and boilers. The results from the oxy-fuel measurements were presented in **Paper VII**.

In **Chapter 5**, measurement related equipment, such as lasers and detectors, are presented as well as typical optical setups used for extinction, LII, and ELS. The main results from Paper I - VII will be presented along with some unpublished results in **Chapter 6**, followed by a summary and outlook in **Chapter 7**.





# Chapter 2

## Combustion and Gasification

In this chapter, the concepts of combustion and gasification are introduced. For combustion, premixed and non-premixed flames will be presented as well as the oxy-fuel combustion technique. For gasification, a general introduction is presented together with gasification techniques such as entrained-flow gasification and fluidized bed gasification.

### 2.1 Combustion

Combustion is exothermic reactions between a fuel and an oxidant, often oxygen. The combustion phenomenon has been around on earth since the first wildfires occurred around 420 million years ago when the oxygen content in the atmosphere had reached at least 13 % [16, 17]. The first human-controlled fires occurred much later, between 0.2 and 1.7 million years ago [18].

The energy released from a combustion process depends on what fuel is being used and can be calculated by using enthalpies of the reactants and products. For the theory of heat release and heating values, textbooks on combustion can advantageously be consulted, see for example [19, 20]. The maximum energy release will theoretically occur for the stoichiometric mixture, i.e. the mixture for which all fuel and oxidizer are consumed and has created only carbon dioxide and water (for hydrocarbon fuels). The energy released during the combustion process will be used to heat the product gases. The actual temperature will depend on what environment the fuel is being burnt in, the energy losses, and the heat capacities of the products. For example, burning a fuel in only oxygen will result in much higher temperatures compared to burning fuel in air, since the energy released will also be used to heat the inert nitrogen during combustion in air [20].

### 2.1.1 Premixed and Non-Premixed Flames

A flame can either be premixed or non-premixed, often referred to as a diffusion flame. Three images showing one diffusion (candle light) and two premixed flames with different ratios of fuel and air can be seen in Fig. 2.1. For a premixed flame, the fuel and oxidizer are mixed before burning. The relation between the fuel and oxidizer can be described by the equivalence ratio,  $\phi$ . The fuel-air equivalence ratio is defined as:

$$\phi = \frac{\left(\frac{n_{\text{fuel}}}{n_{\text{oxidizer}}}\right)_{\text{mixture}}}{\left(\frac{n_{\text{fuel}}}{n_{\text{oxidizer}}}\right)_{\text{stoichiometric}}}, \quad (2.1)$$

where  $n_{\text{fuel}}$  and  $n_{\text{oxidizer}}$  represents the number of moles of the fuel and oxidizer respectively. For a stoichiometric mixture, where ideally the fuel and oxidizer are consumed and creating carbon dioxide and water, the equivalence ratio equals to 1. If the mixture contains more fuel than oxidizer compared to the stoichiometric mixture then  $\phi > 1$ , which is referred to as a fuel-rich flame [20]. On the other hand, if the mixture contains more oxidizer in relation to fuel, then the flame is referred to as a fuel-lean flame with  $\phi < 1$  [20].

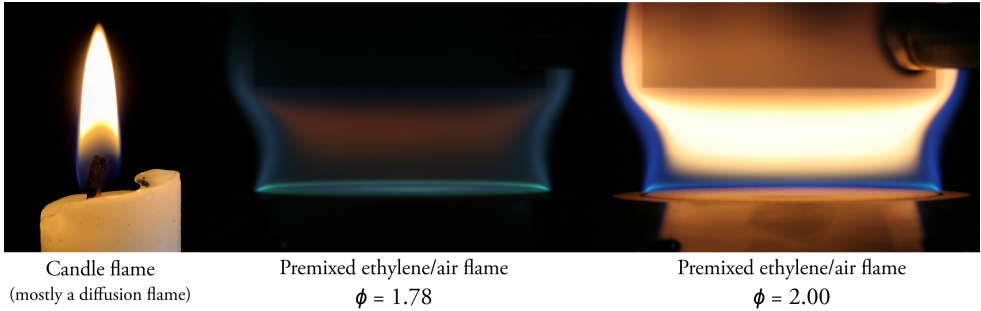
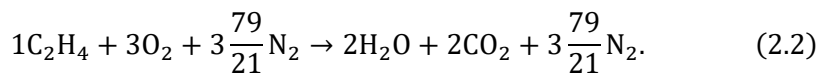


**Figure 2.1**

Flame images of one candle flame (mostly a diffusion flame), and two premixed ethylene/air flames on a McKenna burner. Both premixed flames are fuel rich, where the premixed flame with equivalence ratio 1.78 shows some initial soot formation and the flame with equivalence ratio 2.0 show clear visible soot emissions.

Premixed ethylene/air flames have been used in measurements throughout the work for this thesis, and would therefore serve as a good candidate for an example. The balanced stoichiometric equation for burning ethylene in air is:



The stoichiometric ratio,  $(n_{\text{fuel}}/n_{\text{oxidizer}})_{\text{st}}$ , between the fuel and oxidizer for burning ethylene/air is in this case  $1/3$ . If the amount of fuel is doubled, while keeping the amount of air constant, the equivalence ratio will also be doubled:

$$\phi = \frac{\left(\frac{n_{\text{fuel}}}{n_{\text{oxidizer}}}\right)_{\text{mixture}}}{\left(\frac{n_{\text{fuel}}}{n_{\text{oxidizer}}}\right)_{\text{stoichiometric}}} = \frac{\frac{2}{3}}{\frac{1}{3}} = 2. \quad (2.3)$$

For a non-premixed flame, or diffusion flame, the fuel and oxidizer are introduced separately. The name diffusion flame comes from the fact that the fuel and oxidizer primarily are transported to the reaction zone by diffusion from opposite sides [20]. For a diffusion flame, mixing between the fuel and oxidizer are important for the combustion reactions to occur. A common example of flame that is mainly a diffusion flame is a normal candle light, see Fig. 2.1, where the fuel burns on a wick surrounded by ambient air as an oxidizer. The candle light process starts with some of the wax is being melted by the heat from the flame. The melted wax is then transported upwards on the wick through capillary action, where the wax is vaporized due to increased temperature. The vapors then break down into smaller hydrocarbons through pyrolysis when transported towards the surface of the flame. At the same time oxygen moves from the surrounding atmosphere to the flame surface through convection and diffusion, which then leads to combustion and to the formation of soot.

For a diffusion flame it is difficult to discuss an equivalence ratio as the input of fuel and oxidizer is not mixed. However, a local equivalence ratio can often be defined for a specific volume in a diffusion flame. In large-scale enclosed systems, such as in gasifiers or furnaces, an overall equivalence ratio is often defined. For these applications it is more common to use the air-fuel equivalence ratio, often referred to as lambda,  $\lambda$ . The air-fuel equivalence ratio is defined as the ratio between the stoichiometric air-to-fuel ratio (AFR) and the actual air-to-fuel ratio. The air-fuel equivalence ratio is also equal to the inverse of the fuel-air equivalence ratio,  $\phi$ , and can be expressed as:

$$\lambda = \frac{AFR_{\text{stoichiometric}}}{AFR_{\text{actual}}} = \frac{1}{\phi} \quad (2.4)$$

### 2.1.2 Oxy-fuel Combustion

In oxy-fuel combustion, the oxidizer is oxygen and is often mixed with carbon dioxide. Oxy-fuel in combination with carbon storage has in recent years gained increasing interest due to its potential as a method for either neutral or negative net emissions of carbon dioxide for fossil fuels and biofuel, respectively [19]. Techniques for carbon storage are described in, for example [21]. An advantage of the oxy-fuel technique is

that it can often be applied in existing systems with only minor retrofitting, and thereby reducing the cost and taking advantage of earlier investments [19].

A negative aspect of the oxy-fuel combustion technique is the increased temperatures, which is a result of the increased oxygen concentration. When burning solid fuels, such as coal or biomass, the increased temperatures causes a significant increase in char combustion and volatile components [19]. By recirculating some of the flue-gas, which include primarily carbon dioxide and excess oxygen, into the combustion chamber, the temperature effect caused by the increased oxygen levels can be lowered. For example, the heat capacity of carbon dioxide is higher than the heat capacity of nitrogen, which means that having 21 % oxygen and 78 % carbon dioxide in the inlet oxidizer would result in lower temperatures compared to if air had been used (21 % O<sub>2</sub> and 78 % N<sub>2</sub>). However, the recirculated flue-gas containing CO<sub>2</sub> and O<sub>2</sub> would have a higher initial temperature compared to if air with ambient temperature were used as oxidizer, which would decrease the effect of using recirculation. This problem could be minimized if some part of the heat from the recirculated flue-gas were used for other purposes before the flue-gases are circulated back into the reactor.

Even though most nitrogen has been removed when using oxygen and recirculated carbon dioxide instead of air, various NO<sub>x</sub>-compounds can often be found in large-scale systems, especially when burning solid fuels [19]. These NO<sub>x</sub> molecules originate from the oxidation of nitrogen in the volatile fuel components and from char. However, the recirculation allows re-burning of previously formed NO<sub>x</sub>, since up to 70 % of the flue-gases are recirculated in practical devices [19]. Furthermore, the lower temperatures due to recirculation inhibits the formation of thermal NO<sub>x</sub>. For combustion in oxy-fuel environments the amount of NO<sub>x</sub> created is often decreased by a factor of at least three compared to normal combustion [19].

## 2.2 Gasification

The main purpose of gasification is to convert solid carbon fuels to a gaseous or liquid, and a more usable product, which can be used as a versatile fuel compared to the solid counterpart. The gas produced often includes carbon monoxide, water, hydrogen, and methane, and is often referred to as synthetic gas or syngas [22, 23]. The thermal conversion of solid fuels includes several steps and occurs in substoichiometric (in terms of lambda value) conditions, sometimes with less than 35 % of the amount of oxygen needed for complete combustion [22]. The first step in the conversion process occurs when the fuel is heated and drying commences, which results in the release of water. The next process is devolatilization, where pyrolysis occurs. During this process char is created and volatiles are released. Gasification then occurs where the solid carbon reacts with, for example, hydrogen, steam or carbon dioxide [22]. If the fuel conversion process is halted after the partial conversion, the process is called gasification. If full

conversion of the solid fuel to a product gas with no residual heating value has taken place, then the process is combustion [23], which is discussed in section 2.1.

The first commercial use of gas produced from gasification of coal was for lighting of the Westminster Bridge in London in 1812 [23]. A few years later, in 1816, the first plants opened in the United States in order to produce gas for street lights in Baltimore, and soon thereafter also in Boston and New York City [22]. The use of coal has been, and continues to be, the primary fuel source for producing gas through conversion of solid fuels using gasification.

In recent years the interest of using biomass instead of coal for gasification has increased. This is a result of the biogas produced, compared to the fossil alternatives such as gas produced from coal gasification or natural gas, will be a renewable source of energy. Furthermore, as with gasification in general, the goals are to create a versatile and a more homogenous fuel with a more concentrated energy content compared to the original form of the biomass [22]. This is important as the definition of biomass is quite broad, and includes, for example, mixed waste, wood residues, and sewage sludge [22, 23], which means that the heating values or energy content of different biomass sources varies significantly. There might also be large variations of heating value for the same type of fuels, which is especially notable in mixed waste. This means that it is not only hard to estimate the fuel consumption for producing biogas, it will also be difficult to design a gasification plant suitable for a broad range of biomass [22].

The main chemistry for gasification of carbonaceous fuels are the same regardless of if biofuels or pure coal is used to produce the synthetic gas. In [22], ten reactions that are probable to occur during gasification are presented, they are denoted (a) to (j) here:



According to [22], the first three reactions, (2.5a) to (2.5c), are the primary consumers of the supplied oxygen. These reactions will provide heat for drying and devolatilization, break up chemical bonds, and increase the temperature inside the reactor in order for reactions (2.5d) to (2.5j) to take place. These reactions are referred to as the gasification reactions, and depends strongly on pressure and temperature. The reactions are described in more detail in [22].

During gasification, unwanted products such as soot and tars may also be formed depending on reaction temperatures, air-fuel equivalence ratios ( $\lambda$ ), and how well mixing occurs inside the gasifier [24]. The largest difference in terms of products between coal and biomass gasification are the solid rest products. The ash content, i.e. the inorganic components, differs significantly between coal and biomass. The main ash components found in coal includes silica, alkali metals, and ferric oxide to mention a few. In most biomass sources the main ash components are salts [23]. In Paper IV, measurements in a gasifier were presented, showing significant differences in soot concentration depending on the fuel used. It was speculated that one cause of this was the ash components, as salts, especially salts containing alkali and alkaline earth metals, could affect the soot formation [13, 14, 25]. The effects of salts on soot formation was studied in laboratory flames with the work being presented in Paper V and Paper VI.

The syngas produced during gasification has to go through several steps before being a useful fuel, for example, a gas cleaning processes in order to remove soot, tars and unwanted products. However, this will not be discussed in this thesis. For a more thorough review of pre-treatment of solid fuels, gas cleaning, reactor designs, and a more deepened knowledge regarding the chemical reactions and kinetics, see for example [22, 23].

### 2.2.1 Gasification Techniques

There are several different types of gasification techniques/processes, and all have their advantages and disadvantages. Two common types of gasification are entrained-flow gasification and fluidized bed gasification.

For entrained-flow gasification the fuel and oxidizer, often oxygen or air, are introduced together in the same direction, most commonly top-fired or side-fired, using one or several burners. An advantage of using entrained-flow gasification is that most types of coal-based fuels can be used, given that they are milled to a small enough size (less than 100  $\mu\text{m}$  for coal) [23]. Small particles are required for good transport of the fuel within the reactor, and is a consequence of the short residence time, which is often only around a few seconds [23]. Furthermore, due to the short residence time, high temperatures are needed for good carbon conversion. The high temperature will make most entrained-flow gasifiers operate in slagging mode, which means that the rest products (ash) are transported out from the reactor as a melted slag.

An atmospheric top-fired entrained-flow gasifier, located at RISE ETC in Piteå, Sweden, was investigated using two different fuels, peat (fossil fuel) and milled stem wood (biomass). This investigation was presented in Paper IV. For more information regarding the gasifier, see section 3.2.3.

In fluidized-bed gasification, fuel and oxidizer are often introduced separately but directly into the bed material, consisting of either silica sand, quartz sand or any other suitable material. This allows for very good mixing between the fuel and the oxidizer.



The oxidizer is often a mixture of oxygen and steam, however for biomass gasification, air is often used. The fuel size is important in fluidized bed gasification, since fuel particles that are too small may leave the fluidized bed and follow the raw syngas upwards and exit the reactor. This might cause clogging of the equipment and should be avoided. Large particles (larger than 10 mm for coal) should also be avoided, as it might be difficult to fluidize these particles [23]. The residence time for a fuel particle in the fluidized bed varies significantly. Some particles may leave the bed together with the ash particles before full conversion is complete, and some particles may be fully converted. The obtainable conversion-ratio for a fluidized bed gasifier is therefore often lower compared to entrained-flow gasification, 97 % and 99 % respectively [23]. The operation temperature inside the reactor is also lower compared to entrained-flow gasification to avoid melting the ash particles, which would cause problems in the fluidized bed.

In Gothenburg, Sweden, a demonstration plant (GoBiGas) for producing biogas from forest residues has been built and has been in operation since 2014. This plant is based on dual fluidized-bed gasification, which uses two fluidized-bed reactors, one for combustion and one for gasification [26]. The plant also includes gas cleaning and processes for increasing the methane content up to 95 %. The produced gas is then being used as fuel in vehicles [27].



# Chapter 3

## Soot and Experimental Soot Sources

In this chapter soot is presented to give an insight into what soot is and how soot is formed. This chapter also includes most of the experimental soot sources that have been used in the work for this thesis, including laboratory burners, a soot generator, and practical combustion devices.

### 3.1 Soot

The definition of soot varies depending on literature source, but in short, soot is particles resulting from incomplete combustion of hydrocarbon fuels, and consists mainly of carbon and to some extent also hydrogen ( $\sim 1\%$  by weight) [19, 28]. Soot is sometimes referred to as black carbon (BC) when it comes to atmospheric research [29, 30]. In the atmospheric research community another type of less absorbing particles with high organic content is called brown carbon (BrC), where brown carbon often is considered to originate from burning biofuels [29]. For flame soot originating from gaseous hydrocarbon fuels, the equivalent optical properties of brown and black carbon are found in what will be referred to as nascent and mature soot, where nascent soot absorb less light compared to the more graphitized and mature soot particles, see [31] and Paper II.

Soot primary particles are approximately spherical with a diameter of 1 - 50 nm [32-34]. However, significantly larger soot structures can be formed when a few or many primary particles create a soot aggregate. Soot aggregates are often described mathematically as fractal structures [11] and can be several hundred nanometers in size.

#### 3.1.1 Soot Formation

Soot is a result of incomplete combustion in regions with excess carbon atoms relative to what would be found if complete combustion occurred. For a premixed flame with an equivalence ratio,  $\phi > 1$ , there is excess fuel in relation to oxidizer, which may result in the formation of soot when the equivalence ratio approaches two. The description of the soot formation process in this section will assume a premixed

environment, as most of the investigated flames in this thesis have been premixed. For flames with equivalence ratios larger than 1, water and carbon dioxide will be formed, but also other molecules due to the excess amount of carbon atoms in the mixture. For a slightly rich flame, i.e. with an equivalence ratio of just above 1, carbon containing molecules such as carbon monoxide will be formed. The carbon monoxide concentration will increase with increased equivalence ratio, and for increased equivalence ratio other larger carbon molecules may also be formed leading up to formation of soot particles. The soot formation limit in terms of equivalence ratio, i.e. critical equivalence ratio, varies from fuel to fuel, and has, for example, been found to be 1.82 for ethylene and 1.56 for propane [19].

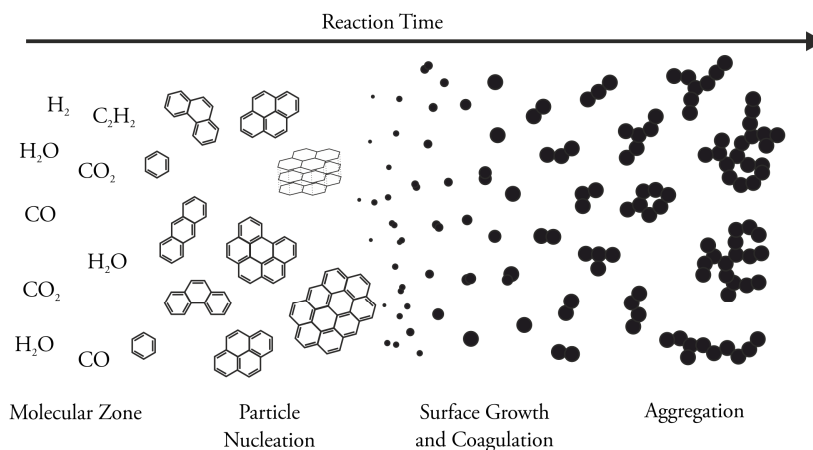


**Figure 3.1**

An illustration of the soot formation process for a fuel-rich premixed flame, going from molecules in the product zone to soot aggregates in the later stages of the formation process.

In Fig. 3.1, the soot formation process is illustrated. In the early stages of the product zone for a fuel-rich flame, various molecules can be found in gas-phase. These molecules include water, carbon dioxide, hydrogen, carbon monoxide, and various hydrocarbons which have been formed when the fuel molecules have dissociated in the high-temperature regions of the flame. One of the most important hydrocarbons for soot formation is acetylene, C<sub>2</sub>H<sub>2</sub>, which is considered to be among the earliest precursor to soot [34]. From the molecules in the product zone, larger polycyclic aromatic hydrocarbons (PAHs) can be formed through different mechanisms [34], and PAHs are also considered to be precursors to soot [19, 34].

Polycyclic aromatic hydrocarbons of various sizes, from the smallest naphthalene molecules with only two aromatic ring to larger ones with several rings, can be found throughout the product zone in sooting flames [35]. The soot nuclei are assumed to be formed when the two-dimensional PAH molecules attach to each other and form three-

dimensional structures, i.e. particle nucleation. In [34], three pathways of the nucleation process are described. The newly formed soot particles are approximately 1 - 2 nm in size [34, 36] and will grow to particle sizes of up to 50 nm through surface growth and coagulation, which occur simultaneously. The process of surface growth occurs continuously as the soot nuclei are exposed to smaller hydrocarbons present in the flame. The smaller hydrocarbons interact with the surface and results in an increased size of the soot particles. Coagulation is a process where soot nuclei merge to create larger particles. In comparison to surface growth, where the soot volume fraction (the fraction of soot in a confined volume) increases with the increased size, coagulation will not change the soot volume fraction in the gas. However, the number concentration of particles will decrease during the coagulation process. The process of coagulation also explains why the primary soot particles are not entirely spherical.

The final step of the soot formation process is aggregation. The primary soot particles which have grown through coagulation and surface growth, group together and form large structures of various sizes. These structures can contain hundreds of almost spherical primary particles and can be several hundred nanometers in size.

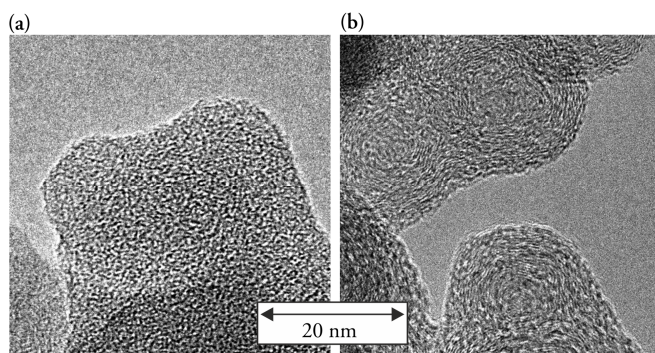


**Figure 3.2**

Two images of sampled soot from the miniCAST soot-generator evaluated in a transmission electron microscope. The image in (a) shows a soot particle from early in the soot formation process with an amorphous structure, while in (b) clear carbon layers are visible indicating a more mature particle. Image courtesy of Sandra Török and Kirsten Kling.

During the soot formation process, the inner structure of the particles changes as well. The newly formed soot particles are often referred to as nascent soot, and have a much more amorphous structure than soot particles in the later stages of formation process. The structure of the more mature particles is more graphitized with clear carbon layers. During the soot ageing process, the particles will lose hydrogen, and at the same time accumulate carbon from the carbon rich surrounding atmosphere. This may result in  $sp^2$ -bonds, which are present in graphite, and thereby be part of the graphitization process [37]. A comparison between nascent and more mature particles can be seen in Fig. 3.2, where two high-resolution transmission electron microscopy images are

shown, one of nascent soot (Fig. 3.2a), and one of a more mature soot particle (Fig. 3.2b). Differences in the soot structure can be seen in these images, where the more mature particles have visible carbon layers around an amorphous core, while no apparent structures can be seen in the image of the nascent particles. For further reading regarding soot formation, see for example [34, 38, 39].

## 3.2 Experimental Soot Sources

In this section several types of combustion devices are presented, including burners, an engine, a gasifier and a furnace. The most commonly used flames and operating conditions for these systems are also presented.

### 3.2.1 Laboratory Burners

#### *The McKenna Burner*

The McKenna burner is a porous-plug burner manufactured by Holthius and Associates [40]. An image of the McKenna burner is shown in Fig. 3.3a. The burner consists of a porous sintered inner plug of either bronze or stainless steel with a diameter of 60 mm. The outer porous ring is a shroud ring of bronze, used for a co-flow gas with an inner and outer diameter of 62.6 mm and 73.5 mm, respectively. The burner is water-cooled through a cooling circuit inside the inner plug. A sketched drawing showing a cross-section of the burner is showed in Fig. 3.3b.

In the community of laser-induced incandescence, primarily two flames on the McKenna burner are used for soot diagnostics. These are premixed ethylene/air flames with equivalence ratios,  $\phi$ , of either 2.1 or 2.3. The total flow of fuel and air through the center plug are often kept at 10 l/min (1 atm, 273 K). To stabilize the flames, either air or nitrogen is often used as co-flow gas. The flow of gas in the outer ring is often selected to match to cold gas velocity of the fuel and air in the center plug. To stabilize the flame further, a plug of stainless steel, with a diameter of 60 mm, is placed with its lower edge 21 mm above the burner surface.

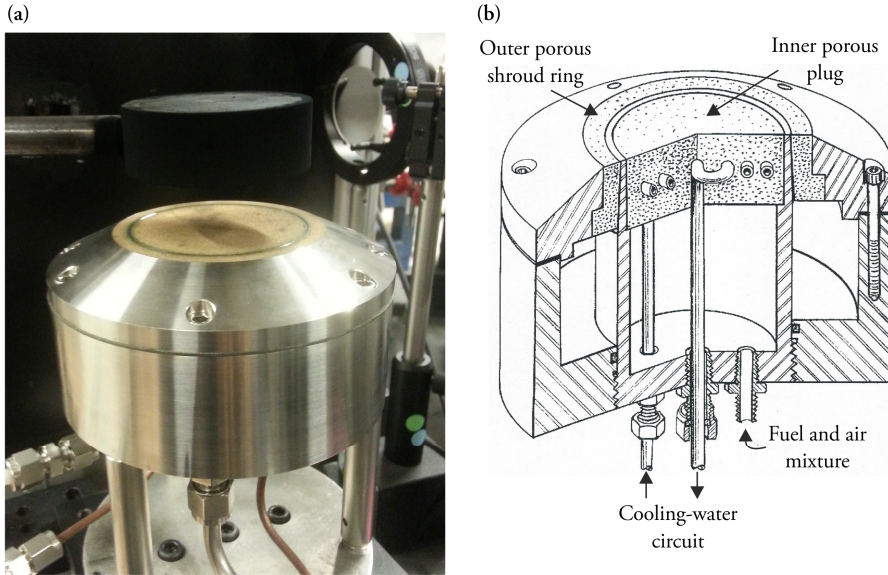


**Figure 3.3**

In (a), an image of the McKenna burner is shown together with the stainless steel stabilizer plug placed with its lower edge 21 mm above the burner surface. In (b) a sketch of a cross-section of the McKenna burner is shown with some of the connectors marked.

The flames produced on the McKenna burner are often considered to be flat flames, meaning that their properties only change with height above burner (HAB) and are constant in the horizontal plane, i.e. the flames are one-dimensional in nature. However, in work by Olofsson *et al.* [41] and by Migliorini *et al.* [42], this was showed to be questionable, at least for some conditions, with results showing varying soot concentration in the horizontal plane of the burner. Also, Olofsson *et al.* showed that a co-flow of nitrogen leads to cooling effects in the edges of the flame resulting, in lower soot volume fractions and smaller particle sizes, while a co-flow of air resulted in a more even soot distribution. In Fig. 3.4, images of the two commonly used ethylene/air flames with an equivalence ratio of 2.1 and 2.3, where a co-flow of air has been used, are shown. The difference in intensity is due to the increased amount of soot in the  $\phi = 2.3$  flame.

The flames on the McKenna burner have been investigated in work related to Paper I and Paper II and in work presented in numerous other publications, see for example [41-44].

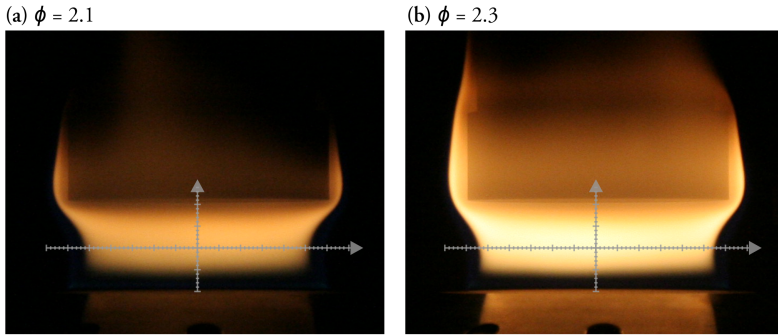


**Figure 3.4**

Images of two ethylene/air flames using shroud gas of air with equivalence ratios of (a)  $\phi = 2.1$ , and (b)  $\phi = 2.3$ . The images have an overlapped mm-cross. Both images have been captured with exposure times of 1/500 s.

### *The Modified PerkinElmer Burner*

The modified PerkinElmer burner produces similar, yet physically smaller flames than the McKenna burner, but allows for seeding of various solutions into the flame. Images of the PerkinElmer burner can be seen in Fig. 3.5. The air, fuel and co-flow gases leave the burner through a mesh top with a diameter of 45 mm with holes of approximately 1 mm in diameter and a depth of 20 mm, see Fig. 3.5b. The inner part of the mesh, with a diameter of 23 mm, is where the mixture of fuel, and air (with seeded solution) exits the burner, and the surrounding mesh is for the co-flow used for stabilization.

For the soot measurements presented in Paper V and Paper VI, an ethylene/air flame with an equivalence ratio of  $\phi = 2.6$  was used. The flow of ethylene was set to 0.27 l/min and the flow of air was set to 1.5 l/min (1 atm, 273 K). These settings resulted in a flame with an approximate diameter of 16 mm at a height above burner of 10 mm. The small flame was quite sensitive to the ambient atmosphere and required a substantial co-flow of air for stabilization. The co-flow was set to 5 l/min. In addition to the co-flow gas, a stabilizer plug in stainless steel with a diameter of 20 mm was placed with its lower edge at 21 mm above the burner surface.

The PerkinElmer burner allows seeding of various solutions into the flame directly through the fuel and air mixture. The solution is pulled from an external container and carried by air from one of the air inlets, see all connectors of the burner in Fig. 3.5c. The solution carried into the burner hits an impact bed and creates an aerosol with small water droplets, which are transported towards the burner head. Larger droplets will not follow the gas flow and are removed and collected in an air-tight drain container.



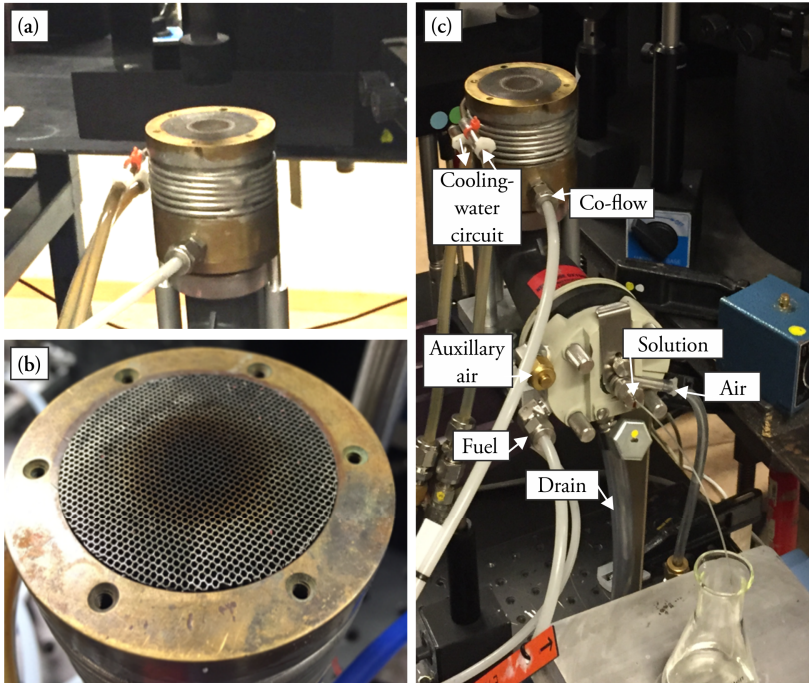


**Figure 3.5**  
 Images of the modified PerkinElmer burner. In (a) the burner and the stabilizer plug are shown, in (b) the mesh for the fuel and air mixture and co-flow are shown, and in (c) all of the connectors to the burner are marked.

In Fig. 3.6, three images of the investigated flame with an overlapped mm-cross are shown, seeded with distilled water, solutions of potassium chloride, and sodium chloride. In the flame seeded with sodium chloride, the typical (589 nm)-emission from sodium is visible at the edges of the sooting flame.

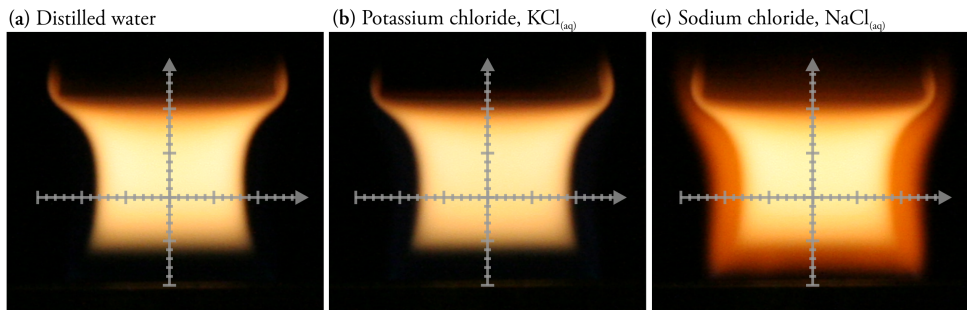


**Figure 3.6**  
 Images of sooting ethylene/air flames with equivalence ratio 2.6 seeded with distilled water (a) and 1 M solutions of potassium chloride (b) and sodium chloride (c). An overlapped mm-scale is shown in each image of the flames.

### 3.2.2 The miniCAST Soot-Generator

The miniCAST soot-generator (model 5201 type C) is a commercial product by Jing Ltd in Switzerland for creating soot with various properties. A photo of the miniCAST can be seen in Fig. 3.7. The settings for operating the miniCAST can be varied to change, for example, soot particle sizes, concentration, and the organic content of the particles. The particle diameters range from 20 to 200 nm, with a concentration of up to  $10^8$  particles per  $\text{cm}^3$  [45]. The miniCAST is operated using propane as fuel, nitrogen as a mixing and quench gas, and air for oxidation and dilution. In Table 3.1, suggested operating points (OP) from the manufacturer are presented. Changes of the dilution air can be performed if the particle concentration needs to be adjusted without changing the particle properties. The operation of the miniCAST, including the control of the built-in mass flow controllers, are managed by a pre-supplied computer program where the different operating points are set by the user.

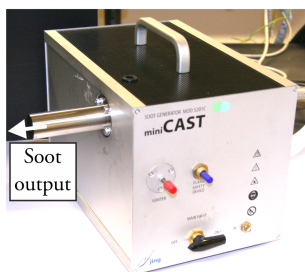


**Figure 3.7**  
A photo of the miniCAST 5201 type C soot-generator.

**Table 3.1**  
The operating points suggested by the manufacturer for the miniCAST [46].

Operating point	Fuel, $\text{C}_3\text{H}_8$	Mixing gas, $\text{N}_2$	Oxidizer air	Quench gas, $\text{N}_2$	Dilution air	
1	0.06 l/min	0 ml/min	1.55 l/min			
2		50 ml/min	1.54 l/min			
3		100 ml/min	1.52 l/min			
4		150 ml/min	1.50 l/min			
5		200 ml/min	1.47 l/min		7 l/min	20 l/min
6		250 ml/min	1.42 l/min			
7		300 ml/min	1.36 l/min			
8		330 ml/min	1.32 l/min			

The fundamental principle of the miniCAST is presented in Fig. 3.8a. A propane diffusion flame is the source of the soot particles. Around the flame, oxidizing air is present. The flame is quenched by nitrogen, resulting in a particle flow leaving the combustion chamber. The flow of quench gas will cool down the particles and suppress

further combustion processes and condensation when soot approaches the ambient atmosphere. The dilution air is added to dilute the particle output stream from the miniCAST. From the data presented in Table 3.1, it is clear that the most significant change between the different operation points is the variation in the amount of mixing gas (nitrogen). The mixing gas is combined with the fuel and will change the soot output significantly. In Fig 3.8b, an exaggerated sketch of flames from three operating conditions (OP1, OP5, and OP7) are shown to highlight how particles with different properties are extracted from the flames when changing the amount of mixing gas. The increased total flow of fuel and mixing gas will allow particles from earlier in the combustion process to be quenched, and thereby result in an output with smaller, less aggregated, and less mature particles.

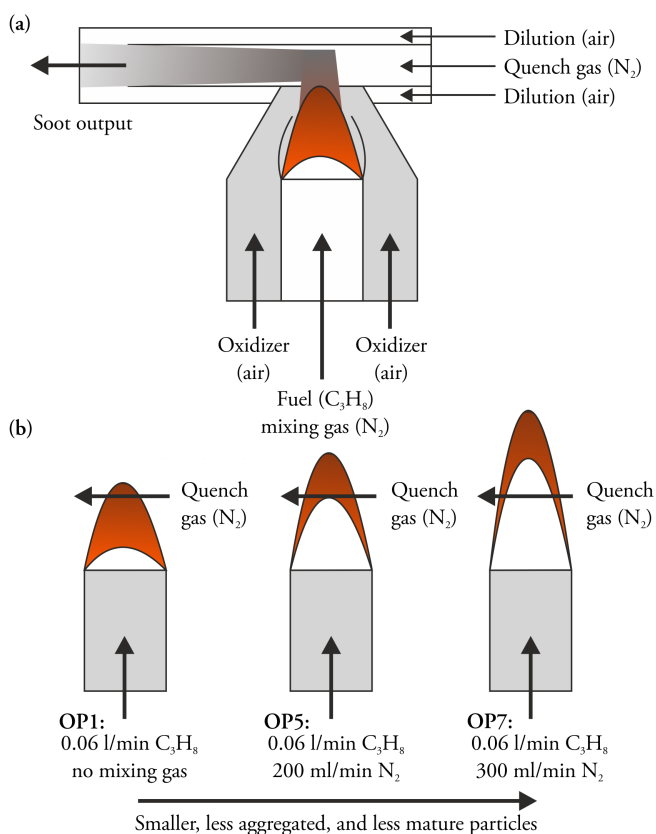


**Figure 3.8**

Illustrations to show how the miniCAST create different types of soot. (a) shows the fundamental principle of the miniCAST and the gases involved in the process, inspired by [46]. (b) shows an exaggerated sketch of how different types of soot are carried out from the miniCAST by changing the amount of mixing gas in the fuel.

Soot from the miniCAST has been investigated using a four-wavelength extinction approach and the results are presented in [47] (Paper R-IV), and some of the results are shown in Chapter 6.

### 3.2.3 Large-Scale and Practical Systems

#### *Atmospheric Entrained-Flow Gasifier*

At RISE Energy Technology Center (ETC) in Piteå, Sweden, they have a top-fired down-draft atmospheric entrained-flow gasifier. This gasifier is sometimes referred to as the vertical atmospheric flexi-fuel rig (VAFF). The gasifier is cylindrical with a flat top and a conical bottom with an inner and outer diameter of approximately 500 mm and 900 mm, respectively. The combustion chamber is surrounded by 200 mm of refractory lining inside the outer steel shell. The height of the gasifier is 3.87 m. In Fig. 3.9, both a sketch and a photo of the gasifier is shown with some dimensions given.

The burner is placed in the top of the rig, creating a down-fired flame. Two different burners can be used with the gasifier. Both burners have an outer diameter of 89 mm with a central fuel pipe which has a diameter of 50 mm. One of the burners is referred to as the “jet burner”, which has the air and fuel inlets parallel to the burner axis creating a flame directed downwards. The second burner has three air registers creating a rotating flow inside the gasifier, and this burner is therefore referred to as the “swirl burner”. The characteristics of the swirl burner can be altered by changing the distribution of air between the different air registers.

The rig can be operated with various fuels, and for the measurements presented in Paper IV, powders of stem wood and peat at various operating conditions were investigated. The flow of fuel was controlled by changing the rotating speed of feed augers originating from the bottom of a fuel hopper. When operating using wood and peat powder, the fuel consumption was on average 20.2 kg/hour and 22.9 kg/hour, respectively, resulting in a fuel load of around 115 kW<sub>th</sub>. The air-fuel equivalence ratio,  $\lambda$ , was adjusted by changing the amount of air, both transport air for carrying the fuel, and burner air through the different air registers. The gasifier was operated at  $\lambda = 1.2$  in combustion mode during the startup process, and from  $\lambda = 0.7$  to  $\lambda = 0.3$  in gasification mode for the measurements. Details of specific air flows and air-fuel equivalence ratios can be found in Table 2 in Paper IV.

Optical measurements in the gasifier were possible as measurement ports were located at different distances from the burner. In Fig. 3.9, these are denoted with ML1 to ML6, where ML stands for measurement level. The extinction measurements presented in Paper IV were performed in measurement ports ML3 and ML4. Furthermore, thermocouples are located both in the refractory lining as well as inside the gasifier at different distances from the burner. These are seen in Fig. 3.9a, and denoted T1 to T16.

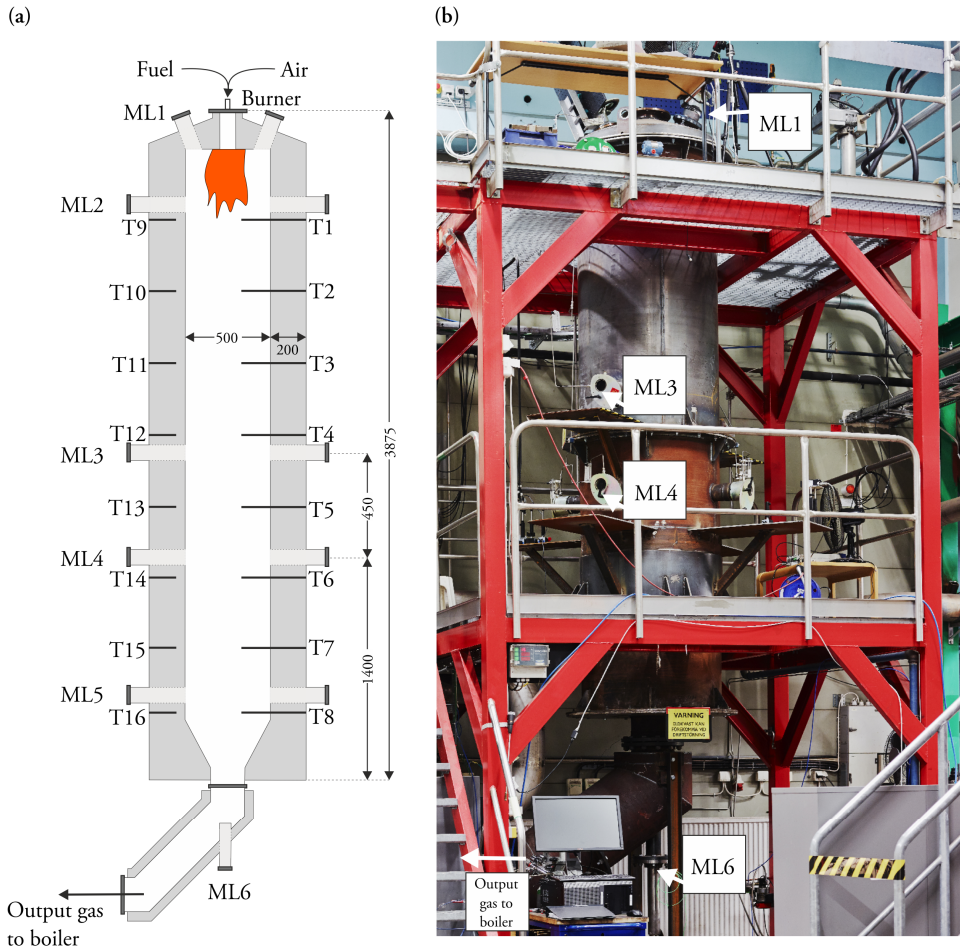


**Figure 3.9**  
 An illustration of the RISE ETC atmospheric entrained-flow gasifier is shown in (a) and an image of the gasifier is shown in (b). The measurement levels are denoted ML1-ML6, and the thermocouples inside the rig and inside the refractory lining are denoted T1-T8 and T9 to T16, respectively.

### *Scania D12 (optical) Engine*

The engine used for the measurements presented in Paper III is a modified Scania D12 heavy-duty direct-injection engine with six cylinders. For the investigated engine, only one of the six cylinders was fired, while the others were motored. The engine has been modified with an extended piston according to a Bowditch design [48] to allow for optical access. The extended piston has a quartz top, allowing for optical access to the combustion chamber from below. In addition, one of the exhaust valves was replaced

by an angled window to allow for optical access from the top of the combustion chamber.

For the soot measurements presented in Paper III, a Scania injector with eight nozzle holes was used for fuel injection along with the Scania XPI common rail fuel injection system, which allows injection pressures of up to 2500 bar. The fuel used for the measurements was Swedish MK1 diesel fuel and the engine was operated at 1200 rpm. To create conditions of exhaust gas recirculation (EGR), an external furnace burning diesel was used. The simulated EGR conditions enabled variations in the intake oxygen concentration from 9 % to 21 % O<sub>2</sub>. For more details regarding the engine and the settings used, see Paper III.

### *Chalmers Oxy-Fuel Test Furnace*

A 100 kW<sub>th</sub> atmospheric oxy-fuel test furnace is located at Chalmers University of Technology in Gothenburg, Sweden. The furnace is a down-fired cylindrical furnace with an outer and inner diameter of 1400 mm and 800 mm respectively. The inner height of the furnace is 2400 mm, and a sketch of the furnace with some dimensions given can be seen in Fig. 3.10a. The furnace uses a swirl burner, for which a sketch can be seen in Fig. 3.10b, and can be operated with both solid and gaseous fuels in oxy-fuel mode, with normal air as well as oxygen-enriched air. The burner has two annular swirling registers, the primary register and the secondary register, with angles of 45 and 15 degrees respectively. The fuel is introduced in the center of the burner. In oxy-fuel mode, some of the dry flue-gas, consisting mainly of carbon dioxide and excess oxygen, is recirculated back into the furnace.

Measurements can be conducted using various techniques at different distances from the burner using measurement ports placed at different vertical positions. The measurement ports are denoted M1 to M8 in Fig. 3.10a, and are also shown in images of the furnace in Figs 3.10c and 3.10d. At each vertical position M1 to M7, four measurement ports are found placed orthogonally to each other. For the extinction and laser-induced incandescence measurements presented in paper VII, three of the four measurement ports at level M3 were used. Previous measurements performed in the furnace have mainly been using probes and extractive techniques, for example, temperature measurements using thermocouples, radiative intensity measurements, and soot sampling for analysis using external instruments [49-51].

For the measurements leading to Paper VII, several measurement cases were investigated as the furnace was operated using propane in oxy-fuel mode, with air, and with oxygen-enriched air. The measurement cases are presented in Table 3.2. For all cases, the overall air-fuel equivalence ratio,  $\lambda$ , was set to 1.15 and the flow of propane was constant at 1.73 g/s, which resulted in an 80 kW propane diffusion flame. To maintain the same overall air-fuel equivalence ratio when increasing the amount of oxygen in the oxidant, both for the oxy-fuel cases and the oxygen-enriched cases, the



oxidant flow has to be decreased. A decrease in oxidant flow decreases the total flow through the reactor resulting in less mixing between the fuel and oxidant.

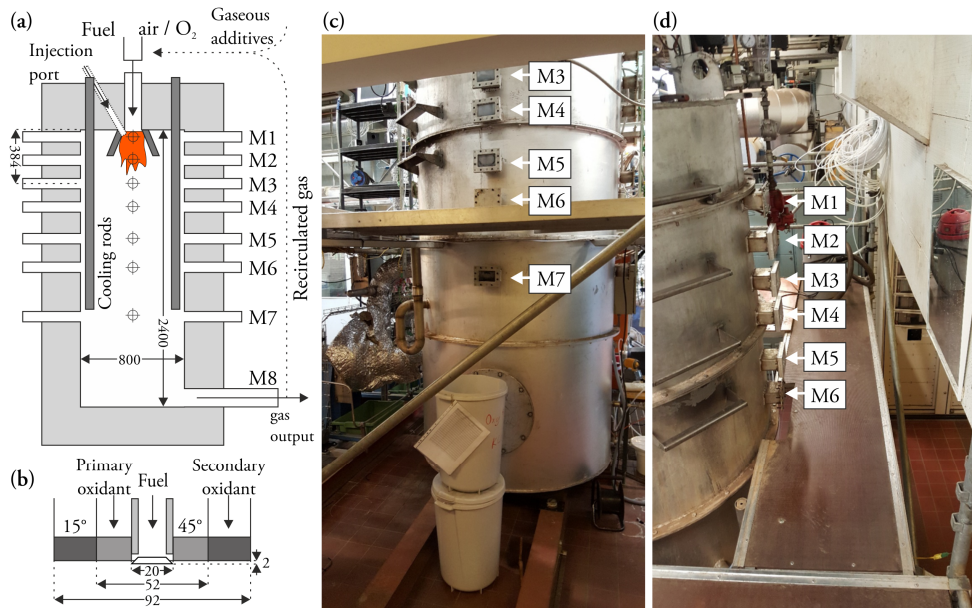


**Figure 3.10**

The oxy-fuel furnace located at Chalmers University of Technology, Gothenburg, Sweden. A sketch of the furnace is shown in (a) and a sketch of the burner used is shown in (b). The measurement ports are denoted M1 to M8. In (c) and (d) images of the furnace at ground level and the upper level is shown. In these images the visible measurement ports are marked.

**Table 3.2**

The different test cases used for the Chalmers oxy-fuel test furnace. The part that is not oxygen in the oxidant is mainly recirculated carbon dioxide for the oxy-fuel cases.

	Test case	Overall air-fuel equivalence ratio	Propane flow [g/s]	Oxygen in oxidant [%]	Oxidant flow [Nm <sup>3</sup> /h]	Primary oxidant register
Oxy-fuel	1	1.15	1.73	25	73.0	Open
	2			30	60.8	Open
	3			35	52.1	Open
	4			40	45.6	Open
	5			42	43.4	Open
Air	6	1.15	1.73	21	86.9	Open
	7			21	86.9	Closed
Oxygen-enriched air	8	1.15	1.73	25	73.0	Open
	9			27	67.6	Open
	10			29	62.9	Open
	11			30	60.8	Open





# Chapter 4 Soot Diagnostics and Theoretical Considerations

In this chapter, techniques for soot diagnostics are presented to give an insight into how they can be used for soot measurements. The chapter also includes the necessary theory for using the techniques for evaluation of, for example, soot volume fractions and particle sizes. The chapter also includes a discussion regarding the assumptions needed for evaluation and uncertainties related to both these assumptions and the measurements.

## 4.1 Extinction

Extinction is a line-of-sight technique where both the incident light intensity,  $I_0$ , and the transmitted intensity,  $I$ , through an optically thin absorbing medium are measured. The decrease in light intensity through the absorbing medium can be related to the extinction coefficient,  $K_{\text{ext}}$ , using the Beer-Lambert law:

$$I = I_0 e^{-K_{\text{ext}}L}, \quad (4.1)$$

where  $L$  is the length of the absorbing medium. The Beer-Lambert law can be understood by looking at Fig. 4.1. Extinction is a combination of both absorption and scattering, and the extinction coefficient is the sum of the absorption coefficient,  $K_{\text{abs}}$  and the scattering coefficient  $K_{\text{sca}}$ , i.e.  $K_{\text{ext}} = K_{\text{abs}} + K_{\text{sca}}$ . In the general case, where an absorbing medium consists of several different species, the extinction coefficient may be written as:

$$K_{\text{ext}} = \sum_i K_{\text{abs},i} + K_{\text{sca},i} = \sum_i K_{\text{abs},i} (1 + \rho_{\text{sa},i}), \quad (4.2)$$

where the absorption and scattering coefficient for each specific species are denoted with an  $i$ . The ratio between the scattering and absorption coefficient is denoted  $\rho_{\text{sa}}$ . Often, only one species is of interest, and therefore it is of great importance that the light used is only absorbed by this specific species.

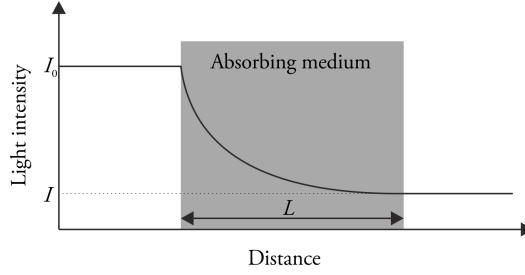


**Figure 4.1**

The light intensity as a function of distance when light is passing through an absorbing medium with absorption length,  $L$ .

When applying extinction measurements on soot, it is possible to estimate soot volume fractions under some assumptions. The primary soot particle diameter,  $d$ , is often around 5-30 nm for soot found in flames [32, 33] and is often investigated using light with wavelengths in the visible and near-infrared regimes. The primary soot particles are often considered to be spherical and isotropic, and are much smaller than the wavelength used, which means that the measurements can be considered to be performed within the Rayleigh limit. In the Rayleigh regime, it is common practice to neglect the scattering as part of the extinction, i.e.  $\rho_{sa}$  is assumed to be zero [52]. This means that the extinction coefficient is equal to the absorption coefficient. For individual particles the absorption coefficient for isotropic spheres is, according to Rayleigh theory given by:

$$K_{\text{abs}} = -\frac{\pi^2}{\lambda} \text{Im} \left( \frac{m^2 - 1}{m^2 + 2} \right) N d^3, \quad (4.3)$$

where  $\lambda$  is the laser wavelength,  $m$  is the complex refractive index of soot,  $N$  is the particle number concentration, and  $d$  is the primary particle diameter. The factor,  $-\text{Im}((m^2 - 1)/(m^2 + 2))$ , is often denoted as the absorption function,  $E(m)$ , which will be discussed further in section 4.1.1.

For larger particles and for soot aggregates, the above mentioned assumptions may no longer be valid, and a more complex theory for particles with arbitrary size and shape may be needed. For diagnostics of soot in flames, the Rayleigh-Debye-Gans (RDG) approximation may work with sufficient accuracy [53]. In this approximation, the absorption cross-section for each individual particle is multiplied with the number of particles in an aggregate of soot. This means that the absorption, as within the Rayleigh limit, is volume dependent, and that Eq. (4.3) should still be valid.

The soot volume fraction,  $f_v$ , can be expressed:

$$f_v = N \frac{\pi d^3}{6}. \quad (4.4)$$

The experimentally measured extinction coefficient, evaluated from Beer-Lambert law, Eq. (4.1) can in combination with Eqs (4.3) and (4.4) give an expression for estimating the soot volume fractions from measurements, given that the scattering contribution can be neglected. The expression for evaluating soot volume fractions from extinction measurements is given by:

$$f_v = \frac{K_{\text{ext}} \lambda}{6\pi E(m)}. \quad (4.5)$$

A consequence of using a line-of-sight technique such as extinction, is that only averaged data along the laser beam path can be obtained. For spatially resolved soot volume fraction measurements, laser-induced incandescence can advantageously be utilized. Extinction measurements have been performed in the work presented in Papers I, III, IV, V, VI, and VII in different environments. Measurements in small-scale laboratory flames were performed in the work presented in Papers I, V, and VI. In Paper III, extinction measurements performed in a diesel engine with optical access was presented. Extinction measurements in an atmospheric gasifier were presented in Paper IV. In Paper VII, measurements performed in a 100 kW<sub>th</sub> oxy-fuel test furnace was shown.

#### 4.1.1 The Complex Refractive Index of Soot

The complex refractive index of soot,  $m$ , is defined as  $m = n - ik$ , where  $n$  is the real part and  $k$  is the imaginary part of the refractive index [54]. When evaluating soot volume fractions it is common to use the absorption function,  $E(m)$ , directly instead of using the refractive index. The absorption function can be calculated from the complex refractive index using:

$$E(m) = -\text{Im} \left( \frac{m^2 - 1}{m^2 + 2} \right). \quad (4.6)$$

From Eq. (4.6) it is clear that a specific complex refractive index will only give one specific value of  $E(m)$ , however, a specific  $E(m)$  will not give just one combination of values for  $n$  and  $k$  for the complex refractive index. In recent years, it has been more common to directly evaluate  $E(m)$  from measurements, see for example Paper II and

[55-58]. This causes no significant problem when evaluating soot concentrations since only  $E(m)$  or  $m$  is required. However, for evaluation of soot particle sizes using a combination of soot volume fraction and scattering measurements, another function of the complex refractive index is also used. This function,  $F(m)$  is defined according to:

$$F(m) = \left| \frac{m^2 - 1}{m^2 + 2} \right|^2, \quad (4.7)$$

and can not be derived only from using the absorption function. The function,  $F(m)$ , is mainly used for particle size evaluations from elastic light scattering measurements, which will be discussed in section 4.3. It is shown here to highlight the issues of performing measurements to evaluate  $E(m)$  instead doing measurements to evaluate the complex refractive index. From a known  $E(m)$ , there is no possibility to calculate an equivalent value for  $F(m)$  without selecting either  $n$  or  $k$  based on some assumptions.

There are also large variations in reported values in the literature for  $E(m)$ ,  $F(m)$  and for the complex refractive index, which will give large uncertainties if a value is assumed in, for example, evaluated soot volume fractions. In Fig. 4.2, reported values of  $E(m)$ , and complex refractive indices converted to  $E(m)$  and  $F(m)$  for soot from various sources are shown. Most of the data in Fig. 4.2 are shown in [37, 59], however, more detailed information on how the values have been obtained is found in [59-71]. The data in Fig. 4.2 are shown to highlight the large spread of values presented in the literature. The values of  $E(m)$  and  $F(m)$  presented in Fig. 4.2 varies from less than 0.1 to values around 0.5. Therefore, depending on the value of  $E(m)$  selected for evaluation of, for example, soot volume fractions, the results may vary significantly.

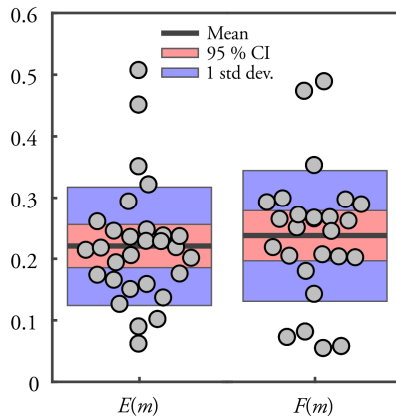


**Figure 4.2**

Values of the absorption function,  $E(m)$  and the function  $F(m)$  of soot from various sources in [59-71]. Most of the values have been calculated from the complex refractive index of soot. The graphs show the mean value, one standard deviation and the 95 % confidence interval (CI).

In the literature, another common representation of the complex refractive index of soot, is the dimensionless extinction coefficient,  $K_e$ . If using Eq. (4.5) and comparing with the expression for evaluating  $K_e$  in [72], then  $K_e = 6\pi E(m)$ . However, the definition of the dimensionless extinction coefficient often includes the ratio between the absorption and the scattering coefficient resulting in  $K_e = 6\pi (1 + \rho_{sa}) E(m)$  [56], which will result in Eq. (4.5) if the scattering contribution to the extinction can be neglected, i.e.  $\rho_{sa} \rightarrow 0$ .

Measurements of  $K_e$  show quite large variations, which also could be seen in measurements of the absorption function. In work by Williams *et al.* [72], they present measurements of  $K_e$  from diffusion flames resulting in values from 5 to 10 for ethylene flames, depending on flame type and wavelength that was used for the investigation. Furthermore, they showed that the dimensionless extinction coefficient is fuel dependent, with lower values for ethylene and methane compared to kerosene flames.

To conclude this section, it is obvious that there will be large uncertainties in the evaluated soot volume fraction, independent on whether  $E(m)$  is used directly or if the complex refractive index or measured values of  $K_e$  are used in evaluations.

#### 4.1.2 Uncertainties – Extinction

The main uncertainty for the extinction measurements and evaluation of soot volume fractions is, as discussed in section 4.1.1, the absorption function,  $E(m)$ . The absorption function may introduce significant errors when evaluating soot volume fractions due to the large spread of values in the literature, as presented in Fig. 4.2. How large the error is will depend on the selected value for the absorption function compared to the actual optical properties of the measured particles. However, there are also other uncertainties when using extinction for soot volume fraction measurements. These uncertainties include estimation of the absorption length, potential absorption by other species than soot, the assumption of neglecting the scattering contribution, and accuracies in the measurements of both the transmitted and the initial intensity.

The difficulty in estimating the absorption length varies depending on whether the measurements have been performed in small-scale laboratory flames or in large-scale systems. For absorption lengths in smaller flames, the uncertainties are often quite small, as the entire measurement region can be imaged using any type of camera, see for example measurements presented in Papers I, V or VI. For these measurements the uncertainties come from the problem of establishing where the soot edge of the flame is located, which may be related to the saturation level on the camera. In large-scale systems, however, it is much harder to estimate the absorption length. For the engine measurements presented in Paper III, the absorption length varied as the piston moved up and down, which was taken into account in the evaluation. Moreover, it is difficult to know if soot is present along the entire beam path. For the measurements performed in the atmospheric gasifier shown in Paper IV, the absorption length was set to the full

inner diameter of the gasifier, as no secondary technique could be used to give a better approximation. A third example is the measurements presented in Paper VII. In this work images obtained using laser-induced incandescence (LII) were used to estimate the absorption length. From the averaged LII images which showed LII signals for only 15 cm of the entire furnace, the absorption length was estimated based on the soot distribution from LII.

When performing soot measurements, it is also of great importance that the laser beam is only absorbed by the soot particles. In sooting flames, polycyclic aromatic hydrocarbons (PAHs) can be found throughout the flame [35], and they absorb strongly in the ultra-violet (UV) and visible wavelength regimes. This was investigated thoroughly and presented in Paper I, where it was shown that wavelengths longer than around 700 nm should be used for soot measurements to avoid absorption by PAHs, in good agreement with results presented in [35]. PAHs are not the only absorbers in a sooting flame. Absorption lines from molecular species such as H<sub>2</sub>O should be avoided.

The scattering contribution in small-scale flames is often small, and does not inflict any large uncertainties. But for larger soot particles, the scattering-to-absorption ratio,  $\rho_{sa}$ , have in some studies been found to be between 0.2 and 0.4 depending on fuel and wavelength [56, 57], which means that the corresponding soot volume fractions measured under the assumption that scattering is neglected might be over predicted by 20 to 40 %. In work presented in Paper IV, the scattering contribution to the extinction was investigated. This was performed by using a second laser for the extinction measurements in the gasifier when burning wood and peat. In this work, it was concluded that the scattering contribution caused an error of less than 10 % for the measured soot volume fractions. For the measurements conducted in the oxy-fuel furnace, presented in Paper VII, no measurements of the scattering contribution were conducted. However, in an earlier investigation by Bäckström *et al.* presented in [51] and [73], similar flames were investigated using a photo-acoustic soot spectrometer (PASS-3). These measurements resulted in single-scattering albedos (SSA), which is the ratio between the scattering and the total extinction, for different wavelengths: 405 nm, 532 nm, and 781 nm. The results showed decreasing SSA for increased wavelength. For 781 nm (extinction measurements conducted using 808 nm) the value for SSA was measured to 0.03, indicating a low influence of scattering to the measurements.

The accuracy of the measurement system for extinction was investigated in work related to Paper I and the measurement uncertainties were found to be very small compared to those originating from the absorption function, the absorption length, and the scattering contribution.

## 4.2 Laser-Induced Incandescence (LII)

Laser-induced incandescence (LII) is a technique for soot diagnostics, where the soot particles are heated by laser pulses to temperatures of around 4000 K [9, 10, 74]. The increase of temperature will increase the Planck radiation emitted from the soot particles and will also lead to emitted radiation shifted toward shorter wavelengths. The increased radiation compared to the natural flame luminosity is in this context, referred to as the LII signal, and has been shown to be approximately proportional to the soot volume fraction [75].

Besides soot volume fraction measurements, which has been the primary use in the work of this thesis, LII can also be used for soot primary particle size evaluation and soot temperature measurements, which will briefly be described in section 4.2.2.

The LII process and the mass-energy balance for a soot particle can be described by several physical processes. These are mainly absorption, radiation, heat conduction, and sublimation. By absorbing energy, the internal energy of the soot particle will increase, resulting in higher particle temperatures. The increased soot particle temperatures will result in radiation and heat conduction losses. If the particle temperature reaches above ~3400 K, see paper II, the soot particle will start to sublime and lose mass. The mass-energy balance in a particle can be described by the following equation:

$$\dot{Q}_{\text{int}} = \dot{Q}_{\text{abs}} - \dot{Q}_{\text{rad}} - \dot{Q}_{\text{con}} - \dot{Q}_{\text{sub}}, \quad (4.8)$$

where the different terms are describing rates in energy for different physical properties related to the LII process. The change in internal energy for the individual soot particle is described by  $\dot{Q}_{\text{int}}$ . The energy increase and losses due to absorption and radiation are denoted  $\dot{Q}_{\text{abs}}$  and  $\dot{Q}_{\text{rad}}$  respectively, while  $\dot{Q}_{\text{con}}$  is the term for energy changes due to heat conduction. The final term,  $\dot{Q}_{\text{sub}}$  describes the changes in energy due to sublimation, i.e. the loss of mass due to very high particle temperatures, which is a result of high internal energy. The energy required to reach sublimation temperatures varies depending on the soot optical properties and the laser wavelength used. Using a laser with a wavelength of 1064 nm, sublimation often occurs for a fluence larger than 0.15 J/cm<sup>2</sup> [31], but depends strongly on the absorption properties of the soot particles. For example, nascent soot particles require more energy to reach sublimation temperatures compared to more mature particles, see Paper II, where it was shown that nascent particles are more transparent than the more graphitized and mature particles. The concepts of mass and energy balance can also be depicted as shown in Fig. 4.3. For more detailed information regarding the different terms in the mass-energy balance equation, see for example [76].

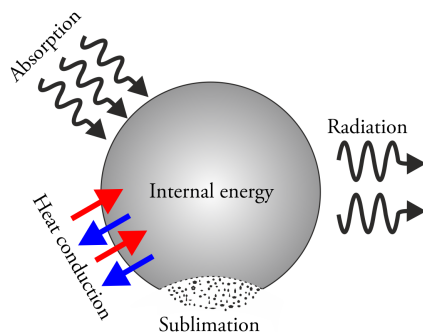


**Figure 4.3**

The physical mechanisms in the LII process including absorption, radiation, heat conduction, and sublimation.

The laser-induced incandescence signal is only approximately proportional to the soot volume fraction, and does not result in quantitative soot volume fraction data without being calibrated with a secondary technique. Extinction measurements have often been performed simultaneously as LII measurements in order to calibrate the LII signals to soot volume fractions. Laser-induced incandescence has been used in work related to Papers II, V, VI and VII. In the work presented in Paper II, time-resolved measurements were conducted in combination with elastic light scattering. Two-dimensional LII measurements were presented in Papers V, VI and VII. In these papers, the LII signal was calibrated to soot volume fractions using extinction.

#### 4.2.1 Laser Profiles and Fluence Curves

The laser-induced incandescence signal from soot is highly dependent on the incident laser energy, or laser fluence (energy per unit area), and on the spatial profile of the used laser beam. It is therefore of importance to investigate the LII signal response as a function of laser fluence, i.e. to measure a fluence curve. This is performed to ensure that a suitable laser energy is used for the intended measurements and that the laser beam has the intended profile. A typical fluence curve has a rapid initial increase in LII signal as a function of fluence, until the soot reaches sublimation temperatures. Then the signal can either continue to increase, plateau, or decrease with increased fluence depending on the spatial profile of the laser beam.

There are three commonly used spatial profiles for LII; the Gaussian beam, the Gaussian sheet and the top-hat profile. The different profiles can be seen in Fig. 4.4.



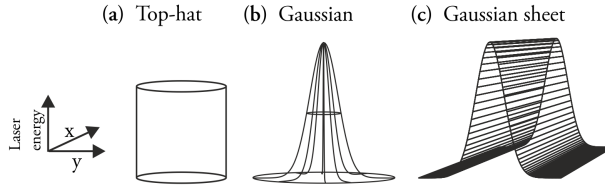


**Figure 4.4.** Three different ideal laser-profiles, (a) the top-hat profile, (b) the Gaussian beam, and (c) the Gaussian sheet

In Fig. 4.5, modelled fluence curves from the three profiles shown in Fig. 4.4 are presented. For the top-hat profile (Fig. 4.4a), which theoretically has an even laser fluence over the cross-section of the entire beam, the LII signal will increase up to a maximum value and then start to decrease. The decrease is caused by sublimation, and with increased laser energy, the sublimation will increase as the entire heated soot region will start to sublime, resulting in lower signals for higher fluence.

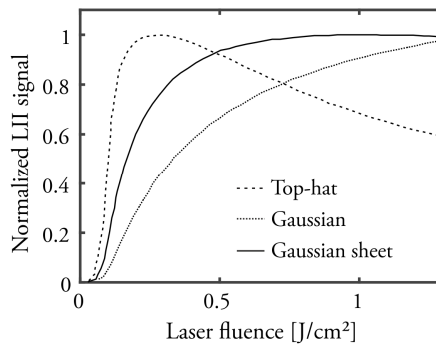


**Figure 4.5** Modelled normalized LII signals for the top-hat profile, the Gaussian beam, and the Gaussian sheet as a function of laser fluence for soot with a primary particle diameter of 100 nm. This graph has been adapted from work presented by H. Bladh and P.-E. Bengtsson in [77].

For the Gaussian beam (Fig. 4.4b), which has the highest laser fluence in the center of the profile and decreasing fluence towards the edges, the LII signal will continue to increase with increased laser fluence, even after sublimation temperatures have been reached in the center. This is a combined effect of both sublimation and increased LII signals at the edges. The increased LII signal at the edges, caused by increased fluence will, in this case, result in higher overall LII signals. The signal decrease caused by sublimation in the center of the beam profile is smaller than the increase in signal at the edges. The overall LII signal will therefore continue to increase with increased fluence for a laser beam with a Gaussian beam profile.

For the Gaussian sheet (Fig. 4.4c), which has constant fluence in one direction and a Gaussian profile in the opposite direction, there will be a combined effect of what occurred for the top-hat profile and the Gaussian beam. This combination will lead to a fluence curve that approximately reaches a plateau, i.e. giving an LII signal which is approximately independent on laser fluence after the initial signal increase. An advantage of using a laser fluence on this so-called plateau during measurements, is that fluctuations in laser energy will barely affect the emitted LII signal. For applied measurements with only small absorption of the laser beam, the laser fluence is often still high enough to be on the plateau. However, for cases with high absorption of the laser beam, it is possible that the fluence decreases below the fluence plateau, making the soot measurements very sensitive to laser energy changes.

#### 4.2.2 Time-Resolved LII Measurements

When the laser pulses get absorbed by the soot particles leading to LII, the temperature and the LII signal increase rapidly. The reached temperature depends strongly on the absorption properties. For example, heating nascent soot particles to the same temperature as mature soot requires more laser energy, see the results presented in Paper II. When the laser pulse has passed through the flame and has been partially absorbed, the soot particles start to cool down to ambient flame temperatures. This cool-down process is strongly dependent on particle size. Larger soot particles have smaller surface-to-volume-ratios, which results in a slower cool-down process in comparison to smaller particles. In Fig. 4.6, two decay curves are shown from measurements performed in an ethylene/air flame. These curves are measured at two different heights above burner (HAB), 8 mm and 12 mm respectively, where the soot at 12 mm shows a slower decrease in LII signal. The difference seen for these two curves is mainly a size effect, as increased particle sizes are observed at higher heights above burner. Increased soot aggregation could also partially contribute to the slower cool-down process observed at higher heights [78].

Numerical models of LII, see for example [79], can be used to simulate the LII signal response for different laser energies and measurement conditions, for example, conditions found in flames. LII signal decay curves can, for example, be generated for different particle sizes. Measured curves can then be numerically fitted with modelled curves and enable particle size estimations directly from LII measurements without using combined measurements with elastic light scattering. Furthermore, if a two-color LII setup is used, i.e. measuring the LII signal at two different wavelengths or wavelength regions simultaneously, it is possible to evaluate soot particle temperatures. If temporally resolved measurements have been performed, it is also possible to evaluate the temperatures during the entire cool-down process to ambient flame temperatures using pyrometry [58, 80].

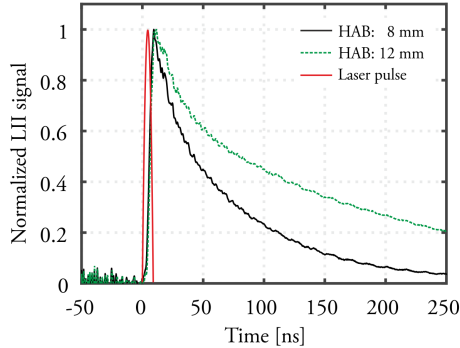


**Figure 4.6**

Two LII curves measured at two different heights above burner (8 mm and 12 mm) in a ethylene/air flame with an equivalence ratio of 2.3 on a McKenna burner.

A disadvantage of temporally resolved measurements is that the measurements are normally limited to point measurements in a specific probe volume, as cameras for two dimensional measurements are usually too slow to capture the decay curve. However, measurements in stable flames can be performed by moving or scanning the gate in attempts to measure parts of the decay curves using cameras, see for example [81]. When performing point measurements for decay curves or temperature measurements it is important that the soot in the entire measurement region is heated to the same temperature. Therefore, the top-hat laser profile is the most suitable laser profile for these measurements.

### 4.2.3 Time-Gated LII Measurements

Time-gated measurements can be performed by measuring the time-resolved LII signal and then only use a specific part of the signal, often a few nanoseconds around the peak LII signal, see Fig. 4.7a. Another option is to use a camera, where the camera gate is overlapped with the laser pulse. In Fig. 4.7b, a sketch of a camera gated measurement is shown, where the gate is overlapped with the laser pulse and peak LII signal. The camera gate is usually longer compared to the gate used in time-resolved measurement to increase the signal-to-noise ratio. Using a camera allows for two-dimensional imaging measurements, which can give instantaneous soot volume fractions for the entire cross-section of a flame in one image. Most often, time-resolved measurements are performed in fundamental studies while camera gated measurements are performed for applied studies.

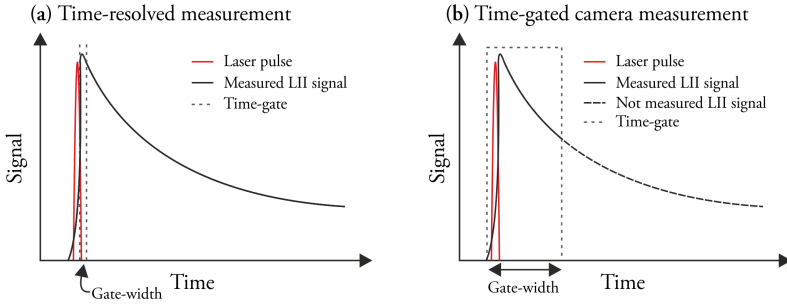


**Figure 4.7**

These graphs illustrate the differences when using time-gated measurements for (a) a temporally resolved measurement and (b) a time-gated camera measurement. The gate-widths are not to scale, but highlights that usually longer gate-widths are used for camera measurements.

#### 4.2.4 Calibration of LII signals to Soot Volume Fractions

The calibration of LII signals to soot volume fractions are based on the assumption that the LII signal is proportional to soot volume fraction. This proportionality between the LII signal and soot volume fraction has been investigated in work by Melton [82] and Bladh *et al.* [75], showing an approximate proportionality between the LII signal and the cube of the soot particle diameter. The general calibration procedure can be described in three steps.

The first step is to evaluate the soot volume fraction in the investigated flames using, for example, extinction. When LII measurements have been performed in a single point, as is most common for temporally resolved measurements, the extinction measurements and soot volume fraction have to be evaluated at the same point for calibration to be possible. When performing two-dimensional LII measurements, the extinction measurements can be performed at any position where the LII signal has been measured, which can then be used to calibrate and translate the entire LII image to soot volume fractions. For evaluation of soot volume fraction using extinction, see section 4.1. The second step is to estimate the LII signal corresponding to the evaluated soot volume fraction. The third step is to calculate a calibration factor that transfers the LII signal to soot volume fractions. This factor is valid as long as the measurements have been performed using the same measurement settings.

#### 4.2.5 Uncertainties - LII

The measurement uncertainties for laser-induced incandescence are estimated to be quite low compared to those which are inferred from the extinction measurements when evaluating soot volume fractions to calibrate LII. In this thesis, laser-induced incandescence has mainly been used for soot volume fraction measurements in combination with extinction. The uncertainty discussion in this section will therefore primarily deal with issues related to soot volume fraction measurements using LII.

The detection wavelength used for measuring LII is important for several reasons. In work by Melton *et al.* [82] results are presented indicating that the LII signal proportionality with soot volume fraction will be more valid if a long detection wavelength is used. On the other hand, with a longer detection wavelength, the background flame luminosity will increase significantly. For example, for a blackbody with a temperature of 1500 K, the Planck radiation will increase by a factor of 390 when comparing the intensity at 400 nm with the corresponding value at 600 nm. It is therefore important to select a detection wavelength that is suitable for the specific measurement case. For the LII measurements conducted using two-dimensional imaging, presented in Papers V, VI and VII, short-pass filters were used with a cut-off wavelength either at 425 nm or 450 nm. These filters were used to suppress as much background radiation as possible to increase the signal-to-noise ratio. However, for the LII measurements presented in Paper II using sensitive photomultiplier tubes, longer detection wavelengths were used, 575 nm and 684 nm.

For accurate LII measurements, it is important to subtract the remaining background luminosity. For a stable flame with a constant background, it is quite simple to measure the background luminosity between the LII signal measurements. However, for a turbulent flame, for example the flames presented in Paper VII, this approach is not possible as the background changes and other approaches were therefore necessary. In the work for Paper VII a double gate option in the camera was utilized, where a measurement of the background was performed a few microseconds before each LII measurement.

Variations in laser pulse energy can also be a problem. However, if the measurements are conducted on the fluence plateau as discussed in section 4.2.1, the problems resulting from energy variations are minimized. However, if measurements are conducted in a soot rich environment it is possible that the laser fluence decreases below the plateau, which will increase the uncertainties. Measurements below the fluence plateau could result in patterns related to energy variations in the spatial laser profile, as the LII signal is very sensitive to small energy changes below the plateau. It is also difficult to use the calibration factor from extinction measurements if LII measurements have been performed below the plateau, since the same soot volume fraction might result in different LII signals, due to laser energy changes.

### 4.3 Elastic Light Scattering (ELS)

Elastic light scattering (ELS) is a diagnostic technique where the light scattered from, for example, soot particles are measured. The theory presented in this section are based on information presented in [11, 54]. For elastic light scattering, the measured light is at the same wavelength as the incident light from the laser onto, in this case, the soot particles. Elastic light scattering can in combination with LII or extinction be used for particle size measurements. Measurements of elastic light scattering from soot are often presented as  $Q_{\nu\nu}$ -factors, where the two  $\nu$ 's indicate the polarization observed by the detector, and the polarization of the incident beam, respectively. For an assumed spherical soot particle, the  $Q_{\nu\nu}$ -factor is given by:

$$Q_{\nu\nu} = N \left( \frac{2\pi}{\lambda} \right)^4 \left( \frac{d}{2} \right)^6 \left| \frac{m^2 - 1}{m^2 + 2} \right|^2, \quad (4.9)$$

where  $N$  is the particle number concentration,  $\lambda$  is the laser wavelength,  $d$  is the primary particle diameter and  $|(m^2 - 1)/(m^2 + 2)|^2$  is a function of the complex refractive index, called  $F(m)$ , as presented in section 4.1.1. For aggregated particles, both the number of primary particles per aggregate,  $n$ , as well as the aggregate number concentration,  $N_a$ , have to be taken into account. This will result in a modified expression for the  $Q_{\nu\nu}$  factor as:

$$Q_{\nu\nu} = N_a n^2 \left( \frac{2\pi}{\lambda} \right)^4 \left( \frac{d}{2} \right)^6 \left| \frac{m^2 - 1}{m^2 + 2} \right|^2 S(q). \quad (4.10)$$

The factor  $S(q)$ , is a structure factor, describing the physical properties of the aggregate and depends on the radius of gyration,  $R_g$ , and the scattering wave vector,  $\vec{q}$ . The expression for  $S(q)$  depends on the size and magnitude of the scattering wave vector and is described for three different regimes. These are the Rayleigh, Guinier and power law regimes, and the structure factor are described in these regimes respectively by:

$$S(q) = 1 \text{ if } qR_g \ll 1, \quad (4.11a)$$

$$S(q) = 1 - \frac{q^2 R_g^2}{3} \text{ if } qR_g \lesssim 1, \quad (4.11b)$$

$$S(q) = C(qR_g)^{-D_f} \text{ if } qR_g > 1, \quad (4.11c)$$

where  $D_f$  is the fractal dimension of the aggregate,  $q$  represents the inverse of the length of the scattering vector, and  $C$  is a coefficient determining the cut-off between the power law and the Guinier regime.

Calibration of elastic light scattering measurements are often conducted using either nitrogen or air with known scattering cross-sections, which for a given temperature and pressure will give known  $Q_{vv}$ -factors, or equivalent depending on which polarization that is being calibrated. The ELS measurement from  $N_2$  or air can then be used to estimate a calibration factor used to transfer scattering data from soot to  $Q_{vv}$ -factors.

### 4.3.1 Soot Particle Size Measurements

In combination with soot volume fraction measurements, either performed by laser-induced incandescence calibrated using extinction measurements or from extinction measurements directly, ELS can be used for particle size measurements. This is possible as the soot volume fractions according to Eq. (4.4) is dependent on the cube of the primary particle diameter and the ELS signal is dependent on the primary particle diameter to the power of six. A combination of Eqs (4.4) and (4.9) will yield a theoretical expression for the primary particle diameter for a spherical non-aggregated particle, and if also combined with Eq. (4.5), an experimental expression will be given:

$$d = \sqrt[3]{\frac{Q_{vv} 2\lambda^4}{f_v} \frac{1}{3\pi^3} \frac{1}{F(m)}} = \sqrt[3]{\frac{Q_{vv} 4\lambda^3 E(m)}{K_{\text{ext}} \pi^2} \frac{1}{F(m)}} \quad (4.12)$$

For an aggregated particle the expression for the soot volume fraction has to be changed to take the parameters from aggregation into account. The number of particle concentration,  $N$ , used in Eq. (4.5) will be replaced by a factor of the number aggregate concentration,  $N_a$ , and the number of particles per aggregate,  $n$ , as given by:

$$f_v = N_a n \frac{\pi d^3}{6}. \quad (4.13)$$

If the expression for  $Q_{vv}$  for soot aggregates, Eq. (4.10), is combined with Eqs (4.5) and (4.13) both a theoretical and experimental expression for the primary particle size is given by:

$$d = \sqrt[3]{\frac{Q_{vv} 2\lambda^4}{f_v} \frac{1}{3\pi^3} \frac{1}{F(m)} \frac{1}{n} \frac{1}{S(q)}} = \sqrt[3]{\frac{Q_{vv} 4\lambda^3 E(m)}{K_{\text{ext}} \pi^2} \frac{1}{F(m)} \frac{1}{n} \frac{1}{S(q)}}. \quad (4.14)$$

From the equations presented, it is clear that the size evaluation depends on several parameters with various uncertainties. The methodology for evaluation of particle sizes, presented in the present section, has been used for particle size evaluation in Paper VI.

### 4.3.2 Uncertainties - ELS

The uncertainties for the elastic light scattering measurements are often quite low compared to those uncertainties that arise from using the measured results in evaluations of, for example, soot particle sizes. This section will therefore primarily discuss uncertainties regarding evaluation of primary particle sizes. Evaluation of particle sizes using ELS and LII will for a certain measurement positions, only result in one averaged value of the soot particle size. However, the actual particle sizes are found to have a broad distribution, which clearly can be seen in the evaluation of TEM images in Papers V and VI.

One of the uncertainties when evaluating primary particle sizes is the complex refractive index of soot, which is discussed in section 4.1.1. In both Eq. (4.12) and Eq. (4.14) it becomes clear that uncertainties in  $E(m)$  and  $F(m)$  will have a large impact on the evaluated particle sizes as a ratio of these parameters is used. For example, if an established value of  $E(m)$  is used, as discussed in section 4.1.1, there might not be a corresponding value for  $F(m)$  since  $E(m)$  could have been evaluated directly from measurements and not derived from the complex refractive index. This will result in uncertainties, as values of  $F(m)$  reported in the literature are less common than values of  $E(m)$ .

Another uncertainty is whether it is possible to evaluate particle sizes without taking the aggregation into account. The short answer is no. In work presented in Paper VI, the primary soot particle sizes were evaluated both from sampled soot analyzed in a transmission electron microscope (see section 4.4) as well as using a combination of LII and ELS. The images from transmission electron microscopy (TEM) clearly show that the soot particles had started to form aggregates already at a height above burner of 10 mm (visible soot started to appear at 4 mm HAB). The LII/ELS evaluation using Eq. (4.12) resulted in evaluated soot particles a factor 3 larger than the sizes evaluated from the TEM images. This deviation is unreasonable, and it is therefore important to take the aggregation into account.

If aggregation is taken into account, two additional parameters come into the evaluation: an average value of the number of primary particles per aggregate, and the structure factor. The primary particle diameter is proportional the cube root of these parameters, which means that the effect on the particle size will be smaller than the uncertainty in the specific parameter.

To estimate an average value of the number of primary particles per aggregate, soot samples from flames have to be evaluated, for example using TEM. This process is extremely time consuming as will be discussed in section 4.4.1. Furthermore, if



evaluation of particle sizes should be performed at multiple heights above burner, then soot samples are needed from all heights of interest, as the number of particles per aggregate may change with height. The increased number of samples will increase the evaluation time significantly; it is therefore extremely time-consuming to estimate this parameter with high accuracy.

The structure factor has according to Eq. (4.11) a maximum value of 1, which occurs if scattering in the Rayleigh regime is assumed. Using a structure factor of 1, means that the particle sizes may be underestimated. In work by Reimann *et al.* [83], they investigated similar flames as the one presented in Papers V and VI, and they present experimental values of  $S(q)$  between approximately 0.75 and 1. If these values applied to our case it could infer a bias towards underestimated particle sizes by up to 10 %.

To conclude this section, it is clear there are large uncertainties in particle size evaluation and by only using ELS together with LII, it can sometimes be hard to know what assumptions can be made. Optical techniques can still be utilized in applied measurements, also when a secondary technique, such as TEM, can not be applied if the uncertainties have been evaluated in a well-known environment beforehand.

## 4.4 Transmission Electron Microscopy (TEM)

Transmission electron microscopy (TEM) is a technique where an electron beam passes through a sample and creates an image based on the transmitted intensity. A transmission electron microscope has the possibility to observe much smaller structures compared to normal light based microscopes, as the electrons have a very short de Broglie wavelength [84]. For soot diagnostics, TEM can be used for primary particle size evaluation, aggregate size measurements and, also for retrieving the fractal dimension of aggregates [85] on soot sampled using a probe.

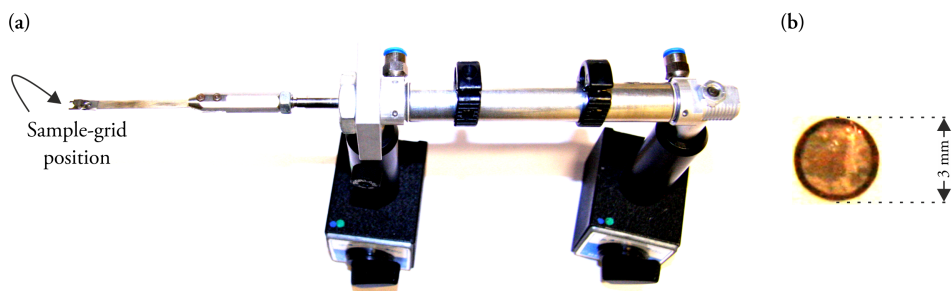
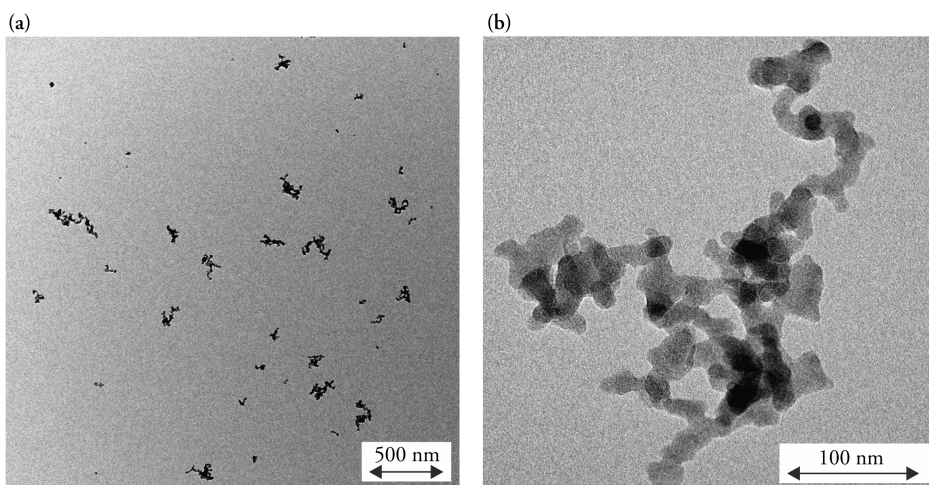


Figure 4.8

Images of (a) the pneumatic probe for soot sampling on TEM grids and (b) an enlargement of a carbon-coated TEM sample grid.

To sample soot for TEM analysis, suitable sample grids are needed. Carbon-coated copper grids can be used for soot sampling and an image of one of these grids can be seen in Fig. 4.8b. A pneumatic probe has been used for controlled soot sampling for the samples collected for TEM imaging presented in Papers V and VI, this probe can be seen in Fig. 4.8a. The pneumatic probe used in these experiments allows for extraction of samples with specific residence times inside the flame and can be accurately controlled from 100 ms and up. The soot is collected on the copper grids based on thermophoresis. This system can also be used for the sampling of cold soot from the miniCAST soot-generator.

The soot samples collected for Papers V and VI have been evaluated in a TEM microscope (FEI Tecnai Spirit BioTWIN), with a maximum magnification factor of 300,000. This magnification is good enough for evaluating soot particle sizes. However, to be able to see the inner structures of the soot particles, a TEM-microscope capable of a larger magnification factor is needed. The images retrieved from the TEM microscope include a scale bar to enable size measurements. In Fig. 4.9, two TEM images are shown, one overview image showing several soot aggregates and one image of a magnified soot aggregate.



**Figure 4.9**

Two typical TEM images of soot, one overview image of several soot aggregates in (a) and one image of a single soot aggregate in (b).

The evaluation of, for example, soot particle sizes can then be performed on the given images. This can either be performed by manually or by an automated program, and for the work presented in Papers V and VI, the analysis of TEM images were performed manually.

#### 4.4.1 Uncertainties - TEM

Soot is sampled by inserting a probe into the flame at around 100 ms. This means that the method is an intrusive way of measuring on soot compared to using laser diagnostics, since the probe will perturb the flame. Inserting a sample grid into a flame will lead to uncertainties in what soot has been collected, as soot may not only be collected inside the flame, with contributions also from the flame edge. The vertical spatial resolution is neither as good nor as accurate as laser measurements, since the probe is mechanically inserted and might vibrate during insertion, which may cause soot sampling at unintended heights above burner. These experimental uncertainties are hard to avoid, and can therefore be said to an inherent part of the sampling technique.

The uncertainties caused by the specific TEM microscope will not be discussed here, but the microscope most likely has some uncertainties in the magnification and given scale factor. When performing sampling and retrieving images for evaluation, one of the largest uncertainties comes from not having a large enough statistical data set. For evaluation of primary particle sizes, it is relatively easy to get a large statistical data set, as one soot aggregate includes many primary particles. However, particles from many aggregates need to be evaluated as the primary particles size distribution in one aggregate may not represent the overall size distribution. For the number of primary particles per aggregate it is much more time consuming and difficult to retrieve a good statistical data set. The uncertainties here relate to two different problems, firstly, it is hard to know whether the sampled data is representing the actual spread of aggregates in the flame and if the probability for an aggregate to stick to the TEM grid is size dependent. Secondly, the selected samples for evaluation also have to represent the distribution, which might be hard when aggregates for evaluation are selected manually when operating the TEM microscope.

Evaluation of primary particle sizes can be performed either by hand or by using a computer program based on image analysis. In the work presented in Papers V and VI, the soot particle sizes were evaluated by hand, i.e. two opposite edges of each primary particle were determined by hand and then evaluated to particle diameter in a computer program. This method comes with the uncertainty that the edges have to be determined by the user, which can be difficult as the particles in an aggregate are not always clearly defined. Furthermore, this method assumes the particles to be spherical. During the preparation of Paper VI, the TEM images of some cases were evaluated twice to gain knowledge on how much the particle sizes differed between the two evaluation rounds to estimate the uncertainty in the evaluation routine. Differences of a few percent were found when doing the manual evaluation twice. This does not mean that an automated system will evaluate the particle sizes with a better accuracy, as the threshold level for the edges has to be decided using a suitable method. However, repetitive analysis by an automated program should yield the same result for a given image.



# Chapter 5      Optical Arrangements and Experimental Equipment

In this chapter typical optical arrangements for extinction measurements, laser-induced incandescence (LII) and elastic light scattering (ELS) will be presented. Furthermore, key components such as lasers and detectors used in the experiments leading to this thesis will be presented. For details regarding a specific setup used for individual measurement, see the paper(s) where these measurements have been presented.

## 5.1 Extinction Measurements

The setup used for extinction measurements consists mainly of a laser system using a diode laser, two detectors (photodiodes), and some additional optical components. Two typical setups used for extinction measurements are presented in Fig. 5.1.

The highly divergent laser beam emitted from a laser diode is first collimated with an aspherical lens placed just a few millimeters from the laser diode. The beam is then divided using a beam-splitter, where one of the laser beams is directed onto a photodiode measuring a reference intensity. The second laser beam is directed through the absorbing soot region and then onto a photodiode measuring the transmitted light intensity.

For the setup shown in Fig. 5.1a, a lens is placed prior to the beam-splitter in order to achieve high spatial resolution at the location of the burner. This setup is mainly used for fundamental studies using laboratory burners. For the setup presented in Fig. 5.1b, the laser beam remains collimated when it passes through the beam-splitter cube and the absorbing region, and is focused using lenses near the detectors. This approach can advantageously be used for more applied large-scale measurements, as longer beam paths can be used and the spatial resolution is not critical. Furthermore, the lens placed after the absorbing region reduces the effects of beam steering caused by temperature gradients inside the large-scale systems.

The laser system was controlled by a LabVIEW program using a data-acquisition (DAQ) card, which also collected all signals from the photodiodes. The LabVIEW program allowed for preliminary evaluation during measurements based on user input on absorption length and value of the absorption function,  $E(m)$ . The laser diodes were

modulated on and off through signals from the LabVIEW program and the DAQ-card, enabling background measurements during the laser-off periods. If several lasers were used simultaneously, as for the work presented in Paper IV and [47] (Paper R-IV), the LabVIEW program was set to pulse these lasers intermittently with off periods in between. This made sure that the lasers would not overlap in time and that measurements of flame background could be performed.

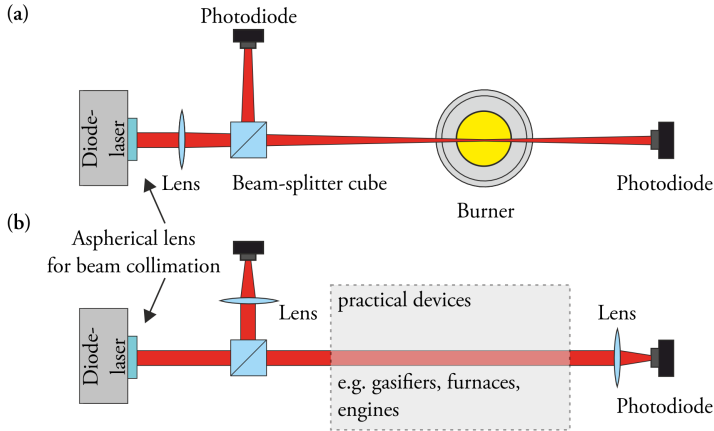


**Figure 5.1.** Two typical setups used for extinction measurements. The setup presented in (a) was used for more fundamental studies where high spatial resolution is required, while the setup in (b) was used for more applied measurements.

### 5.1.1 Diode Laser System

For the performed extinction measurements, a diode-laser system was used. Diode lasers can advantageously be used as they are available at various wavelengths, are relatively cheap, and are easy to handle due to their small size. A typical transistor outline (TO)-can diode laser has a diameter of either 3.8, 5.6 or 9.5 mm, and two typical laser diodes of this type can be seen in Fig. 5.2, along with a diode-pumped solid state (DPSS) laser.

For a stable operation of the diode lasers a constant and controlled temperature is essential. The diodes were mounted in a temperature controlled mount (Thorlabs TCLDM9) connected to temperature and current controllers (Thorlabs TED200C and LDC205C). The laser diodes used can be found in a wavelength range from 405 nm to 1064 nm with output power from 10 mW to 1400 mW. The laser diodes used are presented in Table 5.1.



**Figure 5.2**

Three different laser diodes, the first one from the left is a 9.5 mm TO-can diode laser, the second one is a 5.6 mm TO-can laser, and the third one is a diode-pumped solid state (DPSS) laser with an output of 532 nm.

**Table 5.1**

The diode lasers used for the extinction measurements presented in Papers I – VII.

Wavelength [nm]	Power [mW]	Model	Manufacturer/Supplier	Used in:
405	20	DL4146-101S	Sanyo	Paper I
450	1400	LD-450-1400MG	Roithner LaserTechnik	Paper IV
532	10	DJ532-10	Thorlabs	Paper I
635	15	SDL-7501-G1	SDL	Paper I
655	10	QL65F6SA	Roithner LaserTechnik	Paper I
670	10	QL67F6SA	Roithner LaserTechnik	Paper I
685	30	QL68I6SA	Roithner LaserTechnik	Paper I
690	30	HL6738MG	Hitachi	Paper III
780	10	L780P010	Thorlabs	Paper I
808	10	L808P010	Thorlabs	Paper I, VII
808	500	ADL-80V03TL	Thorlabs	Paper IV
850	10	L850P010	Thorlabs	Paper I, V, VI
904	10	L904P010	Thorlabs	Paper I
980	10	L980P010	Thorlabs	Paper I
1064	10	QLD-1060-10S	QPhotonics	Paper I

### 5.1.2 Photodiodes and Data Collection

Photodiodes were used as detectors for the extinction measurements. Primarily silicon photodiodes (Thorlabs PDA100-EC) were used in combination with most diode lasers, presented in Table 5.1. The silicon photodiodes were used mainly because of their broad wavelength range, 340 nm to 1100 nm, for the detection, and large active area (100 mm<sup>2</sup>). It was found that measurements with the longest wavelengths, i.e. 980 nm and 1064 nm, were not as stable as the measurements performed using shorter wavelengths. It was speculated that these problems were caused by potential heating of the photodiodes due to flame radiation, and the very steep sensitivity curve found for wavelengths longer than 950 nm for the silicon photodiodes.

To achieve accurate measurements for the wavelengths above 950 nm, germanium photodiodes (Thorlabs PDA50B-EC), sensitive in the wavelength range 800 nm to 1800 nm, were used. However, a disadvantage of using these photodiodes was the

significantly smaller active area ( $19.6 \text{ mm}^2$ ) compared to the silicon photodiodes ( $100 \text{ mm}^2$ ).

Two different data-acquisition cards from National Instruments (NI USB-6251 BNC and NI USB-6363), were used for collecting the signals from the photodiodes, depending on application. For acquiring signals for data collection, the specifications for the two DAQ-cards are quite similar. However, for control of lasers, they can give output signals for up to either two or four lasers simultaneously.

## 5.2 LII and ELS Measurements

The setups used for LII and ELS are quite similar and will be described together in this section. A typical setup for LII or ELS consist of a pulsed laser, a beam attenuator, beam shaping optics, a soot source, and a detector. Two setups used for LII and ELS are shown in Fig. 5.3, one setup mostly used for fundamental studies and one setup used primarily for more practical applications.

For the measurements presented in this thesis, an Nd:YAG laser (Quantel Brilliant B) operating either at the fundamental wavelength (1064 nm) or the second harmonic (532 nm) have been used. The most commonly used laser wavelength for heating soot when performing LII measurements is 1064 nm, as this will prevent fluorescence from polycyclic aromatic hydrocarbons, which strongly absorb light in the UV and visible wavelength regimes. Sometimes, often in more practical situations, it is considered advantageous to use 532 nm, due to alignment and safety issues with the invisible 1064 nm beam. The use of 532 nm would, however, infer some uncertainties due to fluorescence from PAHs. For elastic light scattering, 532 nm is the most commonly used wavelength and has also been used for the ELS measurements presented in this thesis.

The measurement setup presented in Fig. 5.3a, is mainly used for temporally resolved LII or ELS measurements, often for more fundamental studies. In this setup the laser beam passes through a beam attenuator, which is used to change the laser energy without changing the laser beam properties. The center part of the beam is cut-out in order to create an approximate top-hat profile. The beam is then relay imaged using lenses to create a top-hat profile of suitable size at the location of the burner. The induced signal or scattering is then detected using photomultipliers. In Fig. 5.3a, the LII signal is detected at two different wavelengths simultaneously, often referred to as two-color laser-induced incandescence [58, 86], which would allow for soot temperature evaluation using pyrometry. To ascertain that the beam has its intended top-hat profile at the position of the burner, the laser beam was imaged on the CCD-chip of a laser beam profiler (DataRay WinCamD UCD15) to make sure that the energy variations in the spatial profile of the laser beam are acceptable.



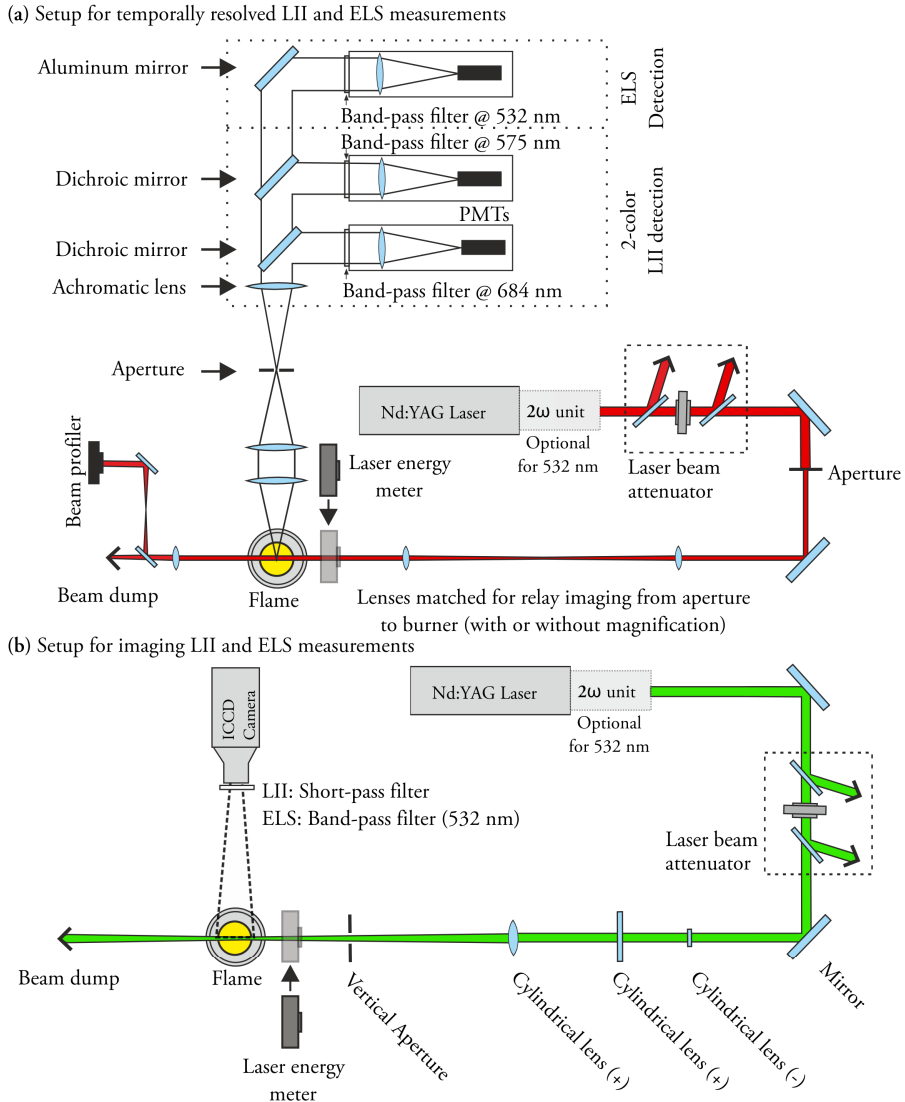


**Figure 5.3**  
 Typical experimental setups for LII and ELS measurements. The setup shown in (a) is for temporally resolved measurements using PMTs and the setup shown in (b) is for two-dimensional imaging LII or ELS using an intensified CCD camera.

The other setup, presented in Fig. 5.3b, is a setup for two-dimensional imaging LII or ELS and is often used in more applied measurements. The setup can of course also be used for fundamental research if two-dimensional soot data is needed. The laser beam, either with a wavelength of 532 nm or 1064 nm, passes through a beam attenuator.

The beam is then formed to a Gaussian sheet using, in this case, three lenses and an aperture. The aperture is used to cut-out a center part of the vertically stretched beam in order to get an as homogeneous laser energy profile in the vertical direction as possible. The induced signal or scattering is then collected by an intensified CCD camera (Princeton Instruments PIMAX IV) using a camera lens and suitable filters, i.e. short-pass filter for LII and a band-pass filter at 532 nm for ELS.

The setup used for the laser-induced incandescence measurement can advantageously be combined with an extinction measurement setup. The extinction measurements can then be used for calibration of LII, as discussed in section 4.2.4.

# Chapter 6      Results

In this chapter, the main results from the measurements presented in Paper I – VII will be shown along with some related results. In the first part, section 6.1, measurements conducted in laboratory flames to investigate soot optical properties using extinction measurements and laser-induced incandescence (LII) will be presented. Some applied measurements using extinction measurements in practical devices will be presented in section 6.2. In section 6.3, results from using LII, elastic light scattering (ELS), and extinction to investigate the effect of metal salts on the soot formation will be presented. In the final section of this chapter, section 6.4, results from measurements conducted in a large-scale oxy-fuel furnace using combined LII and extinction measurements will be shown.

For the evaluation of soot volume fractions, the absorption function has for all measurements presented in this chapter been set to a value of  $E(m) = 0.35$ . This value has been selected based on measurements for mature soot in premixed flames, see Paper II or [58].

## 6.1 Investigation of Soot Optical Properties

The results presented in this section primarily focus on fundamental measurements in laboratory flames for determination of soot optical properties presented in Paper I and Paper II.

In order to be able to perform accurate measurements on soot to evaluate, for example, soot volume fractions, particle sizes, and soot temperatures using optical diagnostics, it is of great importance to know how the optical properties behave related to soot maturity and as a function of wavelength. Extinction measurements using twelve different wavelengths in the wavelength range from 405 nm to 1064 nm have been performed at several heights above burner (HAB) in two flames on the McKenna burner. In Fig. 6.1, the measured transmission using extinction are shown for the flames with equivalence ratio,  $\phi = 2.1$ , and  $\phi = 2.3$ .

Extinction is, as discussed in section 4.1, a technique primarily used for soot volume fraction measurements. For Rayleigh theory, the absorption coefficient, or extinction coefficient if the scattering contribution can be neglected, is inversely proportional to wavelength. A result of the inverse proportionality can be seen in Fig. 6.1, where the beams with longer wavelengths have a higher transmission through the flames, i.e. are

attenuated less. If assuming that scattering is negligible and that the absorption coefficient from Rayleigh theory is valid, the only optical property that could have a wavelength dependence when evaluating soot volume fractions is the complex refractive index, and consequently the absorption function  $E(m)$ , i.e.  $m(\lambda)$  and  $E(m, \lambda)$ . This means that the measured extinction coefficient will be proportional to wavelength according to:

$$K_{\text{ext}} \propto \frac{1}{\lambda} E(m, \lambda). \quad (6.1)$$

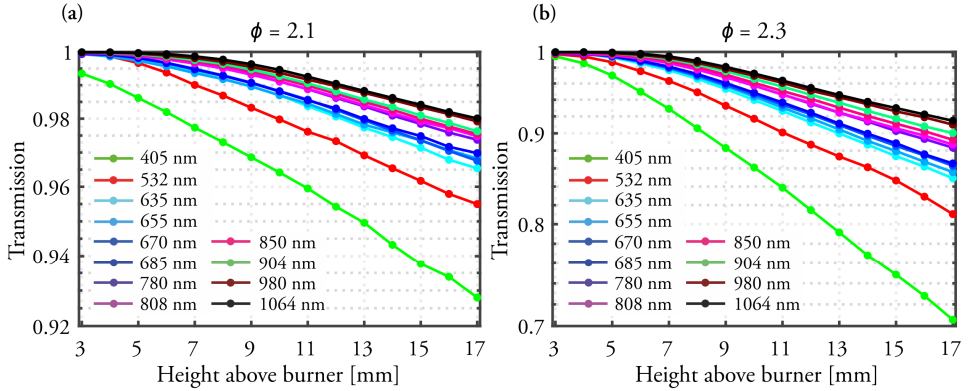


**Figure 6.1** Transmission as a function of height above burner for extinction measurements conducted at twelve wavelengths on two flames on a McKenna burner with equivalence ratios, (a)  $\phi = 2.1$ , and (b)  $\phi = 2.3$ .

The wavelength dependence of the absorption function can also be expressed by the coefficient,  $\alpha$ . This coefficient is sometimes referred to as the dispersion coefficient/exponent [87], however, in the atmospheric research community it is often referred to as the absorption Ångström exponent [88]. The absorption function can with this coefficient be expressed as:

$$E(m, \alpha) = \frac{1}{\lambda^{\alpha-1}} E(m)_{\text{ref}}, \quad (6.2)$$

where  $E(m)_{\text{ref}}$  is the value of the absorption function at a reference wavelength and the exponent  $\alpha$  expresses the deviation from the theoretical inverse relation to wavelength according to Rayleigh theory. If Eqs (6.1) and (6.2) are combined the wavelength dependence of the extinction coefficient can be described as:

$$K_{\text{ext}} \propto \lambda^{-\alpha}. \quad (6.3)$$

From the extinction measurements, shown in Fig. 6.1, extinction coefficients were evaluated for all the investigated wavelengths. Based on this evaluation and Eq. (6.3), dispersion coefficients could be estimated at multiple heights above the burner surface for both flames. In Figs 6.2a and 6.2b, dispersion coefficients as a function of height above burner (5 mm to 17 mm) are presented. The dispersion coefficients have been evaluated for two different wavelength intervals, either with all lasers with wavelengths between 405 nm and 1064 nm, or the between 685 nm and 1064 nm.

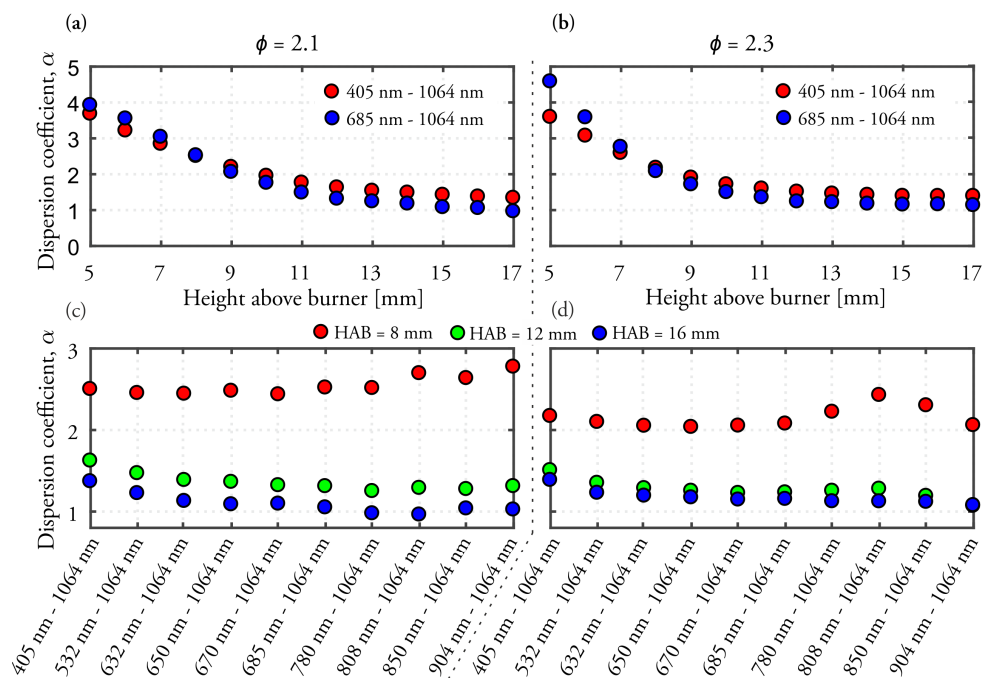


**Figure 6.2**

Dispersion coefficients evaluated using extinction measurements in flames on a McKenna burner. In (a) and (b) the dispersion coefficients are presented as a function of height above burner evaluated using two different wavelength intervals (405 nm – 1064 nm and 685 nm – 1064 nm) for  $\phi = 2.1$  and  $\phi = 2.3$ , respectively. In (c) and (d) the dispersion coefficients have been evaluated at three different HAB to show differences in the dispersion coefficients depending on wavelength interval for equivalence ratio  $\phi = 2.1$  and  $\phi = 2.3$ , respectively.

The evaluation results in dispersion coefficients approaching unity for increased height above burner for both flames. However, for dispersion coefficients evaluated in the full wavelength interval, the dispersion coefficient levels off at a value of approximately 1.3, compared to a value of approximately 1 for the coefficients evaluated in the range 685 nm to 1064 nm. An  $\alpha$ -value of 1 means that the extinction follows the expected wavelength dependence from Rayleigh theory, i.e.  $K_{\text{ext}} \propto \lambda^{-1}$ . The value of the dispersion coefficient of around 1 found for more mature soot in both flames, is reached

at a lower HAB for the  $\phi = 2.3$  flame, which can be associated with a faster soot formation rate. The increased value for the full interval is most likely a result from additional absorption by PAHs, which has been found to absorb strongly in the UV and visible wavelength regimes [35, 89], which therefore does not affect the results in the same way when evaluating using wavelengths longer than 685 nm.

Evaluation of dispersion coefficients in the interval 405 nm to 1064 nm is assumed to include the combined wavelength dependence information for both PAHs and soot particles. For the smaller interval, 685 nm to 1064 nm, the assumption is that only the wavelength dependence of soot is evaluated. This could mean that when these two evaluations show the same value, the wavelength dependence of the PAHs and the soot particles at that specific height are the same. For the flame with an equivalence ratio of 2.1, this occurs at an HAB of 8 mm. The dispersion coefficient at lower HAB (less than 8 mm) is larger for the soot particles than the combined for both soot and PAHs, most likely a result of the PAHs wavelength dependence decreases the overall wavelength dependence. The opposite effect is seen at higher HAB (higher than 8 mm), where the dispersion coefficient approaches 1 for the soot particles, but are shown to be slightly higher when the PAHs are also included.

In an attempt to show how different wavelengths affect the evaluated dispersion coefficients, the evaluation has been performed at three heights above burner. Initially all wavelengths were included in the evaluation. Evaluations then followed where one wavelength was excluded at a time until the evaluation only included the three longest wavelengths. These results are shown in Figs 6.2c and 6.2d. The evaluations performed for the intervals 685 nm to 1064 nm and 780 to 1064 nm, show approximately the same values for the wavelength dependence, and should only vary for changed soot maturity, as discussed above.

The results for the flame with  $\phi = 2.1$ , presented in Fig. 6.2c, show several effects that can be discussed. Firstly, for the less mature particles found at an HAB of 8 mm, the dispersion coefficients are as expected, quite high, but are fairly constant independent of included wavelengths. The main reason for this could be that both soot and PAHs have the same wavelength dependence at this HAB, and inclusion of shorter wavelengths which are absorbed by PAHs therefore does not affect the evaluation. For the measurements evaluated at 12 mm and 16 mm HAB, a decrease can be seen for the evaluated dispersion coefficients when removing the shorter wavelengths. This is expected, as absorption in the PAH molecules here would increase the overall evaluated wavelength dependence. The reason for the slight increase seen for the evaluation at a height above burner of 8 mm, especially visible for the  $\phi = 2.3$  flame for the interval 808 nm to 1064 nm, is unknown, but could be related to absorption in, for example, water.

Based on the fact that PAHs absorb strongly in the UV and visible regimes, which was shown both here and in Paper I, wavelengths longer than about 700 nm should be used when evaluating soot volume fractions using extinction measurements. Another result from the measurements is that the absorption function,  $E(m)$ , only shows a small

dependence on wavelength for more mature particles, i.e. particles at higher heights above burner.

Extinction measurements have also been performed in soot from the miniCAST soot-generator. A four-laser approach was utilized with lasers operating at wavelengths of 405 nm, 655 nm, 850 nm, and 1064 nm. These lasers were operated simultaneously, and modulated on and off intermittently in order to evaluate dispersion coefficients for soot with different properties. The setup used for these measurements can be seen in Fig. 6.3a. The settings for the different operation points (OP) can be seen in section 3.2.2 and Table 3.1. The soot from the miniCAST has either been transported directly to the measurement cell, or passed through either a thermodenuder (250 °C) or a thermodenuder and an oven (500 °C).

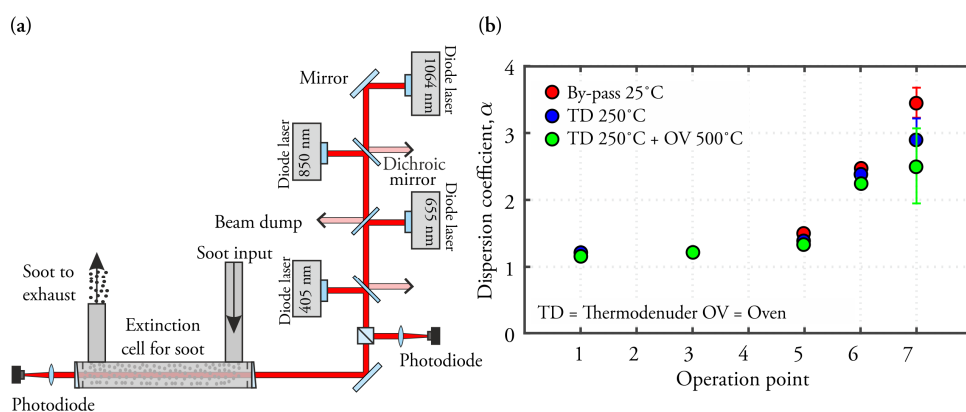


**Figure 6.3**

Extinction measurements of miniCAST soot performed using a four-wavelength approach. The setup is presented in (a) and dispersion coefficients for different operating points of soot are presented in (b). Measurements have also been performed on miniCAST soot that has passed through either a thermodenuder or an oven.

The results, presented in Fig. 6.3b, show for the more mature particles, associated with operation points 1, 3 and 5, values that approach 1, which are similar to the results found at higher heights above burner in flames. For OP6 and OP7, the results are more similar to those for less mature soot particles, at lower HAB in flames. The values for the mature particles in Fig. 6.3b are more similar to those found measuring using the entire wavelength interval presented in Figs 6.2a and 6.2b. This is most likely a result of absorption by PAHs for the beam with a wavelength of 405 nm. When the soot particles, especially for OP7, has passed through either the thermodenuder or both the thermodenuder and the oven before the extinction cell, the dispersion coefficients are lowered, which could be a result related to organics being removed when the soot particles are heated to either 250 °C or 500 °C. Nevertheless, the heating of the soot particle does not decrease the dispersion coefficient to a value close to 1, which indicates that the soot core shows a larger wavelength dependence. The extinction measurements

presented here is part of a larger study of soot produced by the miniCAST using various techniques, where extinction was one of the techniques. The work is presented in [47] (Paper R-IV).

$$\phi = 2.1$$

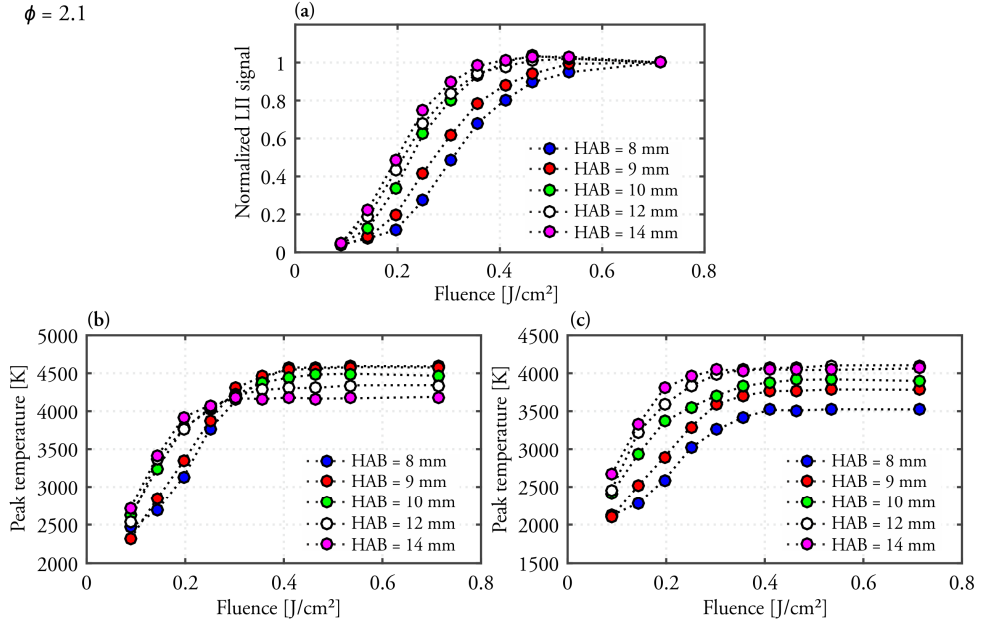


**Figure 6.4**

Measurements using time-resolved LII at different heights above burner in a flame with  $\phi = 2.1$  on a McKenna burner. A fluence curve measured at 684 nm showing normalized LII signal as a function of fluence is shown in (a). Evaluated soot peak temperatures as a function of fluence are shown in (b), assuming a wavelength independent absorption function. In (c), peak temperatures as a function of fluence are shown using a wavelength dependent  $E(m)$  based on the dispersion coefficients shown in Fig. 6.2a. The time-resolved measurements have been evaluated during 0.8 ns around the peak LII signal for both 684 nm and 575 nm.

The wavelength dependence of the absorption properties shown by the dispersion coefficients are also important for LII measurements, for example, when evaluating soot peak temperatures using laser-induced incandescence and pyrometry, see section 4.2. In Paper II, it was shown that the dispersion coefficients have a large impact on the results. In Fig. 6.4a fluence curves for five different HABs are shown. The presented fluence curves have been measured at 684 nm, and can if combined with simultaneous measurements at 575 nm be used to evaluate soot peak temperatures using pyrometry. The evaluation of temperature can be performed using the Wien approximation for blackbody radiation, resulting in an expression for temperature given by:

$$T = \frac{hc}{k_b} \left( \frac{1}{\lambda_2} - \frac{1}{\lambda_1} \right) / \ln \left( \frac{I_1 E(m, \lambda_2)}{I_2 E(m, \lambda_1)} \left( \frac{\lambda_1}{\lambda_2} \right)^6 \right), \quad (6.4)$$



where,  $I_1$  and  $I_2$  represent the intensity of the LII signal measured, calibrated to the sensitivity of the detector for each wavelength, respectively. The constants  $h$  and  $k_b$  are the Planck constant and the Boltzmann constant. If the ratio between the absorption function at the two different wavelengths were replaced by Eq. (6.2), it would yield the following expression for temperature:

$$T = \frac{hc}{k_b} \left( \frac{1}{\lambda_2} - \frac{1}{\lambda_1} \right) / \ln \left( \frac{I_1 \lambda_1^{\alpha-1} E(m)_{\text{ref}}}{I_2 \lambda_2^{\alpha-1} E(m)_{\text{ref}}} \left( \frac{\lambda_1}{\lambda_2} \right)^6 \right). \quad (6.5)$$

By assuming a wavelength-independent absorption function, i.e.  $\alpha = 1$ , for all heights above burner, when calculating the soot peak temperatures, the results presented in Fig. 6.4b are obtained. The results show rapidly increasing temperatures as a function of laser fluence until a plateau is reached due to sublimation. This plateau is reached at lower laser fluence for the more mature particles at higher HAB, which is expected as more mature particles are more effective at absorbing laser light, see for example Paper II or [31]. The reached temperature intervals are in agreement with previously reported values [90-92]. However, the less mature particles, at lower HAB, reaches higher temperatures compared to the soot at higher HAB. This is quite unexpected as graphite has been found to have a very high sublimation temperature, and soot found at higher heights above burner is more graphitized, see section 3.1.1.

If the dispersion coefficients found using the extinction measurements, presented in Fig. 6.2 and Paper I, are applied for the different HABs, the soot peak temperatures change drastically, as seen in Fig. 6.4c, with differences of around 1000 K for the soot at 8 mm HAB. The temperatures presented in Fig. 6.4c, are now increasing with height above burner, as expected from a physical perspective as the soot matures and becomes more graphitized with increased HAB. Thus, accurate dispersion coefficients are crucial for evaluation of temperatures using LII and pyrometry.

## 6.2 Applied Extinction Measurements

The system used for extinction measurements for the fundamental studies, presented in section 6.1 and Paper I, has also been applied in more practical systems in order to evaluate soot volume fractions under various operating conditions.

Measurements have been performed in a heavy-duty diesel engine, presented briefly in section 3.2.3, modified to obtain optical access to the combustion chamber. The extinction measurements, were made with a diode laser operating at a wavelength of 690 nm, which was selected to avoid as much absorption from PAHs as possible, while still having a visible laser beam to ease alignment through the engine. The full measurement setup, and more details regarding the engine, can be found in Paper III.

Measurements were performed while modulating the laser on and off at a frequency of 72 kHz, which allowed for a measurement resolution of 0.1 crank angle degrees (CADs) at 1200 rpm. In Fig. 6.5, results from the engine measurements are shown when using different concentrations of oxygen in the inlet oxidizer, i.e. different degrees of EGR. The results are presented as transmitted light and as evaluated extinction coefficients, both as a function of CAD after top dead center (ATDC). The data presented in Fig. 6.5, have been averaged over 29 full (fired) cycles, and the extinction data were calibrated between injections, which was possible as injection only occurred every second full cycle. However, it was not possible to measure more than some tens cycles due to build-up of soot deposits on the windows used for optical access.

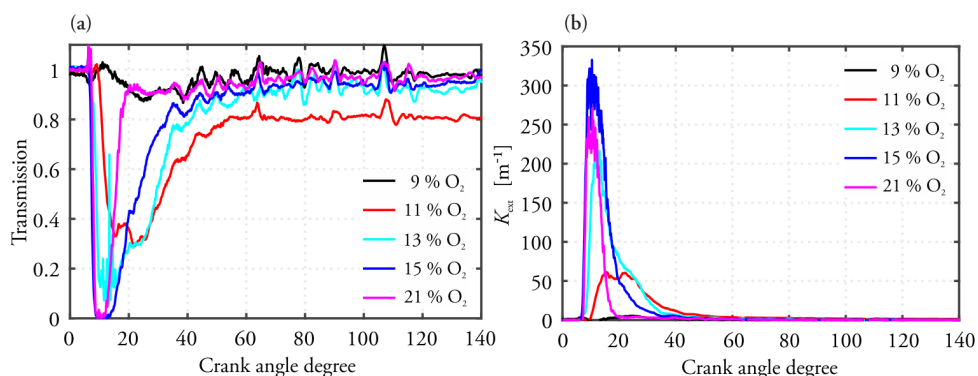


**Figure 6.5**

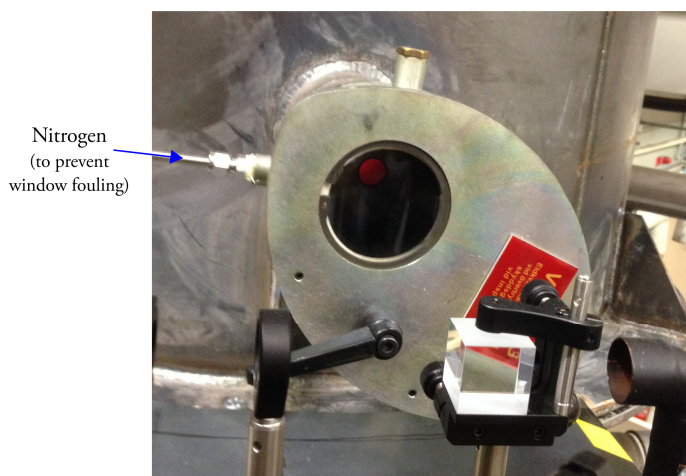
Results from the extinction measurements in the heavy-duty diesel engine for different oxygen concentrations in the inlet oxidizer. The results are presented as transmission data in (a) and as evaluated extinction coefficients in (b) based on absorption lengths corresponding to length of the combustion chamber.

In both graphs of Fig. 6.5, it is clear that after the fuel injection there is a significant increase in absorption, most likely caused by soot particles. This absorption then decreases at different rates depending on the oxygen content. For most cases, the transmission values return to the levels before injection at approximately 40 CAD ATDC. However, the data for 11 % oxygen still shows significant soot concentration throughout the presented interval. For this case, the data does not return to the values found before injection until the exhaust valve is opened, which occurs late in the cycle. The transmission data presented in Fig. 6.5a, shows decreased transmission with increased oxygen concentration. However, as can be noted for the 15 % and 21 % concentrations of oxygen, the transmission reaches zero a few CADs after injection, which makes it difficult to draw conclusions. The uncertainties in these measurements are much larger than extinction measurements performed in laboratory flames. The uncertainty problems are especially clear at CADs from 40 to 140 where the transmission results vary significantly, which could be a result from vibrating and moving parts inherent to an engine.

For the evaluated extinction coefficients, see Fig. 6.5b, using Beer Lambert law (Eq. 4.1), larger variations are found between the cases. Furthermore, the length of the combustion chamber, which varies during a cycle, has been taken into account when evaluating the extinction coefficient. A problem with evaluating the extinction coefficient, is that the absorption length used only takes the length of the combustion chamber into account, and not the actual length where soot is present.

An estimation of the oxidation rate was also performed based on the data from the extinction measurement, i.e. change in extinction versus CAD. These results were compared to data from heat release curves, and was found to show similar trends. This means that the heat release curves could possibly be used as a diagnostic tool for the soot oxidation rates.

Extinction measurements have also been conducted in a large-scale entrained-flow gasifier operating at atmospheric conditions, see section 3.2.3 and Paper IV. Extinction measurements were conducted using two overlapped laser beams originating from laser diodes with wavelengths 450 nm and 808 nm. The measurements were conducted through measurement ports and one of these can be seen in Fig. 6.6.



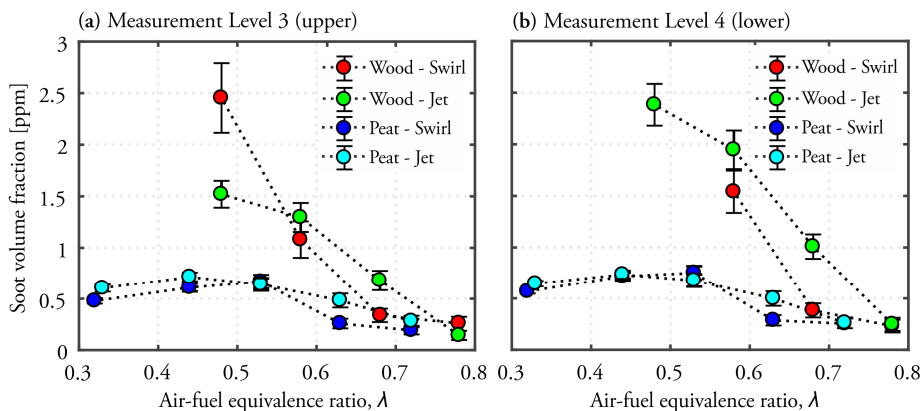
**Figure 6.6**

Image of one of the measurement ports with optical access on the atmospheric entrained-flow gasifier used in the work presented in Paper IV.

The purpose of these measurements were to investigate how the soot concentration varied for different operating conditions using two different fuels, powder from stem wood and peat powder. Furthermore, two different burners were used in the investigation, where one creates a rotating flow inside the gasifier and is referred to as the swirl burner. The other burner has the fuel and air inlets parallel to the burner axis and is referred to as the jet burner. Measurements were also conducted at two different

vertical levels (measurement level 3 and 4 in Fig. 3.9) in the gasifier in order to investigate how the soot concentration changed downstream in the gasifier.

Soot volume fractions were evaluated from the data obtained for wavelength 808 nm. The laser with a wavelength of 450 nm, was used with the purpose to estimate the scattering contribution to the extinction, for more details regarding this estimation see Paper IV or section 4.1.2. In Fig. 6.7, soot volume fractions as a function of the air-fuel equivalence ratio are shown for the different measurement cases presented above. Some data points for the lower air-fuel equivalence ratios are missing due to high concentrations of soot, which resulted in no evaluable transmission of the laser beams through the gasifier.



**Figure 6.7**

Soot volume fractions as a function of air-fuel equivalence ratios measured using extinction in an atmospheric entrained-flow gasifier. Two different fuels (stem wood and peat), and two different burners (swirl and jet) have been used and the measurements have been conducted at two different measurement levels. Measurements at measurement level 3 level 4 are shown (a) and (b), respectively.

A comparison between the two measurement levels, presented in Figs 6.7a and 6.7b respectively, separated by 45 cm, show the same trends. The differences in measured soot volume fractions between the two burners are small when using peat as the fuel. For wood powder, the use of the swirl burner seems to result in more soot. This is not entirely noticeable for measurement level 4 since a data point is missing at  $\lambda = 0.5$  for wood powder using the jet burner. However, a missing data point means that the concentration for this point is actually higher, compared to the measured value using the swirl burner, since it could not be measured. Higher soot concentrations for the jet burner also at  $\lambda = 0.5$ , is in agreement with the results presented for measurement level 3. For the jet burner, using wood as the fuel, there is a clear increase in soot volume fractions downstream in the reactor, i.e. higher soot volume fraction at level 4 compared to level 3. This could be a result from ongoing soot formation. The same effect is not

seen for the swirl burner, most likely due to that the swirl burner leads to increased mixing and a faster reaction process.

The most significant difference for these measurements is observed between the two fuels. Using peat powder results in much lower soot concentrations compared to using powder from stem wood. There could be multiple reasons for this effect, but the main reason is most likely the difference in volatile concentration in the fuels, where peat powder has a much lower volatile concentration, see the fuel analysis shown in Table 1 in Paper IV. Another plausible explanation is the fact that the peat powder has a larger concentration of ash components, which include various metal compounds. Some metal additives have been shown to decrease the soot concentration in flames [13, 14, 93].

### 6.3 Influence of Metal Salts on Soot Formation

The large variations in soot concentrations found when using different fuels in gasification could, to some extent, be a result of metal compounds affecting the soot formation. However, in large-scale systems it is difficult to isolate specific causes of such variations. A small-scale investigation in a lab-scale burner, where salts were seeded into flames to study the effect on soot formation, was therefore designed. The salts investigated were selected based on metals commonly found in the ash components of the bio-fuel feedstock. The full investigation is presented in Paper V and Paper VI.

The effects of seven metal salts: sodium chloride (NaCl), magnesium chloride (MgCl<sub>2</sub>), aluminum chloride (AlCl<sub>3</sub>), potassium chloride (KCl), calcium chloride (CaCl<sub>2</sub>), iron chloride (FeCl<sub>3</sub>), and zinc chloride (ZnCl<sub>2</sub>), on the soot formation were investigated. The salts were dissolved in water at three different concentrations (0.01 M, 0.1 M and 1 M), and were seeded into an ethylene/air flame with an equivalence ratio,  $\phi = 2.6$ , on the modified PerkinElmer burner, described in section 3.2.1.

Measurements were conducted using imaging laser-induced incandescence and elastic light scattering, see section 4.2 and 4.3. In order to calibrate the measured LII data to soot volume fractions, extinction measurements (see section 4.1) were conducted at 10 mm HAB simultaneously as the LII measurements were performed for all cases. Extinction measurements were performed using a laser-diode operating at a wavelength of 850 nm. The typical setups used for LII, ELS and extinction can be found in Chapter 5, for the actual combined setup, see Paper V or Paper VI. The measurements for each salt were conducted from the lowest to highest concentration, and each measurement was repeated three times. For each measurement 100 single-shot images were collected and averaged. In Fig. 6.8, LII and ELS signals, normalized using measurements conducted in a reference flame seeded only with water, are presented. The results in Fig. 6.8 show how different concentrations of the salts affect

the LII and ELS measurements. Each data point is an average at 10 mm HAB for the three measurements conducted.

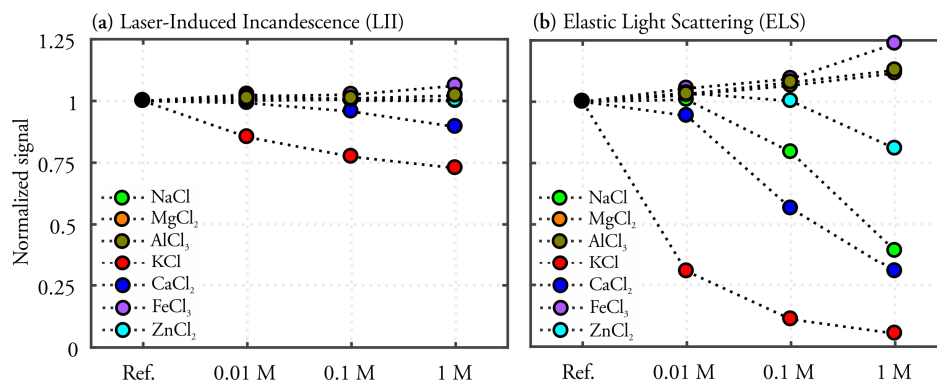


**Figure 6.8** Measurements using laser-induced incandescence (a) and elastic light scattering (b) showing signals normalized against the reference flame for the different salts and concentrations. Data shown are for HAB = 10 mm.

The results in Fig. 6.8 show a clear reduction in LII signal for the flame seeded with KCl. The flame seeded with the highest concentration of CaCl<sub>2</sub> also showed a significant reduction of LII signal. A reduction in LII signal implies that the soot volume fraction has been reduced since the LII signal is approximately proportional to soot volume fraction, as discussed in section 4.2. The other salts are only resulting in minor changes of the LII signal. However, for the ELS measurements, clear decreases in signal can be observed for potassium chloride, calcium chloride, sodium chloride and zinc chloride, in order of significance. For the other salts slight increases can be seen, which is most likely a result of scattering from the salt particles themselves. The reason for the larger effect found for the ELS measurements is due the ELS signal being much more sensitive to changes in particle size, as discussed in relation to Fig. 6.11. The LII signal is proportional to the cube of primary particle diameter and the ELS is proportional to the primary particle diameter to the power of six, see Eqs (4.4) and (4.9).

The largest effect on soot formation seems to occur with the salts containing either alkali or alkaline earth metals, especially potassium chloride. This effect has also been seen in, for example [13, 93-95], why the focus will be on these salts in the forthcoming presentation of results. In Fig. 6.9, soot volume fractions (LII) and  $Q_{vv}$ -factors (ELS) are shown as a function of height above burner for NaCl, MgCl<sub>2</sub>, KCl, and CaCl<sub>2</sub>. The soot volume fraction has been evaluated using Eq. (4.4) with  $E(m) = 0.35$  for all heights above burner. The use of a constant  $E(m)$  for all heights might introduce uncertainties for lower HABs, where the soot volume fractions may be underestimated, as discussed in section 4.1.1 and 4.1.2.

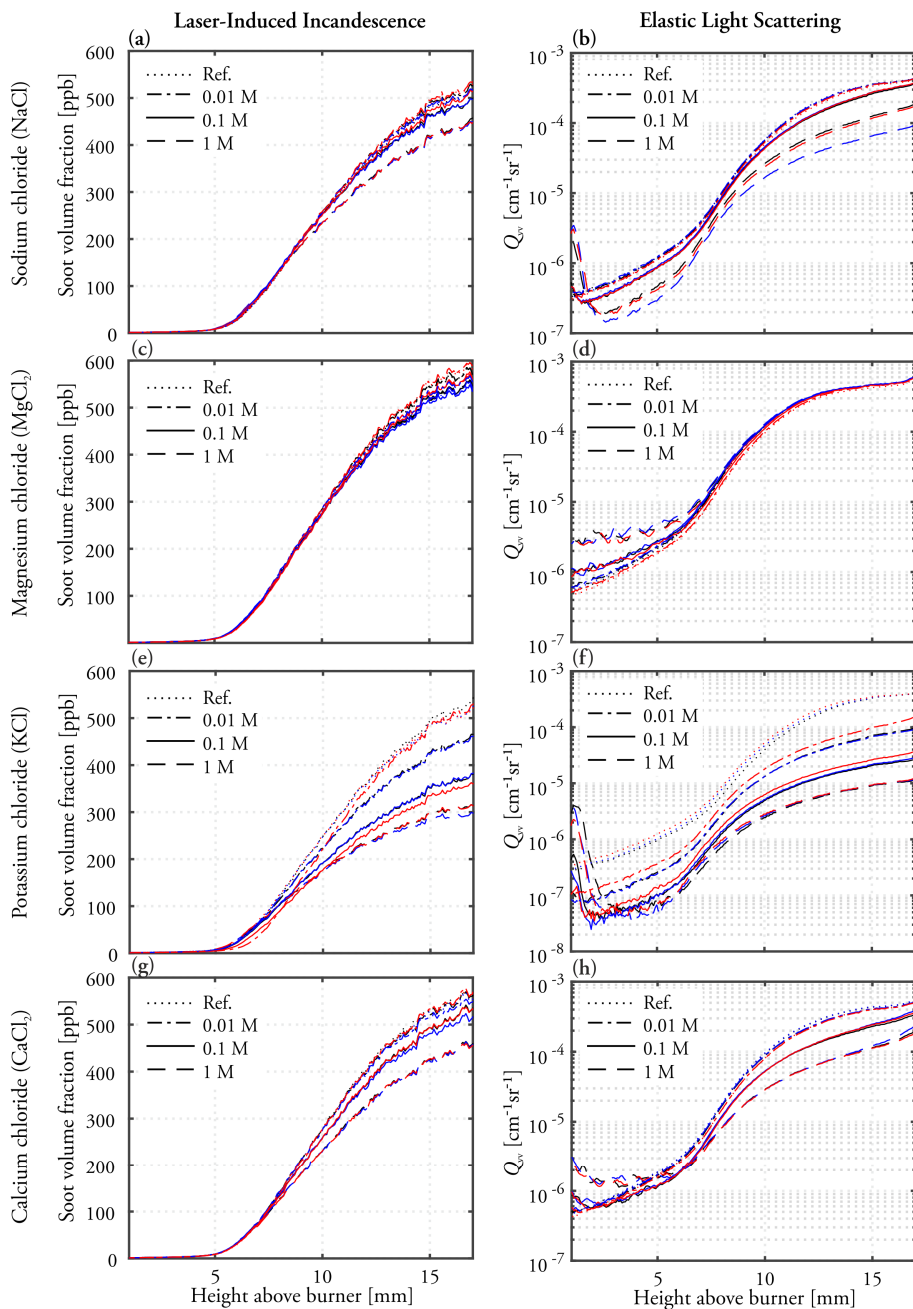


**Figure 6.9**

Soot volume fraction and elastic light scattering signals as  $Q_w$  factors as a function of HAB for NaCl (a, b), MgCl<sub>2</sub> (c, d), KCl (e, f), and CaCl<sub>2</sub> (g, h). For each concentration, three averaged measurements are shown in black, blue and red.

For potassium chloride, calcium chloride, and sodium chloride, presented in Fig. 6.9, the soot volume fraction remains unaffected until an HAB of approximately 8 mm. After 8 mm, there is a decrease in soot volume fractions for increased salt concentration in the soot growth region (8 – 17 mm HAB). However, the effect of seeding magnesium chloride into the flame is negligible. It can therefore not be said that all alkali and alkaline earth metals do affect the soot formation, at least not for magnesium when seeded in as magnesium chloride in this situation.

For the elastic light scattering measurements presented in Fig. 6.9, the effect can be separated into three parts. The first, and largest effect for the soot particles can be seen in the soot growth region. The effect at a higher HAB is largest for potassium chloride, where a clear decrease in  $Q_w$ -factors can be seen for increased salt concentrations. The effects for  $\text{CaCl}_2$  and  $\text{NaCl}$  are quite similar, with decreasing scattering for increased concentration of salts, while magnesium chloride does not show any effect at higher heights above burner.

The second effect in the pre-reaction region, below 2 mm, shows increased scattering signal for increased for all salts along with increased concentrations presented in Fig. 6.9. This is most likely a result from the scattering of the salt particles themselves. For  $\text{KCl}$  and  $\text{NaCl}$ , this additional scattering seems to disappear after the salt particles have passed through the reaction zone, which is probably because the salt particles dissociate at the high temperatures associated with the reaction zone. However, for both  $\text{CaCl}_2$  and  $\text{MgCl}_2$ , the excess scattering from the salt particles persists through to the pre-soot region (2-4 mm HAB), indicating that the salt particles did not dissociate.

The third effect, clearly seen in the pre-soot region, is that the additives of potassium and sodium decrease the scattering significantly before the visible soot starts to appear at 4 mm HAB. This effect indicates that the soot precursors are affected by the additives. For calcium chloride, there appears to be a combined effect of both excess scattering from the calcium chloride particles and an overall decrease in scattering from the soot particles formed, see Fig. 6.9h.

Soot sampling was performed in the flames at a height above burner of 10 mm, in order to be able to evaluate soot particle sizes, and to get an idea of how the soot particles were structured, for example if they were aggregated in soot clusters. The sampling was performed for the reference flame and the flames seeded with the highest concentration (1 M) of the salts. These soot samples were investigated using transmission electron microscopy (TEM), see section 4.4. Images of soot aggregates from this investigation can be seen in Fig. 6.10 for the reference flame and the flames seeded with  $\text{NaCl}$ ,  $\text{KCl}$ , and  $\text{CaCl}_2$ . In Fig. 6.10, statistical information about the primary particle sizes evaluated from the images of several aggregates taken from each flame are shown. The largest effect is, as expected, found for the potassium chloride seeded flame, where the particle sizes are found to be significantly smaller compared to the reference flame. The calcium chloride seeded flame also showed slightly smaller soot primary particle sizes, while the sodium chloride seeded flame was only marginally affected when it came to particle size at 10 mm HAB.



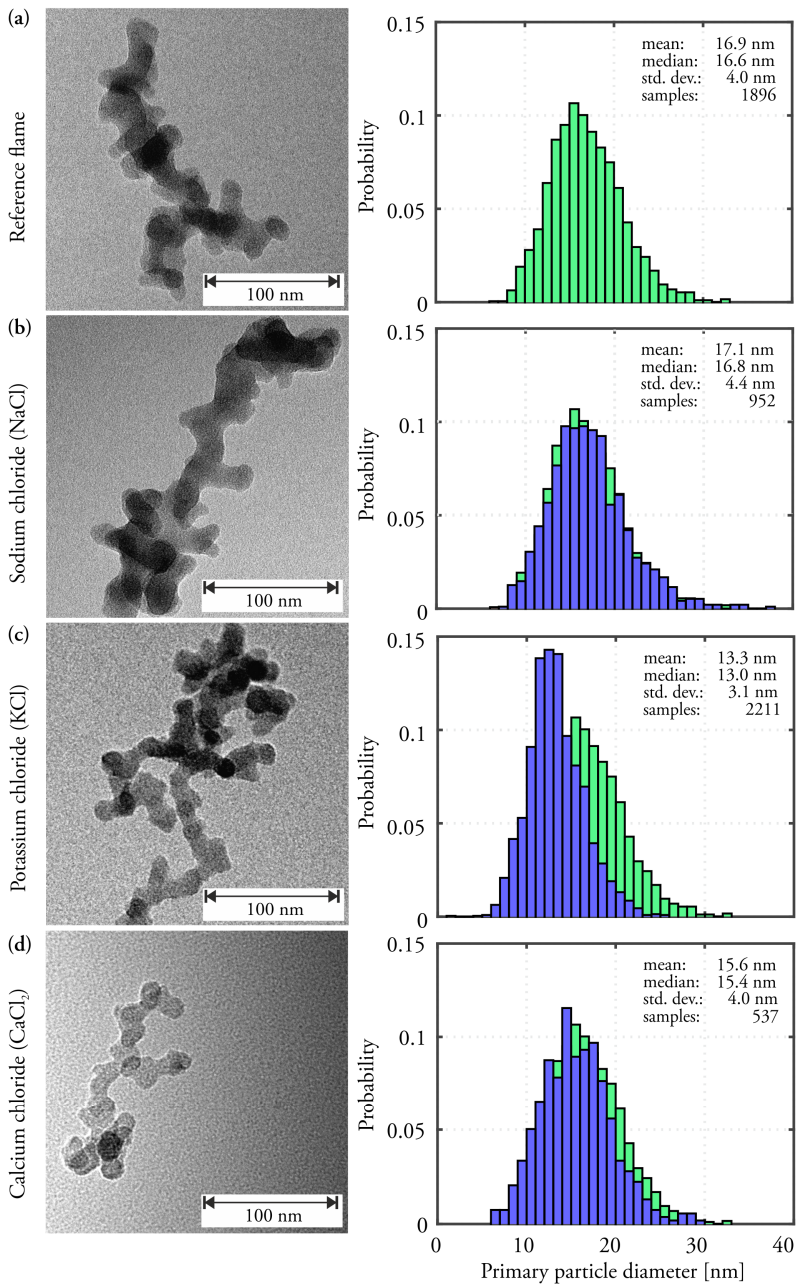


**Figure 6.10** Soot aggregates from TEM measurements for the reference flame (a) and the flames seeded with sodium chloride (b), potassium chloride (c), and calcium chloride (d). Statistical information of evaluated particle sizes can be seen in the second column for each of these flames. The graph for the reference flame is placed in the background of the statistical information graphs of the other salts for comparison.

Soot primary particle sizes can also be evaluated from the LII and ELS data shown in Fig. 6.9, by using the theory presented in section 4.3.1. From the TEM images it is clear that the soot particles have formed aggregates, at least for heights above burner of 10 mm and higher. Therefore, Eq. (4.14) has been used for the primary particle evaluation, as this takes the aggregation into account. However, evaluation of particle sizes requires knowledge of several parameters; both  $E(m)$  and  $F(m)$ , the number of particles per aggregate,  $n$ , and the structure factor,  $S(q)$ , which includes the radius of gyration,  $R_g$ . In the present evaluation of particle sizes,  $E(m)$  was set to 0.35, and  $F(m)$  was calculated to 0.217, based on a value of the complex refractive used for particle size evaluations in [83]. The structure factor was assumed to be 1, and the number of particles per aggregate was assumed to be 20 for all cases and HABs.

In Fig. 6.11, evaluated soot primary particle sizes are shown as a function of height above burner for the flames seeded with sodium chloride, potassium chloride, and calcium chloride. Based on the results from the TEM measurements shown in Fig. 6.10, it is expected that the evaluation of particle sizes from LII and ELS should show the largest effect for KCl, which it does. The results at 10 mm HAB, for the KCl seeded flame, are in fairly good agreement with the results presented using TEM in Fig. 6.10. For the flames seeded with NaCl and CaCl<sub>2</sub>, the results from the optical measurements show larger changes with increased salt concentration than the corresponding changes from the TEM image evaluation. Since there is a large difference in the laser measurements for NaCl, and only small size differences in the TEM images, it is plausible that the sodium chloride particles mainly affect how the particles aggregate, and to minor extent the soot growth process.

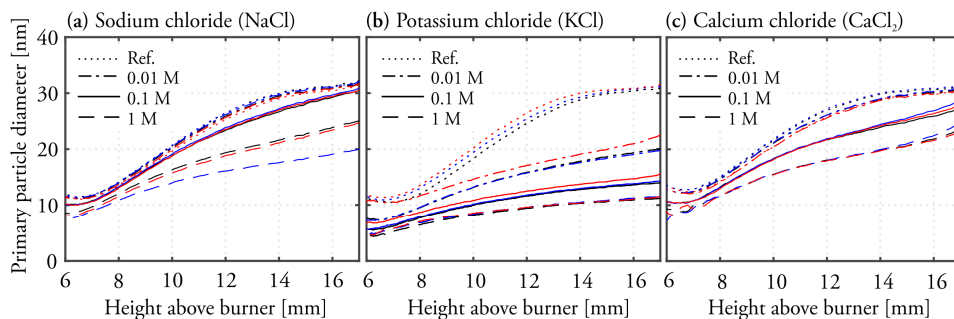


**Figure 6.11**

Evaluated soot primary particle sizes as a function of height above burner for the flames seeded with the three concentrations of (a) sodium chloride, (b) potassium chloride, and (c) calcium chloride. Three averaged measurements are shown for each case in black, blue, and red.

The deviations found between the measurements using LII and ELS compared to the evaluation of TEM images are most likely a result of the limited knowledge on parameter values used in the interpretation of the optical measurement data. For

example, retrieving good statistical data on the number of particles per aggregate for each HAB is very difficult and time consuming. Furthermore, by using a constant value for the number of particles per aggregate for all HAB, the particle sizes may be underestimated and overestimated at a lower and a higher HAB, respectively, since the soot aggregates tend to grow with increased height above burner. For a more detailed discussion regarding the uncertainties, see the discussion in section 4.3.2 and Paper VI.

## 6.4 Applied Measurements Using LII and Extinction

Combined laser-induced incandescence measurements for soot imaging and extinction measurements have been performed in a large-scale oxy-fuel furnace, see section 3.2.3 and Paper VII. Measurements using laser-diagnostics in oxy-fuel and in oxygen-enriched flames have previously been performed by, for example, Shaddix and Williams [96] in small-scale diffusion flames using laser-induced incandescence. Measurements in large-scale oxy-fuel systems have been performed by Stimpson *et al.* [97], where line-of-sight soot volume fraction measurements were performed. The measurements presented in this section were conducted at atmospheric conditions both in oxy-fuel mode with recirculated flu-gases, containing mainly carbon dioxide and oxygen, and using air or oxygen-enriched air as the oxidizer. The measurement cases for the different conditions are presented in Table 3.2.

For the LII measurements, a laser beam from a pulsed Nd:YAG laser was formed into a Gaussian sheet and focused inside the furnace. This beam was overlapped with the extinction laser beam in order to be able to calibrate the LII images to soot volume fractions. The calibration using extinction is based on averaged LII images and extinction measurements, and details regarding this calibration to soot volume fractions can be found in Paper VII. The extinction measurements were performed using a laser operating at 808 nm.

In Fig. 6.12, three single-shot images collected using laser-induced incandescence can be seen, and these images have been calibrated to soot volume fractions. From the images in Fig. 6.12 it is clear that there are soot structures with local high soot concentrations inside the furnace. The local soot concentration seems to depend strongly on the environment used, temperature, and mixing inside the furnace. The overall air-fuel equivalence ratio and the flow of propane are the same for all cases, which means that the total flow inside the furnace has to be decreased when increasing the oxygen content in the oxidizer. This could possibly result in less mixing between the fuel and the oxidizer, and in return result in higher soot concentrations.

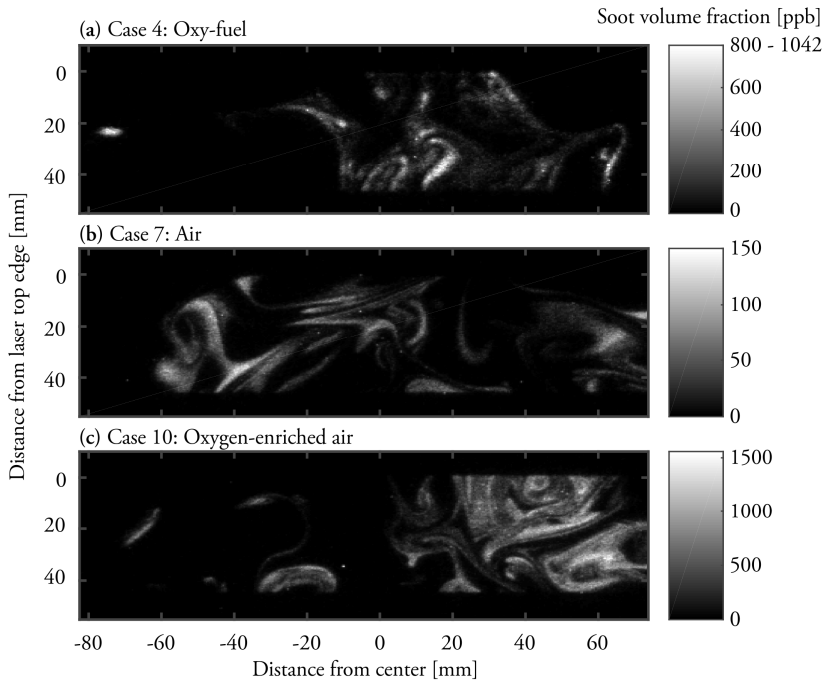


**Figure 6.12**

Single-shot images measured using laser-induced incandescence, calibrated to soot volume fraction using extinction. The images show three cases, (a) one from the oxy-fuel measurements, (b) one from the air-fed cases, (c) and one where oxygen-enriched air was used.

To compare soot concentrations for the measured cases, 500 single-shot LII images were averaged for each case and calibrated to soot volume fractions. The results from this evaluation are shown in Fig. 6.13, for data averaged at the position where the extinction laser overlapped with the LII laser. The results in Fig. 6.13 are shown in a logarithmic scale in order to clearly present the large variation in soot volume fractions found for the different cases.

For the oxy-fuel measurements presented in Fig. 6.13a, there is a strong increase in soot volume fraction as a function of oxygen content in the inlet oxidizer, which is most likely a result of both increased temperature and decreased mixing as discussed earlier. A very clear example of the mixing effect can be seen in Fig. 6.13b for the cases when air (21 %  $O_2$ ) was used. For the case where the primary oxidant register was closed, and all air passed through the secondary register, much higher soot concentrations were observed. This is a result of less mixing inside the furnace, which is a result of both smaller swirl angles in the secondary register, and that the secondary register is located further away from the central fuel pipe.

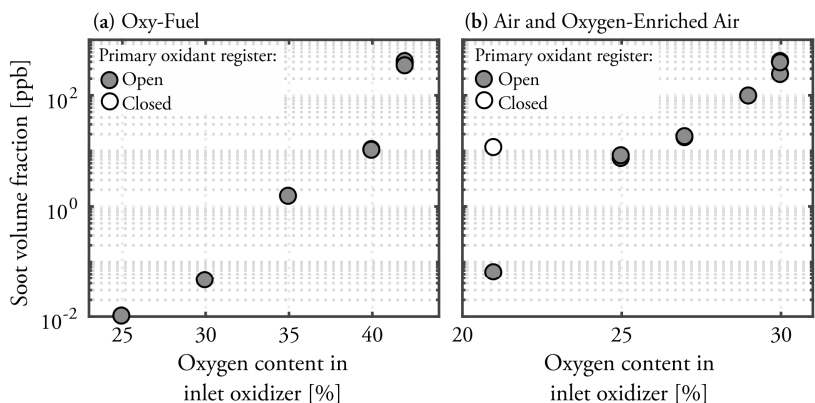


**Figure 6.13**

Measured soot volume fractions as a function of the oxygen content in the inlet oxidizer. The measurement from the oxy-fuel cases are shown in (a), while measurements from the air-fed cases and the oxygen-enriched air cases are shown in (b).

Another interesting observation that can be seen in Fig. 6.13, is that the same level of soot volume fraction is reached for a much lower oxygen content when using oxygen-enriched air, compared to the oxy-fuel cases. This is most likely a temperature effect, since the nitrogen in the air has been replaced with carbon dioxide for the oxy-fuel cases. The replacement of nitrogen with carbon dioxide will result in lower temperatures, due to the higher heat capacity of carbon dioxide.

For some of the measurement cases additives of water, potassium chloride dissolved in water, nitric oxide (NO), or sulfur dioxide (SO<sub>2</sub>) were introduced to investigate how these additives affected the soot formation in a large-scale furnace. The water and KCl<sub>(aq)</sub>, were sprayed directly onto the flames, while NO and SO<sub>2</sub> were added through the inlet oxidizer.

The results from these measurements are shown in Fig. 6.14. For the cases where water and potassium chloride solutions have been sprayed onto the flames, a clear decrease in soot volume fractions can be observed. This was seen in both cases where air and oxygen-enriched air were used. The largest effect on soot concentration seems to come from spraying water onto the flames, indicating that there is a large temperature effect causing the decrease in soot concentrations. However, adding potassium chloride causes some additional decrease, which corresponds to the trend seen for potassium additives in small-scale laboratory flames, see section 6.3. Due to increasing potassium chloride deposits on the windows during the oxy-fuel measurements, these cases could not be evaluated.

The effects of using additives of either NO or SO<sub>2</sub> are quite similar. For the oxy-fuel cases, a slight increase in soot volume fractions can be observed for these additives. However, for the cases where air has been used, the effect is the opposite with decreasing soot concentrations. The reason for this difference is unknown, however, it is plausible

that it could be a temperature effect, as there is a temperature difference when using air compared to the oxy-fuel cases.

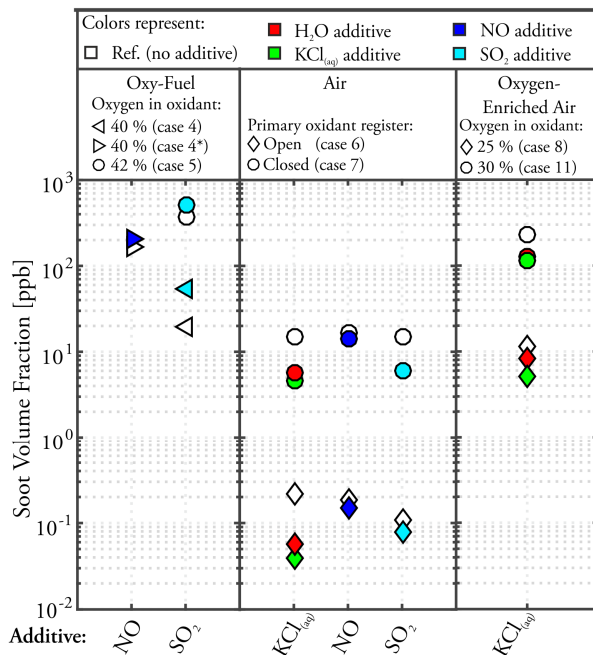


**Figure 6.14**

The effects of different additives, (KCl<sub>(aq)</sub>, H<sub>2</sub>O, NO, and SO<sub>2</sub>) for some of the investigated oxy-fuel, air and oxygen-enriched air cases. The results have been averaged from calibrated LII images. Case 4\* has the same settings as the normal case 4, however, with significant increased soot concentrations probably due to a thermal effect after running the system for a full day.

# Chapter 7

## Summary, Conclusions, and Outlook

In this chapter a summary and the most important conclusions of the conducted work will be presented. The chapter also includes a discussion regarding the impact of the performed work and future possibilities.

### 7.1 Summary and Conclusions

In the work presented in this thesis, primarily three different laser-diagnostic techniques have been used for soot diagnostics. The techniques are extinction, laser-induced incandescence (LII), and elastic light scattering (ELS), and have been used in fundamental measurements in small-scale burners, as well as in applied measurements in large-scale systems.

In the work presented in Paper I and Paper II, optical properties of soot have been investigated for soot produced in two different ethylene/air flames. Extinction measurements were used to investigate the wavelength dependence of the produced soot and this work is presented in Paper I. Twelve different lasers were used with wavelengths in the range of 405 nm to 1064 nm. For the more mature particles at higher heights above burner, the results showed a wavelength dependence in extinction which agrees well with Rayleigh theory for absorbing and isotropic spheres, i.e. a  $\lambda^{-1}$ -dependence. For nascent soot particles, a much stronger wavelength dependence was found. The results also suggested that wavelengths longer than 700 nm should be used when performing extinction measurements of soot, since soot precursors such as polycyclic aromatic hydrocarbons (PAHs) absorb strongly in the UV and visible wavelength regimes.

Combined measurements using laser-induced incandescence and elastic light scattering were presented in Paper II, in order to investigate how soot maturity changed the properties of the soot particles. The results show indications that mature soot is more effective in absorbing light compared to nascent soot, based on decreasing sublimation threshold fluence for increasing height above burner, and fluence curves shifted towards higher fluences. Furthermore, soot peak temperatures measured using a two-color LII setup and pyrometry, were investigated. The results showed significant

differences in evaluated temperatures depending on whether the wavelength dependence of the optical properties, presented in Paper I, was taken into account or not. The differences in evaluated temperature were largest for the nascent particles, for which also the wavelength dependence is the strongest. After the estimated wavelength dependence was applied, increased peak temperatures as a function of height above burner was found, which is expected as graphite has a very high sublimation temperature, and soot has been found to become more graphitized during the ageing process.

The setup used for extinction measurements has also been applied in practical devices, such as a heavy-duty diesel engine and an entrained-flow gasifier. The measurements from the engine are presented in Paper III, where the effect on the soot oxidation for different concentrations of oxygen in the oxidizer were investigated. The results showed decreasing soot oxidation rates with decreased oxygen concentration based on the extinction measurements, which correlate quite well with late cycle heat-release rates. This means that heat-release analysis could possibly be a diagnostic tool for soot oxidation rates.

The extinction measurements conducted in an atmospheric entrained-flow gasifier are presented in Paper IV. The purpose of these measurements was to evaluate soot concentrations for different operating conditions using two different types of fuel and two burners. The fuels used were powder from stem wood and powder from peat, which were burnt at air-fuel equivalence ratios in the range from approximately  $\lambda = 0.7$  to  $\lambda = 0.3$ . The main results from these measurements were that significant differences in soot concentrations, also under the same air-fuel equivalence ratio, were found depending on fuel. Peat powder resulted in considerably lower soot concentrations than wood powder, which is most likely a consequence from the peat powder containing less volatile compounds. Peat also contains more ash components, including metal compounds, for which some has been found to significantly reduce the soot formation.

In large-scale devices, it is often not possible to investigate a specific cause of an observed effect. Therefore, a study where seven different metal salts ( $\text{NaCl}$ ,  $\text{MgCl}_2$ ,  $\text{AlCl}_3$ ,  $\text{KCl}$ ,  $\text{CaCl}_2$ ,  $\text{FeCl}_3$ ,  $\text{ZnCl}_2$ ) were seeded into a small-scale laboratory burner was performed in order to evaluate their effect on the soot formation. For this study, LII, ELS, and extinction measurements were performed in order to evaluate both soot volume fractions and particle sizes. The results presented in Paper V and Paper VI, showed a significant reduction of soot volume fractions for additives of potassium chloride, calcium chloride, and sodium chloride, in order of significance. Soot primary particle sizes were estimated both from sampling inside the flames evaluated using transmission electron microscopy, and from the LII and ELS measurements. For potassium chloride additives, both TEM and the LII/ELS measurements showed significant reductions in particle sizes. However, for additives of  $\text{NaCl}$  and  $\text{CaCl}_2$ , the evaluated particle sizes using TEM only showed minor differences, while the laser measurements indicated larger changes. This suggests that the additives also affect the



soot aggregation, as changes in aggregation were not taken into account in the evaluation.

Soot measurements were also performed in a large-scale (100 kW<sub>th</sub>) oxy-fuel test furnace, where the soot concentration has been evaluated using imaging LII and extinction for various conditions in a propane diffusion flame. The furnace was operated in oxy-fuel environments but also using air and oxygen-enriched air. The results from these measurements showed significant increases in soot concentrations when increasing the oxygen concentration in both oxy-fuel and the oxygen-enriched air cases. This is mainly due to a mixing effect, since the flow inside the furnace is decreased for increased oxygen concentrations in order to maintain a constant air-fuel equivalence ratio. An interesting observation in the results is that similar soot concentrations are achieved for much lower oxygen concentrations for the oxygen-enriched air compared to the oxy-fuel results. This is most likely a temperature effect since the nitrogen has been replaced with recirculated carbon dioxide in the oxy-fuel cases. For some cases, potassium chloride, sulfur dioxide, or nitric oxide were added to the flames. Additives of potassium chloride solution, sprayed directly onto the flames showed decreased soot concentrations. However, the main cause of the decrease seems to arise from lower temperature caused by the water. Sulfur dioxide and nitric oxide showed different results depending on environment, with increasing and decreasing soot concentrations in oxy-fuel and air-fed flames, respectively. The imaging results of the soot volume fractions from these measurements can, for example, be used when modelling the radiative heat transfer in furnaces.

## 7.2 Outlook

The most important findings for the LII community in general are the wavelength dependence and soot maturity work presented in Paper I and Paper II, since these results may have a large impact on evaluation of soot concentrations, particle sizes, and soot temperatures. Soot has, as discussed, been found to be one of the main contributors to global warming, which makes the fundamental work of investigating optical properties important. These properties are of most importance for the atmospheric research community, since optical properties of soot are needed for improving climate models.

For the work related to biomass gasification, the measurements using extinction in the entrained-flow gasifier were important in order to get an idea of what difficulties can be faced when performing such measurements. For example, the problems with very high absorption for some cases, has to be considered if LII or ELS were to be applied in these systems in the future.

The main contribution to the gasification community in this thesis is the impact of some metal salts on the soot formation presented in Papers V and VI. However, this

study should be continued in other types of flames, for example diffusion flames, as the fuel and oxidizer in gasifiers are rarely premixed. It would also be interesting to dope biomass particles with, for example, potassium chloride to see how this affects the formation of soot and PAHs, both in small and large-scale systems.

For lab-scale measurements, initial tests of a system for controlled seeding of biomass particles using a particle disperser have been performed. This allows for measurements in biomass-flames using several techniques in controlled small-scale environments. In such measurements, laser-induced incandescence could be used for soot concentration measurements, while laser-induced fluorescence for measurements could be used for measurements of polycyclic aromatic hydrocarbons (which could be a proxy for tars), and elastic light scattering for measurements of the biomass particles. Combinations of these techniques could be valuable for studies of conversion of biomass fuel with simultaneous measurements of PAHs along with the formation of soot.

# Chapter 8 Bibliography

- [1] IEA, *Key world energy statistics 2017*, International Energy Agency, 2017.
- [2] Energimyndigheten, *Energiläget 2017*, The Swedish Energy Agency, 2017.
- [3] IPCC, *Climate Change 2007: The Physical Science Basis, Summary for Policymakers*, Intergovernmental Panel on Climate Change, 2007.
- [4] IPCC, Summary for Policymakers in: *Climate Change 2013: The Physical Science Basis. Contribution of Working Group I to the Fifth Assessment Report of the Intergovernmental Panel on Climate Change*, T.F. Stocker, D. Qin, G.-K. Plattner, M. Tignor, S.K. Allen, J. Boschung, A. Nauels, Y. Xia, V. Bex, P.M. Midgley (Eds.), Cambridge University Press, Cambridge, United Kingdom and New York, NY, USA, 2013.
- [5] WHO, *Health Aspects of Air Pollution with Particulate Matter, Ozone and Nitrogen Dioxide*, Report No. EUR/03/5042688, Bonn, Germany, 13–15 January, 2003.
- [6] T.C. Bond, S.J. Doherty, D.W. Fahey, P.M. Forster, et al., *Bounding the role of black carbon in the climate system: A scientific assessment*, *Journal of Geophysical Research: Atmospheres* **118**: pp. 5380-5552 (2013)
- [7] Naturvårdsverket, *Utsläpp av sot till luft*. (cited: 2018-01-09). Available from: <http://www.naturvardsverket.se/Sa-mar-miljon/Statistik-A-O/Sot-utslapp-till-luft/>
- [8] A.D. Abid, N. Heinz, E.D. Tolmachoff, D.J. Phares, C.S. Campbell, H. Wang, *On evolution of particle size distribution functions of incipient soot in premixed ethylene-oxygen-argon flames*, *Combustion and Flame* **154**: pp. 775-788 (2008)
- [9] C. Schulz, B.F. Kock, M. Hofmann, H. Michelsen, S. Will, B. Bougie, R. Suntz, G. Smallwood, *Laser-induced incandescence: recent trends and current questions*, *Applied Physics B* **83**: pp. 333-354 (2006)
- [10] H.A. Michelsen, C. Schulz, G.J. Smallwood, S. Will, *Laser-induced incandescence: Particulate diagnostics for combustion, atmospheric, and industrial applications*, *Progress in Energy and Combustion Science* **51**: pp. 2-48 (2015)

- [11] C.M. Sorensen, *Light scattering by fractal aggregates: A review*, *Aerosol Science and Technology* **35**: pp. 648-687 (2001)
- [12] H. Wiinikka, F. Weiland, E. Pettersson, O. Öhrman, P. Carlsson, J. Stjernberg, *Characterisation of submicron particles produced during oxygen blown entrained flow gasification of biomass*, *Combustion and Flame* **161**: pp. 1923-1934 (2014)
- [13] B.S. Haynes, H. Jander, H.G. Wagner, *The effect of metal additives on the formation of soot in premixed flames*, *Symposium (International) on Combustion* **17**: pp. 1365-1374 (1979)
- [14] J.B. Howard, W.J. Kausch Jr, *Soot control by fuel additives*, *Progress in Energy and Combustion Science* **6**: pp. 263-276 (1980)
- [15] P.A. Bonczyk, *Effects of metal additives on soot precursors and particulates in a C<sub>2</sub>H<sub>4</sub>/O<sub>2</sub>/N<sub>2</sub>/Ar premixed flame*, *Fuel* **70**: pp. 1403-1411 (1991)
- [16] T.P. Jones, W.G. Chaloner, *Fossil charcoal, its recognition and palaeoatmospheric significance*, *Palaeogeography, Palaeoclimatology, Palaeoecology* **97**: pp. 39-50 (1991)
- [17] A.C. Scott, I.J. Glasspool, *The diversification of Paleozoic fire systems and fluctuations in atmospheric oxygen concentration*, *Proceedings of the National Academy of Sciences* **103**: pp. 10861-10865 (2006)
- [18] S.R. James, R.W. Dennell, A.S. Gilbert, H.T. Lewis, et al., *Hominid Use of Fire in the Lower and Middle Pleistocene: A Review of the Evidence [and Comments and Replies]*, *Current Anthropology* **30**: pp. 1-26 (1989)
- [19] I. Glassman, *Combustion*, 4<sup>th</sup> ed., Academic Press, San Diego, 2008.
- [20] S. McAllister, J.-Y. Chen, A.C. Fernandez-Pello, *Fundamentals of Combustion Processes*, Springer, New York, 2011.
- [21] L. Zheng (Ed.), *Oxy-Fuel Combustion for Power Generation and Carbon Dioxide (CO<sub>2</sub>) Capture*, Woodhead Publishing Limited, 2011.
- [22] J. Rezaian, N.P. Cheremisinoff, *Gasification Technologies, A Primer for Engineers and Scientists*, CRC Press, Taylor & Francis Group, Boca Raton, Florida, 2005.
- [23] C. Higman, M.v.d. Burgt, *Gasification*, 2nd edition ed., Gulf Professional Publishing, 2008.
- [24] K. Qin, W. Lin, P.A. Jensen, A.D. Jensen, *High-temperature entrained flow gasification of biomass*, *Fuel* **93**: pp. 589-600 (2012)

- [25] E.M. Bulewicz, D.G. Evans, P.J. Padley, *Effect of metallic additives on soot formation processes in flames*, Symposium (International) on Combustion **15**: pp. 1461-1470 (1975)
- [26] H. Thunman, M. Seemann, T. Berdugo Vilches, J. Maric, et al., *Advanced biofuel production via gasification – lessons learned from 200 man-years of research activity with Chalmers’ research gasifier and the GoBiGas demonstration plant*, Energy Science & Engineering **6**: pp. 6-34 (2018)
- [27] Göteborgs Energi, *GoBiGas-anläggningen*. (cited: 2018-02-26). Available from: [https://gobigas.goteborgenergi.se/Svensk\\_version/Anlaggningen](https://gobigas.goteborgenergi.se/Svensk_version/Anlaggningen)
- [28] H.B. Palmer, H.F. Cullis, *The chemistry and physics of carbon*, Dekker, New York, 1965.
- [29] M.O. Andreae, A. Gelencsér, *Black carbon or brown carbon? The nature of light-absorbing carbonaceous aerosols*, Atmospheric Chemistry and Physics **6**: pp. 3131-3148 (2006)
- [30] D. Liu, J. Whitehead, M.R. Alfarra, E. Reyes-Villegas, et al., *Black-carbon absorption enhancement in the atmosphere determined by particle mixing state*, Nature Geoscience **10**: pp. 184-188 (2017)
- [31] N.-E. Olofsson, J. Johnsson, H. Bladh, P.-E. Bengtsson, *Soot sublimation studies in a premixed flat flame using laser-induced incandescence (LII) and elastic light scattering (ELS)*, Applied Physics B **112**: pp. 333-342 (2013)
- [32] H. Bladh, J. Johnsson, P.-E. Bengtsson, *Influence of spatial laser energy distribution on evaluated soot particle sizes using two-colour laser-induced incandescence in a flat premixed ethylene/air flame*, Applied Physics B **96**: pp. 645-656 (2009)
- [33] S. De Iuliis, F. Cignoli, S. Maffi, G. Zizak, *Influence of the cumulative effects of multiple laser pulses on laser-induced incandescence signals from soot*, Applied Physics B **104**: pp. 321-330 (2011)
- [34] H. Wang, *Formation of nascent soot and other condensed-phase materials in flames*, Proceedings of the Combustion Institute **33**: pp. 41-67 (2011)
- [35] S. Bejaoui, X. Mercier, P. Desgroux, E. Therissen, *Laser induced fluorescence spectroscopy of aromatic species produced in atmospheric sooting flames using UV and visible excitation wavelengths*, Combustion and Flame **161**: pp. 2479-2491 (2014)

- [36] H. Bladh, N.-E. Olofsson, T. Mouton, J. Simonsson, X. Mercier, A. Faccinnetto, P.-E. Bengtsson, P. Desgroux, *Probing the smallest soot particles in low-sooting premixed flames using laser-induced incandescence*, Proceedings of the Combustion Institute **35**: pp. 1843-1850 (2015)
- [37] T.C. Bond, R.W. Bergstrom, *Light Absorption by Carbonaceous Particles: An Investigative Review*, Aerosol Science and Technology **40**: pp. 27 - 67 (2006)
- [38] H. Bockhorn (Ed.), *Soot formation in Combustion*, Springer-Verlag, 1994.
- [39] A. D'Anna, *Combustion-formed nanoparticles*, Proceedings of the Combustion Institute **32**: pp. 593-613 (2009)
- [40] L. Holthius, *Holthuis & Associates Flat Flame Burners*. (cited: 2018-01-12). Available from: [www.flatflame.com](http://www.flatflame.com)
- [41] N.-E. Olofsson, H. Bladh, A. Bohlin, J. Johnsson, P.-E. Bengtsson, *Are Sooting Premixed Porous-Plug Burner Flames One-Dimensional? A Laser-Based Experimental Investigation*, Combustion Science and Technology **185**: pp. 293-309 (2013)
- [42] F. Migliorini, S. De Iuliis, F. Cignoli, G. Zizak, *How "flat" is the rich premixed flame produced by your McKenna burner?*, Combustion and Flame **153**: pp. 384-393 (2008)
- [43] J. Zerbs, K. Geigle, O. Lammel, J. Hader, R. Stirn, R. Hedef, W. Meier, *The influence of wavelength in extinction measurements and beam steering in laser-induced incandescence measurements in sooting flames*, Applied Physics B **96**: pp. 683-694 (2009)
- [44] B. Axelsson, R. Collin, P.-E. Bengtsson, *Laser-induced incandescence for soot particle size measurements in premixed flat flames*, Applied Optics **39**: pp. 3683-3690 (2000)
- [45] Jing Ltd., *miniCAST 5201 type C: specification sheet*, Zollikofen, Switzerland, 2014.
- [46] Jing Ltd., *miniCAST 5201 type C: instruction manual*, Zollikofen, Switzerland, 2014.
- [47] S. Török, V.B. Malmberg, J. Simonsson, A. Eriksson, J. Martinsson, M. Mannazhi, J. Pagels, P.-E. Bengtsson, *Investigation of the absorption Ångström exponent and its relation to physicochemical properties for mini-CAST soot*, Aerosol Science and Technology, doi:10.1080/02786826.2018.1457767 pp. 1-33 (2018)

- [48] F.W. Bowditch, *A new tool for combustion research - A quartz piston engine*, SAE Transaction **69**: pp. 17-23 (1961)
- [49] K. Andersson, R. Johansson, F. Johnsson, B. Leckner, *Radiation Intensity of Propane-Fired Oxy-Fuel Flames: Implications for Soot Formation*, Energy & Fuels **22**: pp. 1535-1541 (2008)
- [50] K. Andersson, R. Johansson, S. Hjærtstam, F. Johnsson, B. Leckner, *Radiation intensity of lignite-fired oxy-fuel flames*, Experimental Thermal and Fluid Science **33**: pp. 67-76 (2008)
- [51] D. Bäckström, A. Gunnarsson, D. Gall, X. Pei, R. Johansson, K. Andersson, R.K. Pathak, J.B.C. Pettersson, *Measurement of the size distribution, volume fraction and optical properties of soot in an 80 kW propane flame*, Combustion and Flame **186**: pp. 325-334 (2017)
- [52] M.Y. Choi, G.W. Mulholland, A. Hamins, T. Kashiwagi, *Comparisons of the Soot Volume Fraction Using Gravimetric and Light Extinction Techniques*, Combustion and Flame **102**: pp. 161-169 (1995)
- [53] F. Liu, G.J. Smallwood, *Effect of aggregation on the absorption cross-section of fractal soot aggregates and its impact on LII modelling*, Journal of Quantitative Spectroscopy and Radiative Transfer **111**: pp. 302-308 (2010)
- [54] C.F. Bohren, D.R. Huffman, *Absorption and scattering of light by small particles*, Wiley, New York, 1998.
- [55] S.S. Krishnan, K.C. Lin, G.M. Faeth, *Optical properties in the visible of overfire soot in large buoyant turbulent diffusion flames*, Journal of Heat Transfer **122**: pp. 517-524 (2000)
- [56] S.S. Krishnan, K.C. Lin, G.M. Faeth, *Extinction and scattering properties of soot emitted from buoyant turbulent diffusion flames*, Journal of Heat Transfer **123**: pp. 331-339 (2001)
- [57] A.R. Coderre, K.A. Thomson, D.R. Snelling, M.R. Johnson, *Spectrally resolved light absorption properties of cooled soot from a methane flame*, Applied Physics B **104**: pp. 175-188 (2011)
- [58] H. Bladh, J. Johnsson, N.-E. Olofsson, A. Bohlin, P.-E. Bengtsson, *Optical soot characterization using two-color laser-induced incandescence (2C-LII) in the soot growth region of a premixed flat flame*, Proceedings of the Combustion Institute **33**: pp. 641-648 (2011)

- [59] N.A. Marley, J.S. Gaffney, J.C. Baird, C.A. Blazer, P.J. Drayton, J.E. Frederick, *An Empirical Method for the Determination of the Complex Refractive Index of Size-Fractionated Atmospheric Aerosols for Radiative Transfer Calculations*, *Aerosol Science and Technology* **34**: pp. 535-549 (2001)
- [60] W.D. Erickson, G.C. Williams, H.C. Hottel, *Light scattering measurements on soot in a benzene-air flame*, *Combustion and Flame* **8**: pp. 127-132 (1964)
- [61] W.H. Dalzell, A.F. Sarofim, *Optical constants of soot and their application to heat flux calculations*, *Journal of Heat Transfer* **91**: pp. 100-104 (1969)
- [62] S. Chippett, W.A. Gray, *The size and optical properties of soot particles*, *Combustion and Flame* **31**: pp. 149-159 (1978)
- [63] J. Janzen, *The refractive index of colloidal carbon*, *Journal of Colloid and Interface Science* **69**: pp. 436-447 (1979)
- [64] A.B. Pluchino, S.S. Goldberg, J.M. Dowling, C.M. Randall, *Refractive-index measurements of single micron-sized carbon particles*, *Applied Optics* **19**: pp. 3370-3372 (1980)
- [65] S.C. Lee, C.L. Tien, *Optical constants of soot in hydrocarbon flames*, *Proceedings of the Combustion Institute* **18**: pp. 1159-1166 (1981)
- [66] C.E. Batten, *Spectral optical constants of soots from polarized angular reflectance measurements*, *Applied Optics* **24**: pp. 1193-1199 (1985)
- [67] J. Mullins, A. Williams, *The optical properties of soot: a comparison between experimental and theoretical values*, *Fuel* **66**: pp. 277-280 (1987)
- [68] Z.G. Habib, P. Vervisch, *On The Refractive Index of Soot at Flame Temperature*, *Combustion Science and Technology* **59**: pp. 261-274 (1988)
- [69] H. Chang, T.T. Charalampopoulos, *Determination of the wavelength dependence of refractive indices of flame soot*, *Proceedings of the Royal Society of London: Series A* **430**: pp. 577-591 (1990)
- [70] B.J. Stagg, T.T. Charalampopoulos, *Refractive indices of pyrolytic graphite, amorphous carbon, and flame soot in the temperature range 25° to 600°C*, *Combustion and Flame* **94**: pp. 381-396 (1993)
- [71] J.S. Wu, S.S. Krishnan, G.M. Faeth, *Refractive indices at visible wavelengths of soot emitted from buoyant turbulent diffusion flames*, *Journal of Heat Transfer* **119**: pp. 230-237 (1997)



- [72] T.C. Williams, C.R. Shaddix, K.A. Jensen, J.M. Suo-Anttila, *Measurement of the dimensionless extinction coefficient of soot within laminar diffusion flames*, International Journal of Heat and Mass Transfer **50**: pp. 1616-1630 (2007)
- [73] X. Pei, *A Soot Transformation Study: Interactions Between Soot, Sulfuric Acid and Secondary Organic Aerosol (SOA)*, Department of Chemical and Molecular Biology, Faculty of Science, University of Gothenburg, Gothenburg, Sweden, 2018
- [74] R.J. Santoro, C.R. Shaddix, *Laser-Induced Incandescence in: Applied Combustion Diagnostics*, Taylor and Francis, New York, 2002, pp. 252-286.
- [75] H. Bladh, J. Johnsson, P.-E. Bengtsson, *On the dependence of the laser-induced incandescence (LII) signal on soot volume fraction for variations in particle size*, Applied Physics B **90**: pp. 109-125 (2008)
- [76] H.A. Michelsen, *Understanding and predicting the temporal response of laser-induced incandescence from carbonaceous particles*, Journal of Chemical Physics **118**: pp. 7012-7045 (2003)
- [77] H. Bladh, P.-E. Bengtsson, *Characteristics of laser-induced incandescence from soot in studies of a time-dependent heat- and mass-transfer model*, Applied Physics B **78**: pp. 241-248 (2004)
- [78] H. Bladh, J. Johnsson, J. Rissler, H. Abdulhamid, N.E. Olofsson, M. Sanati, J. Pagels, P.E. Bengtsson, *Influence of soot particle aggregation on time-resolved laser-induced incandescence signals*, Applied Physics B **104**: pp. 331-341 (2011)
- [79] H.A. Michelsen, F. Liu, B.F. Kock, H. Bladh, et al., *Modeling Laser-Induced Incandescence of Soot: A summary and comparison of LII models*, Applied Physics B **87**: pp. 503-521 (2007)
- [80] S. di Stasio, P. Massoli, *Influence of the Soot Property Uncertainties in Temperature and Volume-Fraction Measurements by 2-Color Pyrometry*, Measurement Science & Technology **5**: pp. 1453-1465 (1994)
- [81] R. Hedef, K. Geigle, J. Zerbs, R. Sawchuk, D. Snelling, *The concept of 2D gated imaging for particle sizing in a laminar diffusion flame*, Applied Physics B **112**: pp. 395-408 (2013)
- [82] L.A. Melton, *Soot Diagnostics Based on Laser-Heating*, Applied Optics **23**: pp. 2201-2208 (1984)

- [83] J. Reimann, S.A. Kuhlmann, S. Will, *2D aggregate sizing by combining laser-induced incandescence (LII) and elastic light scattering (ELS)*, Applied Physics B **96**: pp. 583-592 (2009)
- [84] D.B. Williams, C.B. Carter, *Transmission Electron Microscopy, Part 1: Basics*, 2nd ed., Springer, 2008.
- [85] N.J. Kempema, M.B. Long, *Combined optical and TEM investigations for a detailed characterization of soot aggregate properties in a laminar coflow diffusion flame*, Combustion and Flame **164**: pp. 373-385 (2016)
- [86] S. De Iuliis, F. Cignoli, G. Zizak, *Two-color laser-induced incandescence (2C-LII) technique for absolute soot volume fraction measurements in flames*, Applied Optics **44**: pp. 7414-7423 (2005)
- [87] X. López-Yglesias, P.E. Schrader, H.A. Michelsen, *Soot maturity and absorption cross sections*, Journal of Aerosol Science **75**: pp. 43-64 (2014)
- [88] D.A. Lack, J.M. Langridge, *On the attribution of black and brown carbon light absorption using the Ångström exponent*, Atmospheric Chemistry and Physics **13**: pp. 10535-10543 (2013)
- [89] F. Migliorini, K. Thomson, G. Smallwood, *Investigation of optical properties of aging soot*, Applied Physics B **104**: pp. 273-283 (2011)
- [90] D. Snelling, K. Thomson, F. Liu, G. Smallwood, *Comparison of LII derived soot temperature measurements with LII model predictions for soot in a laminar diffusion flame*, Applied Physics B **96**: pp. 657-669 (2009)
- [91] F. Goulay, P.E. Schrader, H.A. Michelsen, *Effect of the wavelength dependence of the emissivity on inferred soot temperatures measured by spectrally resolved laser-induced incandescence*, Applied Physics B **100**: pp. 655-663 (2010)
- [92] S. Maffi, S. De Iuliis, F. Cignoli, G. Zizak, *Investigation on thermal accommodation coefficient and soot absorption function with two-color TIRE-LII technique in rich premixed flames*, Applied Physics B **104**: pp. 357-366 (2011)
- [93] D.H. Cotton, N.J. Friswell, D.R. Jenkins, *The suppression of soot emission from flames by metal additives*, Combustion and Flame **17**: pp. 87-98 (1971)
- [94] B.S. Haynes, H. Jander, H. Mätzing, H.G.G. Wagner, *The influence of various metals on carbon formation in premixed flames*, Combustion and Flame **40**: pp. 101-103 (1981)

- [95] B.S. Haynes, H.G. Wagner, *Soot formation*, Progress in Energy and Combustion Science 7: pp. 229-273 (1981)
- [96] C.R. Shaddix, T.C. Williams, *The effect of oxygen enrichment on soot formation and thermal radiation in turbulent, non-premixed methane flames*, Proceedings of the Combustion Institute 36: pp. 4051-4059 (2017)
- [97] C.K. Stimpson, A. Fry, T. Blanc, D.R. Tree, *Line of sight soot volume fraction measurements in air- and oxy-coal flames*, Proceedings of the Combustion Institute 34: pp. 2885-2893 (2013)



# Acknowledgements

I would like to start by acknowledging my main supervisor, **Per-Erik Bengtsson**, for giving me the opportunity to start working at the Division of Combustion Physics, initially as a master thesis student and later as a PhD student. I would also like to express my gratitude to my first assistant supervisor, **Henrik Bladh**, who left the division in the fall of 2015. You and Per-Erik were such a good team, and your doors were always open for discussions regardless of subject. I would also like to thank my second assistant supervisor, **Christian Brackmann**. I have always appreciated your broad knowledge and our discussions.

I would also like to acknowledge **Nils-Erik Olofsson**, whom I first met when I started my master thesis project in the soot group. You are a bit crazy, and a bit lazy, but still get everything done on time. You showed me that you do not have to work yourself to death while doing a PhD. Furthermore, thank you for showing me everything in the lab, and for being such a good friend. I hope our friendship will be long lasting. I would also like to thank the rest of the soot group, especially **Sandra Török** and **Manu Naduvil Mannazhi**. I have also appreciated sharing an office with **Elias Kristensson**, who conveniently went on parental leave when I wrote this thesis.

During my PhD we have had measurement campaigns in both Piteå and Gothenburg. I would therefore like to thank the people at these places for making me feel welcome during these periods. A special thanks to **Yngve Ögren** and **Henrik Winnikka** at RISE ETC in Piteå, and **Daniel Bäckström** and **Adrian Gunnarsson** at Chalmers in Gothenburg.

During the years I have befriended a lot of kind and funny people at the division: **Nils-Erik Olofsson**, **Sandra Török**, **Moah Christensen**, **Linda Vallenhag**, **Ali Hosseinnia**, **Malin Jonsson**, **Jesper Borggren**, **Kajsa Larsson**, **Elin Malmqvist**, and **Jim Larsson**, to mention some. Even though many of you have finished your PhDs, and left the division already, I would like thank you for making Combustion Physics such a good place to work at, and Elin, I will always make sure to knock on your door.

I would also like to thank my family and friends for always being supportive, especially **Jens** for surviving the emotional roller coaster associated with doing a PhD. Thanks to **Andreas Ericsson**, **John Dahlqvist**, and **Joel Olsson** for all the nice lunches we have had. Friends that should be mentioned for just being there are: **Malin Ahlgren**, **Anders Weddig**, **Anna Svensson**, **Thomas Hjelm**, and **Lina Tingström**. I would also like to mention **Brontë Weddig** for being a good friend and for proof-reading the thesis for grammar and spelling mistakes.

Thank you all!



# Summary of Papers

- I. **J. Simonsson**, N.-E. Olofsson, S. Török, P.-E. Bengtsson, and H. Bladh, *Wavelength dependence of extinction in sooting flat premixed flames in the visible and near-infrared regimes*

In this work, extinction measurements were conducted to investigate the wavelength dependence of the optical properties of soot in two ethylene/air flames. Twelve diode lasers were used, all of which were operated in a wavelength range of 405 nm to 1064 nm. Soot volume fractions were evaluated at different heights above burner (HAB) from the extinction measurements. The inferred soot volume fractions showed a strong dependence on wavelength below 700 nm. This is most likely a result of absorption also from polycyclic aromatic hydrocarbons. Therefore, wavelengths below 700 nm should be avoided when measuring soot for this reason. The wavelength dependence of the absorption function was also evaluated, showing strong dependence on wavelength for nascent soot at lower HABs. For more mature particles at higher HABs, the wavelength dependence of the absorption function was found to be minor.

*I was the main responsible for preparing the experiment, for conducting the measurements, for evaluation of the results, and for writing the manuscript.*

- II. N.-E. Olofsson, **J. Simonsson**, S. Török, H. Bladh, and P.-E. Bengtsson, *Evolution of properties for aging soot in premixed flat flames studied by laser-induced incandescence and elastic light scattering*

In this work, the change in optical properties from nascent to more mature soot was investigated using a combination of elastic light scattering and two-color laser-induced incandescence in a “pump-probe”-experiment. Both of the investigated ethylene/air flames showed that the soot becomes less transparent during the soot growth and maturation process. Soot peak temperatures were also evaluated, and results from Paper I were used in the evaluation, resulting in a discussion on how the sublimation temperatures relates to soot maturity.

*I assisted Nils-Erik Olofsson during the measurements and I was also involved in the discussions of the results and in the preparation of the manuscript.*

- III. Y. Gallo, J. **Simonsson**, T. Lind, P.-E. Bengtsson, H. Bladh, and Ö. Andersson, *A study of in-cylinder soot oxidation by laser extinction measurements during an EGR-sweep in an optical diesel engine*

In this paper, extinction measurements were conducted in a heavy-duty diesel engine with optical access to investigate the correlation between the soot oxidation rates and soot emissions. Soot volume fractions were measured as a function of crank angle degree when the intake oxygen level was varied between 9 % and 21 %. The results showed decreasing soot oxidation rates for decreased oxygen levels in the oxidizer, both from estimation from the extinction measurements of soot and from the rate of heat release curves.

*I was responsible for the laser measurements in this investigation, including the setup of the laser equipment, performing the extinction measurements and evaluation of the results. I was also involved in the discussions of the results and in the preparation of the manuscript. The engine related discussions were mainly performed by Yann Gallo and Öivind Andersson.*

- IV. J. **Simonsson**, H. Bladh, M. Gullberg, E. Pettersson, A. Sepman, Y. Ögren, H. Wiinikka, and P.-E. Bengtsson, *Soot concentrations in an atmospheric entrained flow gasifier with variations in fuel and burner configuration studied using diode-laser extinction measurements*

Extinction measurements using two diode lasers were conducted in an atmospheric entrained-flow gasifier at two vertical positions. Soot volume fractions were evaluated and the results showed significant variations in soot volume fractions for various running conditions. Furthermore, two different fuels were tested (wood powder from stem wood and peat powder) for which peat powder showed much lower soot volume fractions under the same air-fuel equivalence ratios. This is most likely caused by lower volatile content in the peat powder, but could also be related to increased ash components.

*In this work, I was the main responsible for the laser extinction measurements (preparations, measurements and evaluation) and for preparing the manuscript. The measurements performed using secondary techniques were performed by some of the other authors.*



- V. **J. Simonsson**, N.-E. Olofsson, H. Bladh, M. Sanati, and P.-E. Bengtsson, *Influence of potassium and iron chloride on the early stages of soot formation studied using imaging LII/ELS and TEM techniques*

Laser-induced incandescence (LII) and elastic light scattering (ELS) were used to investigate the influence of metal additives on soot formation. In this paper, the results primarily from potassium chloride (KCl) and iron chloride ( $\text{FeCl}_3$ ) seeded flames were shown. The results showed significant reduction of soot volume fraction when seeding KCl solution to the flame. For the  $\text{FeCl}_3$  additives, only a slight increase in ELS signal was observed, most likely a result of scattering from the salt particles themselves. Soot samples were also investigated using transmission electron microscopy, showing decreased particle sizes for the flames seeded with KCl.

*Nils-Erik Olofsson and I did the measurements and initial evaluation together. I was the main responsible for finalizing the evaluation and preparing the manuscript.*

- VI. **J. Simonsson**, N.-E. Olofsson, A. Hosseinnia, and P.-E. Bengtsson, *Influence of potassium chloride and other metal salts on soot formation studied using imaging LII and ELS, and TEM techniques*

This paper is a continuation of the work presented in Paper V. Results from investigating the influence of seven different metal salts (KCl, NaCl,  $\text{CaCl}_2$ ,  $\text{FeCl}_3$ ,  $\text{ZnCl}_2$ ,  $\text{AlCl}_3$  and  $\text{MgCl}_2$ ) on the soot formation using laser-induced incandescence and elastic light scattering are presented. The results indicated that primarily alkali and alkaline earth metals affected the flame with reduced soot volume fractions and either reduced size or concentration of soot precursors. In this paper, further investigation has also been performed for the flame seeded with potassium chloride, including particle size evaluations and temperature measurements using CARS, to ascertain the effect of KCl additives on flame temperature. The temperature measurements showed slightly elevated temperatures for flames with potassium chloride additives.

*The planning of the measurements, building the setup and doing the measurements were performed by Nils-Erik Olofsson and I. I was the main responsible for evaluation of the results and preparing the manuscript. The CARS measurements and evaluation, however, was performed by Ali Hosseinnia and Per-Erik Bengtsson.*

- VII. **J. Simonsson**, A. Gunnarsson, M. Naduvil Mannazhi, D. Bäckström, K. Andersson, and P.-E. Bengtsson, *In-situ soot characterization of propane flames and influence of additives in a 100 kW oxy-fuel furnace using two-dimensional laser-induced incandescence*

In the work presented in Paper VII, soot measurements were conducted in a 100 kW<sub>th</sub> oxy-fuel test furnace where various operating conditions were investigated using propane as the fuel. The furnace was operated at a constant air-fuel equivalence ratio in oxy-fuel mode with various concentrations of oxygen in the inlet oxidizer, resulting in higher soot concentrations for higher oxygen concentrations. The increased soot concentrations were most likely due to the decrease in mixing and total flow through the reactor, which was necessary to maintain the constant air-fuel equivalence ratio.

*I was the main responsible for the laser measurements in this work, assisted by Manu Naduvil Mannazhi, with the authors from Gothenburg operated the furnace. I was also the main responsible for evaluating the results and preparing the manuscript.*



Lund University  
Faculty of Engineering  
Department of Physics

ISBN 978-91-7753-665-9 (print)  
ISBN 978-91-7753-666-6 (pdf)  
ISSN 1102-8718  
ISRN LUTFD2/TFCP-212-SE

